Report on the analogue modelling of the collapse of caldera and volcanic edifices and the associated surface deformation

Deliverable 3.6

Report on the analogue modelling of the collapse of caldera and volcanic edifices and the associated surface deformation

Deliverable 3.6

Version <final>

<Multiple authors>

Work package <WP 3.3>

<September 9th, 2019>

Website: http://www.gemex-h2020.eu

The GEMex project is supported by the European Union’s Horizon 2020 programme for Research and Innovation under grant agreement No 727550

Authors

Marco Bonini, Daniele Maestrelli, Valerio Acocella, Damien Bonté, Gerardo Carrasco-Núñez, Giacomo Corti, Guido Giordano, Federico Lucci, Domenico Montanari, Giovanna Moratti, Gianluca Norini, Federico Rossetti, Stefano Urbani.

T 3.3 Leader: Marco Bonini

WP3 Leader: Damien Bonté

Coordinators:

Domenico Liotta

Víctor Hugo Garduño-Monroy

Contributions

Executive summary: Marco Bonini, Daniele Maestrelli, Giacomo Corti, Domenico Montanari, Giovanna Moratti (CNR-IGG).

Chapter 1: Marco Bonini, Daniele Maestrelli, Giacomo Corti, Domenico Montanari, Giovanna Moratti (CNR-IGG).

Chapter 2: Marco Bonini, Daniele Maestrelli, Valerio Acocella, Damien Bonté, Gerardo Carrasco-Núñez, Giacomo Corti, Guido Giordano, Federico Lucci, Domenico Montanari, Giovanna Moratti, Gianluca Norini, Federico Rossetti, Stefano Urbani.

Sections 2.1- 2.2: Marco Bonini, Daniele Maestrelli, Giacomo Corti, Domenico Montanari, Giovanna Moratti (CNR-IGG).

Section 2.3: Marco Bonini, Daniele Maestrelli, Valerio Acocella, Damien Bonté, Gerardo Carrasco-Núñez, Giacomo Corti, Guido Giordano, Federico Lucci, Domenico Montanari, Giovanna Moratti, Gianluca Norini, Federico Rossetti, Stefano Urbani.

Sections 2.3.1-2.3.4: Marco Bonini, Daniele Maestrelli, Giacomo Corti, Domenico Montanari, Giovanna Moratti (CNR-IGG).

Section 2.3.4: Gianluca Norini (CNR-IDPA)

Section 2.3.5: Stefano Urbani, Valerio Acocella, Guido Giordano, Federico Rossetti, Federico Lucci (UNIROMA TRE).

Section 2.4: Marco Bonini, Daniele Maestrelli, Giacomo Corti, Domenico Montanari, Giovanna Moratti (CNR-IGG).

Section 2.5: Gianluca Norini (CNR-IDPA)

Section 2.6: Stefano Urbani, Valerio Acocella, Guido Giordano, Federico Rossetti, Federico Lucci (UNIROMA TRE).

Section 2.7: Marco Bonini, Daniele Maestrelli, Giacomo Corti, Domenico Montanari, Giovanna Moratti (CNR-IGG).

Chapter 3: Marco Bonini, Daniele Maestrelli, Valerio Acocella, Damien Bonté, Gerardo Carrasco-Núñez, Giacomo Corti, Guido Giordano, Federico Lucci, Domenico Montanari, Giovanna Moratti, Gianluca Norini, Federico Rossetti, Stefano Urbani.

Section 3.1-3.3: Marco Bonini, Daniele Maestrelli, Giacomo Corti, Domenico Montanari, Giovanna Moratti (CNR-IGG).

Section 3.4: Gianluca Norini (CNR-IDPA)

Section 3.5: Stefano Urbani, Valerio Acocella, Guido Giordano, Federico Rossetti, Federico Lucci (UNIROMA TRE).

Chapter 4: Marco Bonini, Daniele Maestrelli, Valerio Acocella, Damien Bonté, Gerardo Carrasco-Núñez, Giacomo Corti, Guido Giordano, Federico Lucci, Domenico Montanari, Giovanna Moratti, Gianluca Norini, Federico Rossetti, Stefano Urbani.

Sections: 4.1.1-4.1.3: Marco Bonini, Daniele Maestrelli, Giacomo Corti, Domenico Montanari, Giovanna Moratti (CNR-IGG).

Section 4.1.4: Gianluca Norini (CNR-IDPA)

Section 4.1.5: Stefano Urbani, Valerio Acocella, Guido Giordano, Federico Rossetti, Federico Lucci (UNIROMA TRE).

Section 4.2: Marco Bonini, Daniele Maestrelli, Valerio Acocella, Damien Bonté, Gerardo Carrasco-Núñez, Giacomo Corti, Guido Giordano, Federico Lucci, Domenico Montanari, Giovanna Moratti, Gianluca Norini, Federico Rossetti, Stefano Urbani.

Chapter 5: Marco Bonini, Daniele Maestrelli, Valerio Acocella, Damien Bonté, Gerardo Carrasco-Núñez, Giacomo Corti, Guido Giordano, Federico Lucci, Domenico Montanari, Giovanna Moratti, Gianluca Norini, Federico Rossetti, Stefano Urbani.

Table of Contents[1]

[1] The content of this report reflects only the authors' view. The Innovation and Networks Executive Agency (INEA) is not responsible for any use that may be made of the information it contains.

List of figures

List of tables

Executive summary

Deliverable D3.6 summarizes the results obtained by Task T3.3 members (CNR-UNIROMA TRE), implementing analogue models with the aim to test hypotheses about the structural evolution of the Los Humeros volcanic complex and Acoculco caldera systems. In this report, we present the results of four experimental series (Series D3.6-1, D3.6-2, D3.6-3, and D3.6-4), which were designed to investigate the collapse of caldera and volcanic edifices, as well as intra-caldera resurgence and associated surface deformation. Specifically, Series D3.6-1 investigates the collapse of symmetric and asymmetric calderas, Series D3.6-2 investigates the influence of pre-caldera volcano-related topography on caldera collapse, D3.6-3 addresses caldera resurgence and pre-existing (sub-vertical) faults, and D3.6-4 addresses the role of caldera resurgence in combination with thrust and normal faults in the basement.

In Chapter 1, we introduce the work of Task T3.3, reporting the regional and the local geological setting of Los Humeros volcanic complex and Acoculco caldera system. In Chapter 2, we briefly introduce the analogue modelling procedure (Section 2.1), we review analogue modelling of caldera collapse and resurgence (Section 2.2), we then describe the modelling strategy (Section 2.3) and the modelling procedures adopted for the four experimental series (Sections 2.4 and 2.5), and, finally, the methodology adopted for monitoring and analysis of models (Section 2.6). In Chapter 3, we describe the results of analogue models for Series 3.6-1, D3.6-2, D3.6-3 and D.3.6-4, while in Chapter 4, we discuss the results and insights into caldera collapse and resurgence from analogue modelling (Section 4.1), as well as the clues provided by these experiments on the evolution of the Los Humeros and Acoculco volcanic systems (Section 4.2). Finally, Chapter 5 outlines the conclusions of this study.

Models of Series D3.6-1 have shown that symmetric caldera collapse is achieved through transient asymmetry steps, and that the development of asymmetric, trap-door caldera collapse systems lead to the formation of peculiar extensional structures accommodating tilting of the caldera roof block.

Models of Series D3.6-2 have shown that the presence of an eccentric volcano edifice induces extra loading on the subsiding block, forcing the caldera to develop a trap-door system.

Models of Series D3.6-3 tested the effect of broad (piston-like) and localized resurgence, providing insights into possible interpretations of the structural pattern of the case studies, particularly the Los Potreros caldera. Series D3.6-4 addresses the role of pre-existing thrust and normal faults on magma resurgence at Los Humeros-Los Potreros system. Finally, Series D3.6-5 explored the role of shallow intra-caldera intrusion, and their implications for the presence of shallow intra-caldera heat sources in geothermal systems.

Some of the performed models show a high similarity with the natural deformation patterns, and may thus help to explain their structural setting and the related evolutionary model.

1 Introduction

Experimental analogue modelling (carried out in the frame of Task 3.3) has focused on the interplay between regional tectonics, fault reactivation and magmatic processes in shaping volcanic edifices, which are aspects relevant for geothermal exploration. Analogue modelling is an experimental technique that allows to study geological processes in the lab, through the analysis of physical models built and deformed at reduced geometrical and temporal scales. In other words, tectonic processes occurring in millions of years, and length scales of tens to thousands of kilometres, are reproduced in the lab in hours/days and centimetre-scale. In the GEMex Project, analogue modelling has addressed two main research questions, particularly (1) interactions between regional tectonics and volcanoes, and (2) collapse of caldera and volcanic edifices and the associated surface deformation. The results of this activity are illustrated in two reports, namely Report D3.5 (*Report on the analogue modelling of the interactions between regional tectonics and volcanoes*), and Report D3.6 (*Report on the analogue modelling of the collapse of caldera and volcanic edifices and the associated surface deformation*). The set-up of analogue models is based on data available in the literature, as well as on new geological and geophysical data obtained through the GEMex Project (particularly from WPs 4 and 5). The results related to Report D3.6 are described below, starting from the geological setting of the study region, and of the Los Humeros volcanic complex and Acoculco caldera complex, which are host to the geothermal fields targeted by the GEMex Project. Analogue modelling carried out in this research has approached the study of the Los Humeros and Acoculco geothermal systems by investigating natural processes from a general point of view, and thus the experimental results provide original hints that can also be applied to other caldera and volcanic complexes worldwide.

All the different series of analogue models have been performed in the frame of Task 3.3 of the GEMex Project, and thus some parts of chapters 1 and 2 are common to deliverables 3.5 and 3.6 (namely, the regional geological setting, analogue modelling of volcano-tectonic processes, and monitoring and analysis of deformation).

Deliverable D3.6 reports the results of five experimental series addressing different aspects related to magmatic-related processes that may be relevant for geothermal exploration, namely: (1) the processes of symmetric/asymmetric caldera collapse (Series D3.6-1), (2) the effect of pre-caldera volcano-related topography (Series D3.6-2), (3) caldera resurgence and interaction with pre-existing structures (both regional inherited fabrics and caldera collapse faults) (Series D3.6-3), (4) combined effects of compressional and extensional tectonics structures and magmatic processes on the Los Humeros Volcanic Complex (Series D3.6-4), and (5) the effect of shallow intra-caldera intrusions (Series D3.6-5). Series D3.6-1, D3.6-2 and D3.6-3 have been performed at the Tectonic Modelling Laboratory of CNR-IGG Firenze, Series D3.6-4 at the laboratory of CNR-IDPA Milano, and Series D3.6-5 at the Laboratory of Experimental Tectonics of University of Roma Tre.

1.1 Regional geological setting

The Los Humeros and Acoculco geothermal fields occur on the eastern sector of the Trans-Mexican Volcanic Belt (TMVB), which is a large-scale ca. 1000 km-long, ESE-trending zone of volcano-tectonic deformation extending through central Mexico, approximately from the mouth of the Gulf of California up to the Gulf of Mexico (Fig. 1.1). The TMVB is a continental volcanic arc resulting from the subduction of the Cocos and Rivera plates beneath the North American plate along the Middle American trench. In the TMVB, magmatic activity started in Early Miocene (ca. 19 Ma) and extensional deformation affected this zone since Late Miocene (Ferrari et al., 2012, and references therein). The evolution of the TMVB is intimately linked to the evolution of subduction of the Farallon plate beneath the North America plate, which stalled in front of Baja California and then the Farallon slab broke at depth and successively slab tearing started to propagate (Burkett and Billen, 2010).

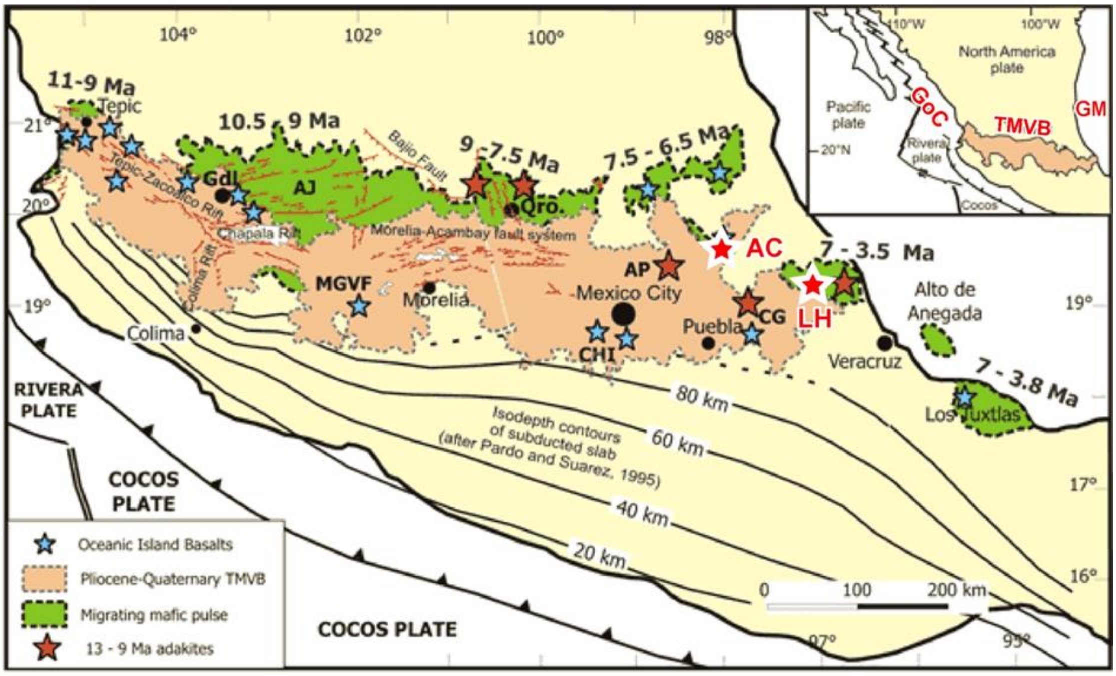

Figure 1.1 Regional geotectonic map of central Mexico, with indication of the study Los Humeros and Acoculco geothermal fields (from Ferrari et al., 2004). LH, Los Humeros geothermal field; AC, Acoculco geothermal field; GoC, Gulf of California; GM, Gulf of Mexico; TMVB, Trans-Mexican Volcanic Belt.

According to Ferrari (2004), magmatism is associated with the lateral propagation of slab detachment beneath the TMVB during the late Miocene. In particular, slab tearing progressed eastward from the Gulf of California to the Gulf of Mexico, in a direction slightly oblique to the trench system (Fig. 1.2; Ferrari, 2004).

Interestingly, the lateral propagation of the slab tear is marked by a pulse of mafic volcanism that migrated from west to east since ~11Ma, reaching the Gulf of Mexico by 7 Ma (Fig. 1.1; Ferrari et al., 2012).

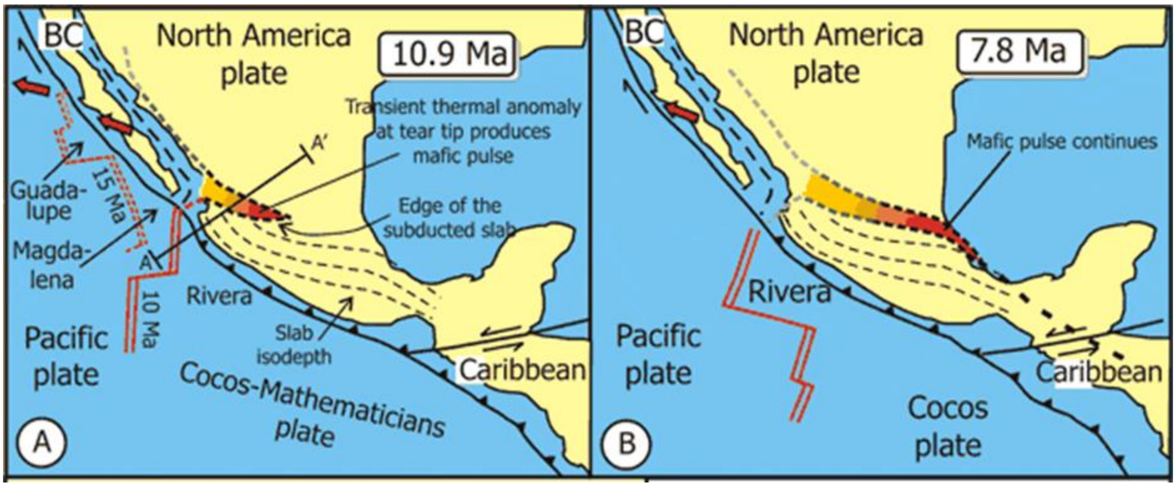

Figure 1.2. Evolution of slab tearing during Late Miocene with proposed location of slab detachment at 10.9 and 7.8 Ma (after Ferrari et al., 2004).

The TMVB covers several ancient fault systems that have been partially reactivated at different times during its evolution. In fact, since the end of the Eocene, the region encompassing the TMVB has been characterized by a broad transtensional kinematics (Alaniz-Álvarez and Nieto-Samaniego, 2007). However, the geometry, kinematics, and time-space distribution pattern of the brittle fault systems affecting the TMVB is complex. In detail, such an extensional deformation affecting the TMVB is relevant west of 100°W, whereas only a limited number of faults, with lesser vertical displacement, can be detected in the eastern TMVB (east of 100°W) (e.g., Suter et al., 2001; Ferrari et al., 2012).

Normal faults affecting the TMVB are generally oriented around East-West, yet variations from ENE to ESE can be observed in the different sectors. Normal faulting shows complex time-space patterns. In the western TMVB, extensional deformation started in Late Miocene (e.g., Rosas-Elguera and Urrutia-Fucugauchi, 1998), with some faults ceasing their activity during Pleistocene (Ferrari et al., 2012), and other showing clear indications of neotectonic (Holocene) activity (e.g., Garduño-Monroy et al., 1993). Some normal faults have been even identified as being seismogenic sources that have produced large historic earthquakes (e.g., the M 6.9 Acambay earthquake of 1912; Suter et al., 1995). Faulting in the eastern TMVB is instead less intense, with the main normal faults being located around Mexico City, where they show evidence of Holocene activity with some left-lateral component of displacement (Norini et al., 2006). The occurrence of normal faults drastically decreases further east in the TMVB, and almost vanish in the area of the Los Humeros and Acoculco (e.g., Ferrari et al., 2012). Although data on age of deformation is partial, a general southward migration of fault activity has been suggested for the western TMVB, while this pattern cannot be identified in the eastern TMVB where a low level of Pleistocene–Holocene tectonic deformation is reported for the Mexico City region (Ferrari et al., 2012). The general distribution and age of faulting pattern may also suggest that tectonic deformation has also been progressing eastward, in a similar fashion of a propagating continental rift.

Regarding the recent/active tectonic stress field operating over the TMVB region, the World Stress Map (Heidbach et al., 2016) reports maximum horizontal stress (S_{Hmax}) axes approximately oriented from ca. E-W to NE, consistent with a N-S to NW-trending extension direction (Fig. 1.3). This extension direction seems to characterize also the eastern part of TMVB, including the study area in easternmost TMVB. Finally, this extension direction is also apparently coherent with a minor left-lateral component of displacement along the rift structure associated with the TMVB.

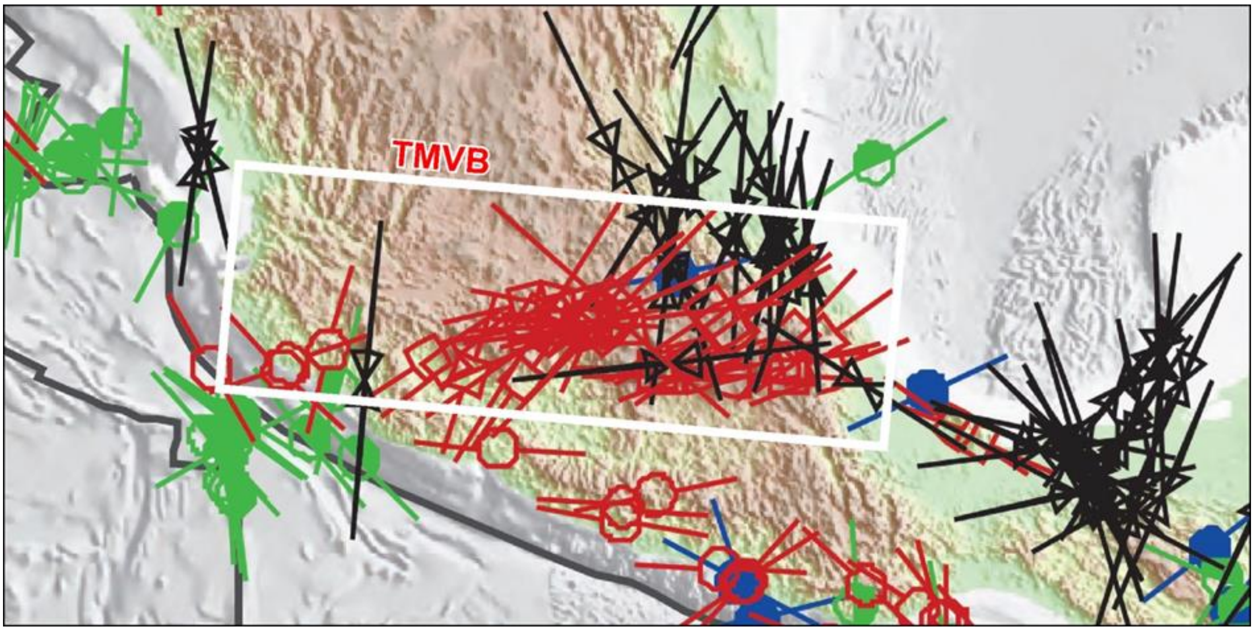

Figure 1.3. Detail of the World Stress Map 2016 for the Trans-Mexican Volcanic Belt (TMVB) (after Heidbach et al., 2016). Colored bars display the orientation of maximum horizontal compressional stress (S_{Hmax}) obtained from different data. The study Los Humeros and Acoculco geothermal fields are located on the easternmost sector of the TMVB (cf. with Fig. 1.1).

1.2 Geological setting of the Los Humeros volcanic complex (LHVC)

The Los Humeros volcanic complex (LHVC) is a prominent calc-alkaline, andesitic to rhyolitic volcanic centre located northwest of Perote town. The Pleistocene Teziutlán andesitic lavas form the main volcanic edifice, which experienced at least two large caldera collapse events (Ferriz and Mahood, 1984). The older caldera collapse produced the 15–20 km-wide Los Humeros Caldera and the emplacement of the 115 km^3

Xaltipan ignimbrite (Fig. 1.4). A second caldera collapse event led to the formation of the rhyodacitic Zaragoza ignimbrite (15 km^3) as well as the nested 8–10 km-wide Los Potreros Caldera (Ferriz and Mahood, 1984; Carrasco-Núñez et al., 2012). The caldera collapse structures and associated Xaltipan and Zaragoza ignimbrite deposits are superimposed onto the older Teziutlán volcanic edifice (see cross section in Carrasco-Núñez et al., 2017a; Fig. 1.4, lower panel).

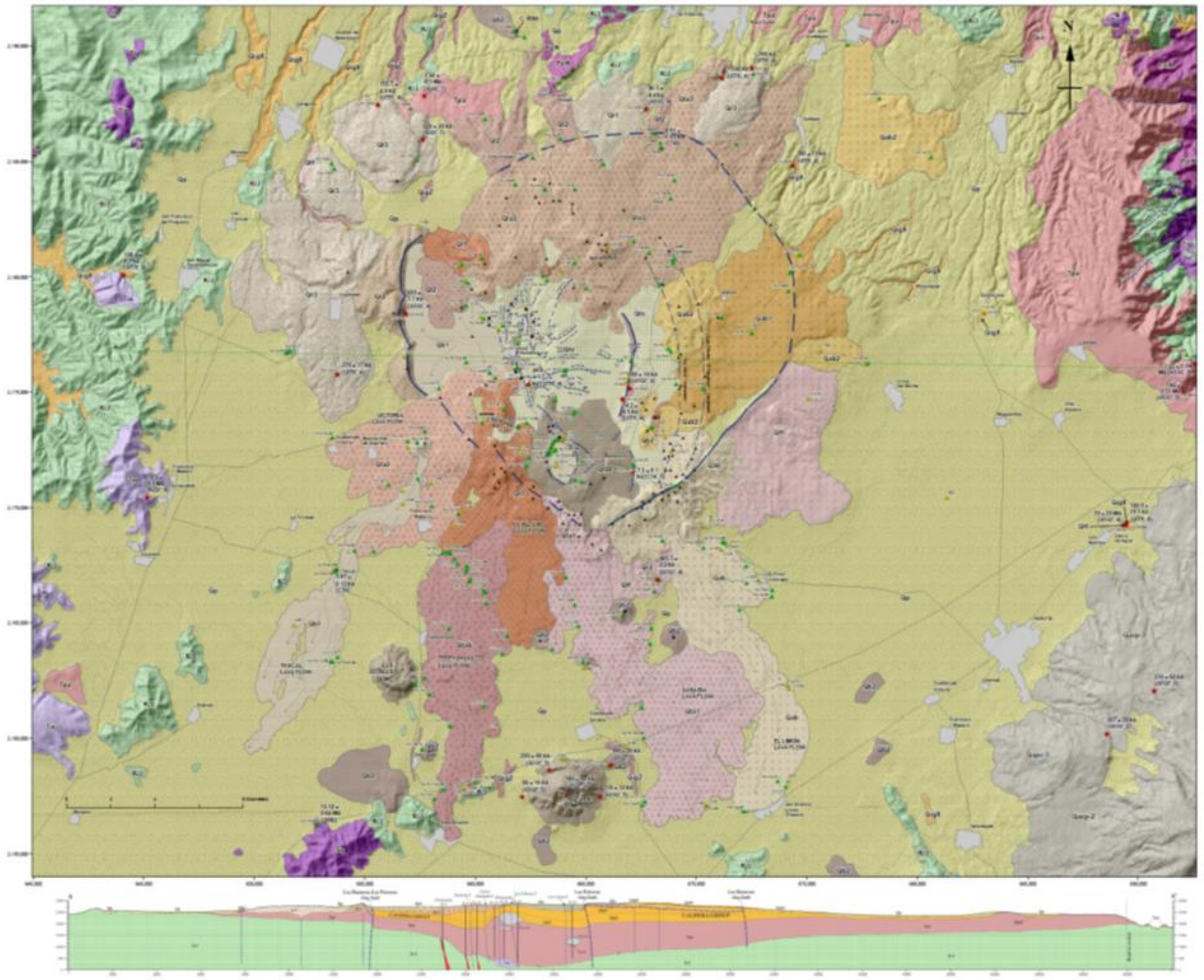

Figure 1.4. Geological map and geological section of the Los Humeros volcanic complex (after Carrasco-Núñez et al., 2017a; for details, the reader is refer to this publication).

Recent radiometric dating yields an age of 1.46 - 2.61 Ma for the Teziutlán andesites, while the Xaltipan and Zaragoza ignimbrites are dated at 164 ka and 69 ka, respectively (Carrasco-Núñez et al., 2018). Interpretative geological cross sections show both caldera structures as being controlled by either inward-dipping (Ferriz and Mahood, 1984; Cedillo-Rodríguez, 1999), or outward-dipping faults (Norini et al., 2015, 2019; Carrasco-Núñez et al., 2017a).

In map-view, the south-eastern margin of the Los Humeros Caldera is bounded by a ca. NE-trending linear scarp referred to as 'Los Humeros scarp', while its south-western rim is apparently controlled by a ca. NW-trending rectilinear structure that is hinted from the clear alignment of several volcanic vents (Carrasco-Núñez et al., 2017a; Fig. 1.4). More specifically, the results carried out in the frame of GEMex activity propose that existing regional structures have been reactivated during the collapse of the Los Humeros Caldera, and have thus controlled caldera rim geometry, particularly along its south-eastern and south-western margins (Fig. 1.5).

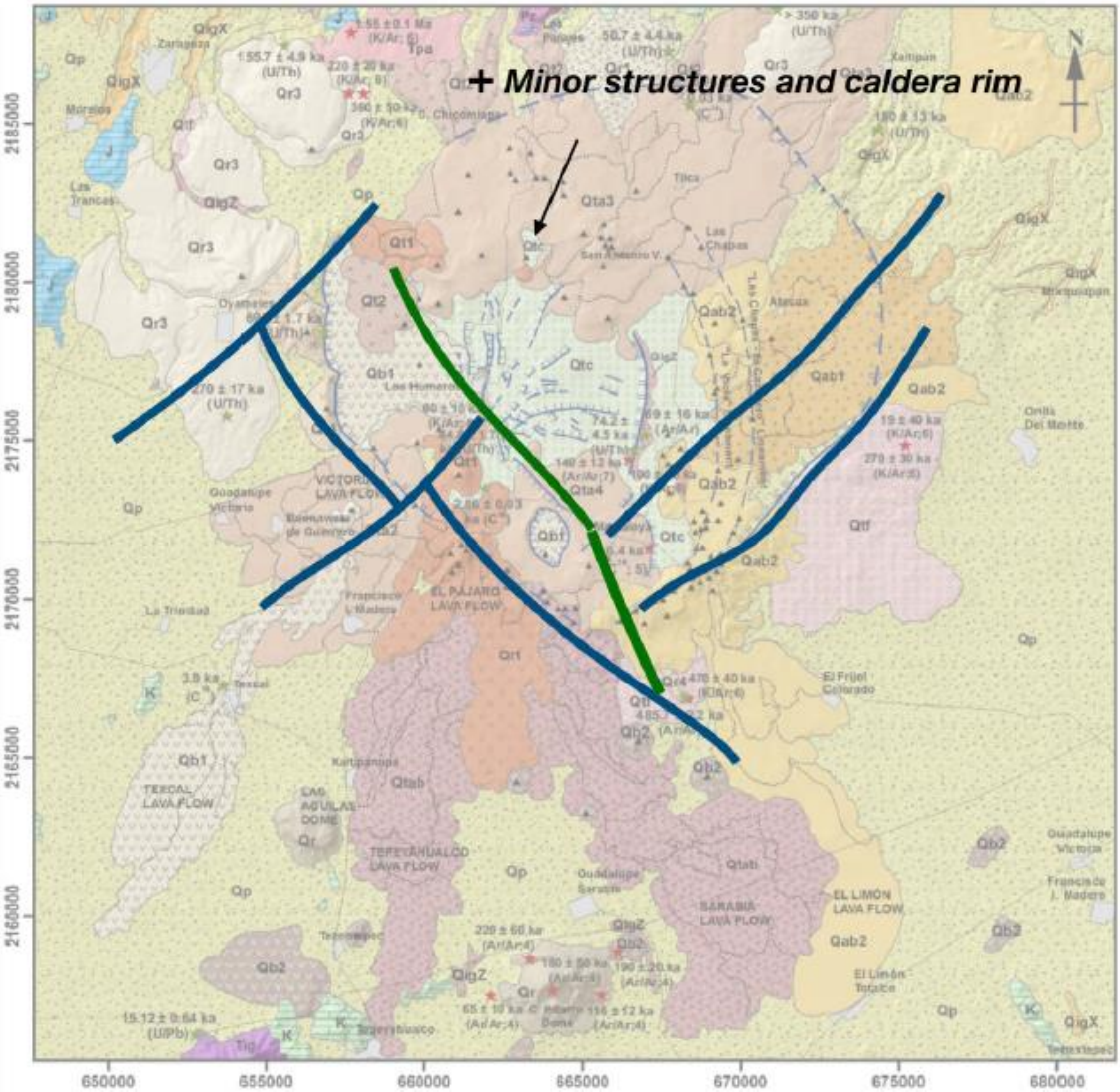

Figure 1.5. Schematic map of existing regional faults (thick blue and green lines) that are hinted to have controlled collapse of the Los Humeros Caldera (after Liotta, 2019).

The Los Potreros Caldera is defined by the ‘Los Potreros scarp’ and the ‘Oyameles scarps’ along its eastern and western margins, respectively (Norini et al., 2015; Fig. 1.4). Such exposed caldera collapse scarps vanish abruptly laterally, or are buried beneath the thick post-caldera products (Fig. 1.4).

A relevant set of faults affects the central part of the Los Potreros Caldera. These intra-caldera faults are characterized by fresh fault scarps denoting recent/ongoing activity. Such a fault system exhibits a complex pattern with fault segments showing two main orientations, particularly (1) faults trending NW to N–S trend, and dipping west (Maztaloya and Humeros faults, as well as some minor faults) and (2) faults striking from E–W to ENE–WSW, dipping north (Las Papas and Las Viboras faults; Fig. 1.6).

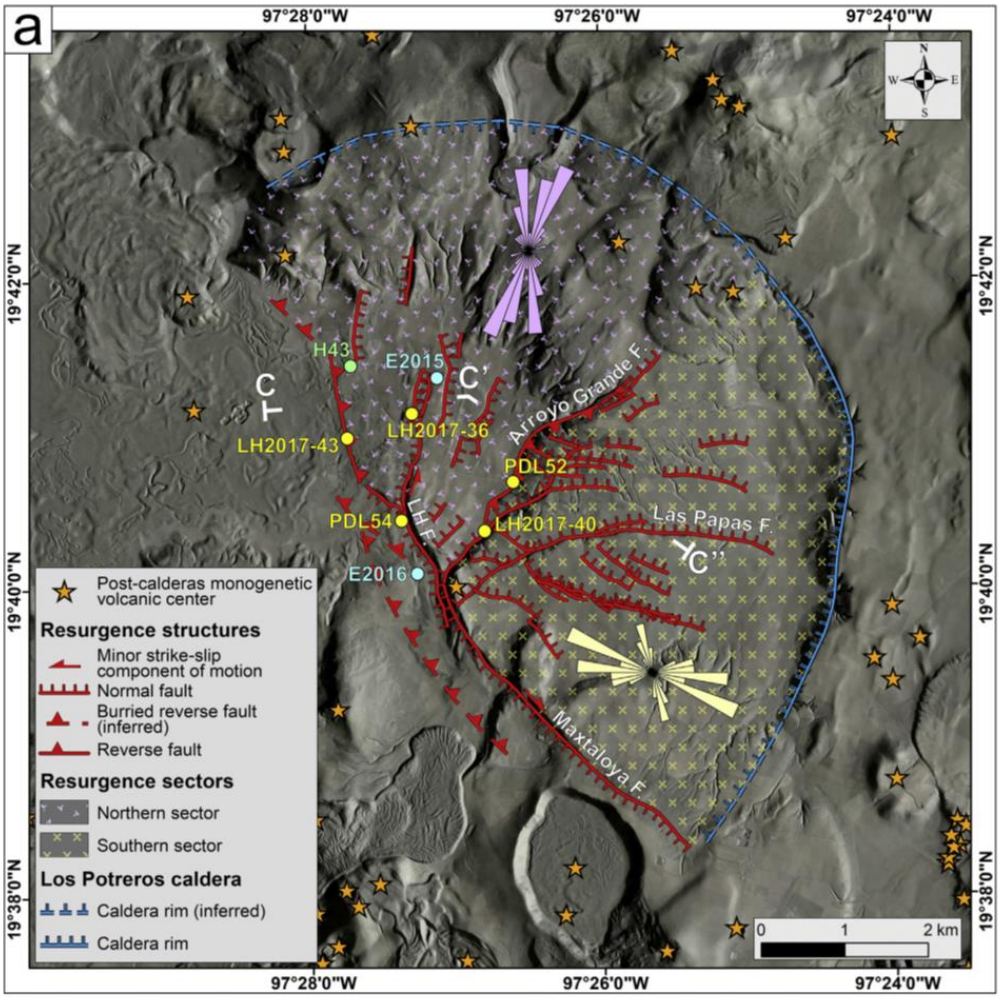

Figure 1.6. Main fault scarps observed within the Los Potreros Caldera together with the interpreted main structural sectors. Northern and southern sectors are interpreted as being related to a resurgent block (after Norini et al., 2019).

It is worth noting that the minor faults within the Los Potreros Caldera branch-off at high angle from the main NW-striking Maztaloya and Humeros faults, defining a sort of ‘horse-tail pattern’ (Fig. 1.6). Importantly, these faults represent the main target of geothermal exploration and production, and are inferred to delimit intra-caldera sectors with similar vertical uplift (Norini et al., 2015). Differential uplift of these blocks has been related to intra-caldera magma resurgence (Norini et al., 2015, 2019; Fig.1.6), which is also suggested by the presence of subsurface rhyolitic domes that have been drilled by geothermal wells (see geological section in Fig. 1.4; Carrasco-Núñez et al., 2017a). Some studies suggest that the magma chamber – that is expectedly sourcing magma resurgence – is currently partly solidified, with present-day temperatures of the order of 600°-650°C (5 to 7–8 km depth; e.g., Verma, 1983, 2000).

1.3 Geological setting of the Acoculco caldera complex

Volcanic activity in the Acoculco caldera complex is characterized by calc-alkaline composition and range in age from Pliocene to Pleistocene (López-Hernández et al., 2009; Avellán et al., 2018; Sosa-Ceballos et al., 2018). Several episodes of volcanism have affected the Acoculco area, producing rhyolitic domes, fissure lava flows, cinder cones, and two large ignimbrite eruptions related to caldera collapse (López-Hernández et al., 2009; Avellán et al., 2018; García-Palomo et al., 2018). The older caldera structure is the 32 km-wide Tulancingo Caldera (3.0–2.7Ma), and the 18 km-wide Acoculco Caldera (1.7 and 0.24Ma) (López-Hernández et al., 2009). The youngest volcanic episode is related to extra-caldera volcanism lasting until 63 ka (Avellán et al., 2018). However, Avellán et al (2018) do not find evidence for the existence of the Tulancingo caldera.

Magmatic activity in the Acoculco caldera complex is structurally controlled by both NE- and NW-trending existing faults in the basement (López-Hernández et al., 2009; Avellán et al., 2018). These faults have been likely reactivated during caldera collapse. In particular, the north-western Acoculco caldera rim follows a NE-SE-trending fault (e.g., Avellán et al., 2018), and the trace of the south-western Acoculco caldera rim is controlled by a NW-SE-oriented fault (Fig. 1.7). Interestingly, also geothermal fluids moved preferentially along NW-SE-oriented faults, as suggested by geothermal alteration that dominantly develops along this fault trend (see Deliverable 4.1 of GEMex Project).

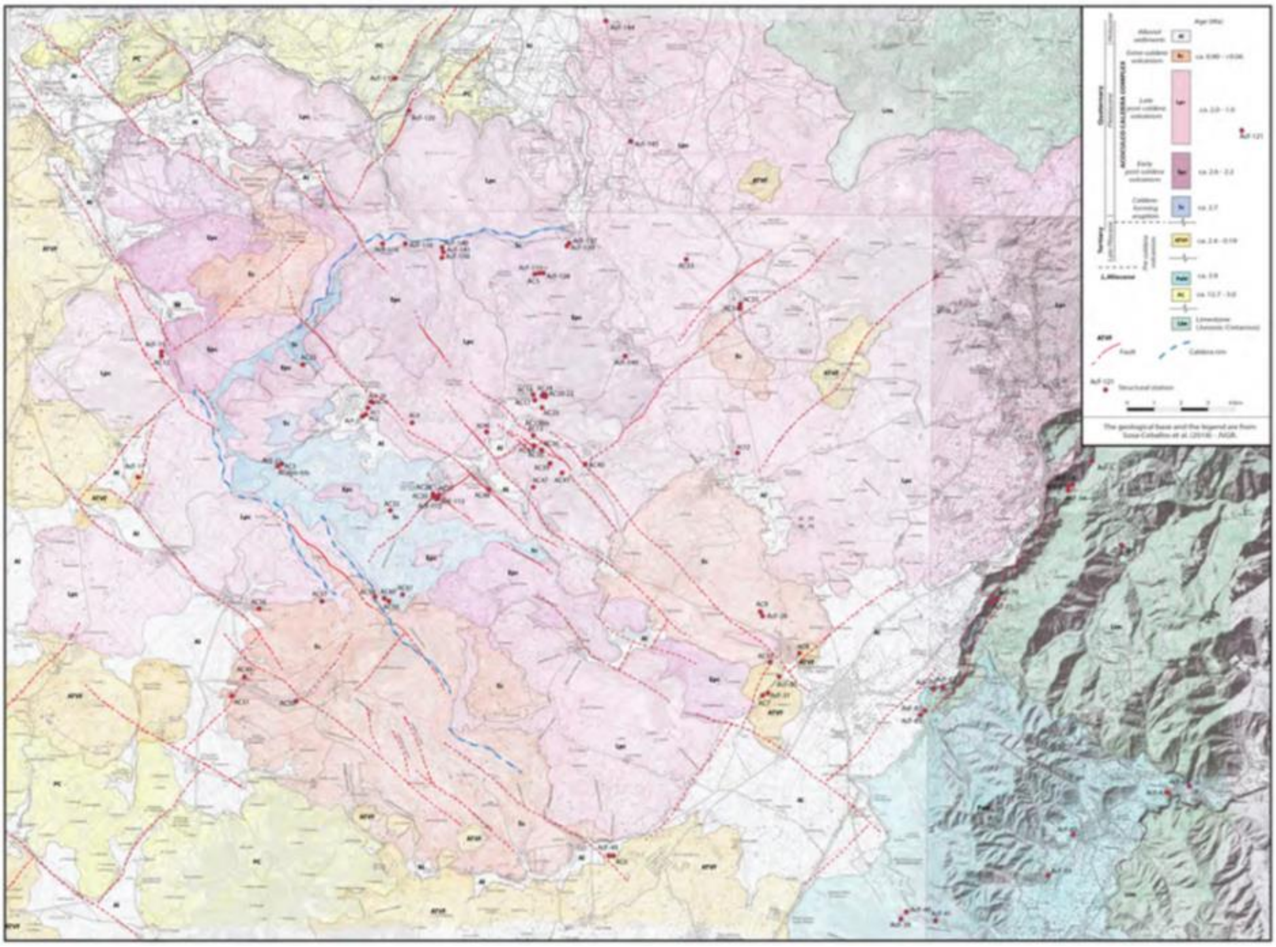

Figure 1.7. Geological map of the Acoculco caldera complex (modified from Sosa-Cabellos et al. 2018, with additional faults surveyed during the GEMex Project) (from Deliverable 4.1 of GEMex Project).

2 Analogue modelling of volcano-tectonic processes

2.1 Short introduction on analogue modelling

Analogue modelling is an experimental procedure that allows to reproduce natural processes at a smaller scale. This means that a model is not only smaller in dimension (property which, of course, is of great advantage for modellers), but also that the complete development of the simulated natural process occurs in a reduced amount of time. This aspect provides the researcher the possibility to control - and monitor step by step - the evolution of a certain geological process, allowing for an in-depth analysis and comprehension of the mechanism that control it in nature. Except for near-instantaneous events, generally the time involved in geological scale processes is largely out of the human monitoring possibilities, therefore analogue modelling is an extremely useful tool. This approach is nowadays well known and largely used in many branches of geology, and benefits from the input deriving from a large variety of datasets (e.g. seismic data, geophysical, structural geology, stratigraphy etc…). Geological information can be simplified in order to be used as "hard data" for model setup, or for comparison, once the models have been obtained. Of course, in order to furnish reliable and well-sounded results, analogue models need to be quantitatively comparable with the case studies, implying the achievement of correct *scaling* (Hubbert, 1937; Ramberg, 1981) of dimensions, physical properties of material, forces, as well as deformation time.

2.2 Short review of analogue modelling of caldera collapse and resurgence

In this paragraph, we report a brief summary of the large amount of work that has been done during the last decades about caldera collapse and resurgence, in order to provide the reader with a general background to understand our modelling. For an in-depth description of caldera collapse modelling we suggest the reader to refer to the recent reviews by Geyer and Martí (2014) and Acocella (2007; Fig. 2.1). The majority of analogue models involving caldera collapse processes can be generally classified into those applying overpressure and underpressure mechanisms, respectively. The first mechanism implies the increase of pressure inside the magmatic chamber, inducing doming at surface and consequent stretching due to tensile stress that is likely responsible for caldera collapse initiation (e.g., Gudmundsson, 1988; Gudmundsson et al., 1997, Burov and Guillou-Frottier, 1999; Guillou-Frottier et al., 2000; Gudmundsson, 2015; 2016). The second mechanism indicates the drop of pressure inside the magmatic chamber due to magma eruption as the driving mechanism for caldera collapse initiation (e.g., Williams, 1941; Druitt and Sparks, 1984; Lipman, 1997). In both models, the complex behavior of the system has been simplified to approximate a purely mechanical deformation. On the other hand, the large amount of experimental work done on this issue demonstrates the reliability of this kind of modeling.

In this frame, various modelling approach have been applied since the ’80. A first attempt was that by Komuro et al. (1984), who modelled caldera collapse applying the overpressure mechanism by pushing a rigid sphere inside granular material, obtaining radial cracking of the resulting dome due to surface tensile stress (Fig. 2.2).

Category of experiment	Analogue modelling study	Materials + apparatus	Main results
Overpressure	Komuro et al. (1984)	Rigid sphere rising in powder	Radial + concentric fractures with depression on crest of dome
	Marti et al. (1994)	Balloon inflated in powder	Outward dipping reverse faults and crestal normal faults
	Walter and Troll (2001)	Balloon inflation in flour	Subsidence of crest of dome with normal faults
	Acocella et al. (2001a)	Silicone intruding in sand	Doming, crestal thinning and depression
	Troll et al. (2002)	Balloon inflation in flour	Formation of piecemeal collapses
	Acocella and Mulugeta (2002)	Silicone rising below sand (centrifuge)	Doming, crestal depression bordered by inward dipping normal faults
Underpressure	Komuro (1987)	Dry ice evaporating in powder	Outward dipping reverse faults
	Marti et al. (1994)	Balloon in powder	Outward dipping reverse faults + subvertical faults
	Roche et al. (2000)	Silicone sinking in sand	Outward dipping reverse faults + inward dipping normal faults Role of root aspect ratio Independence from the reservoir shape
	Acocella et al. (2000)	Silicone sinking in sand	Outward dipping reverse faults + inward dipping normal faults Room problem
	Acocella et al. (2001b)	Silicone sinking in sand	Constant architecture of nested calderas
	Walter and Troll (2001)	Balloon deflating in flour	Outward dipping reverse faults + inward dipping normal faults
	Troll et al. (2002)	Balloon deflating in flour	Piecemeal calderas through inflation-deflation cycles
	Kennedy et al. (2004)	Balloon deflating in sand	Reverse faults + normal faults controlled by the shape of chamber roof
	Lavallèe et al. (2004)	Baloon deflating in sand (topography–cones)	Topography may locally vary the shape of calderas
	Geyer et al. (2006)	Balloon in sand	Roof aspect ratio and magma chamber withdrawal
Regional stress	Cailleau et al. (2003)	Balloon deflating in flour (regional stress)	Caldera elongated accordingly with the regional stress
	Acocella et al. (2004)	Silicone sinking in sand (regional pre-existing faults)	Caldera elongation may depend on regional fault reactivation
	Holohan et al. (2005)	Balloon deflating in sand (regional stress)	Elongation of calderas parallel to minimum compression

Figure 2.1. Table from Acocella (2007) summarizing materials, methods and main findings of several works investigating caldera collapse processes.

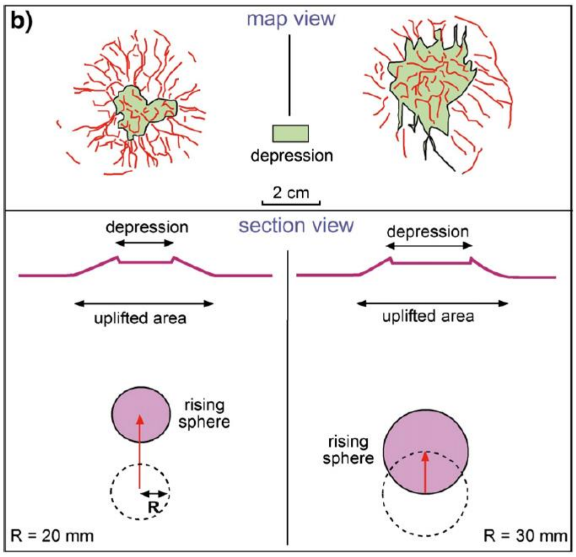

Figure 2.2. Analogue modelling of caldera collapse processes using a moving rigid sphere placed inside a brittle overburden (from Acocella, 2007, redrawn form Komuro et al., 1984).

Many authors followed the same overpressure approach by intruding a viscous material (e.g., silicone) in a brittle layering (Acocella et al., 2001a; Acocella and Mulugeta, 2002) or by inflating a balloon placed at the base of granular material (Martì et al.1994; Walter and Troll, 2001; Troll et al., 2002; Fig. 2.3)

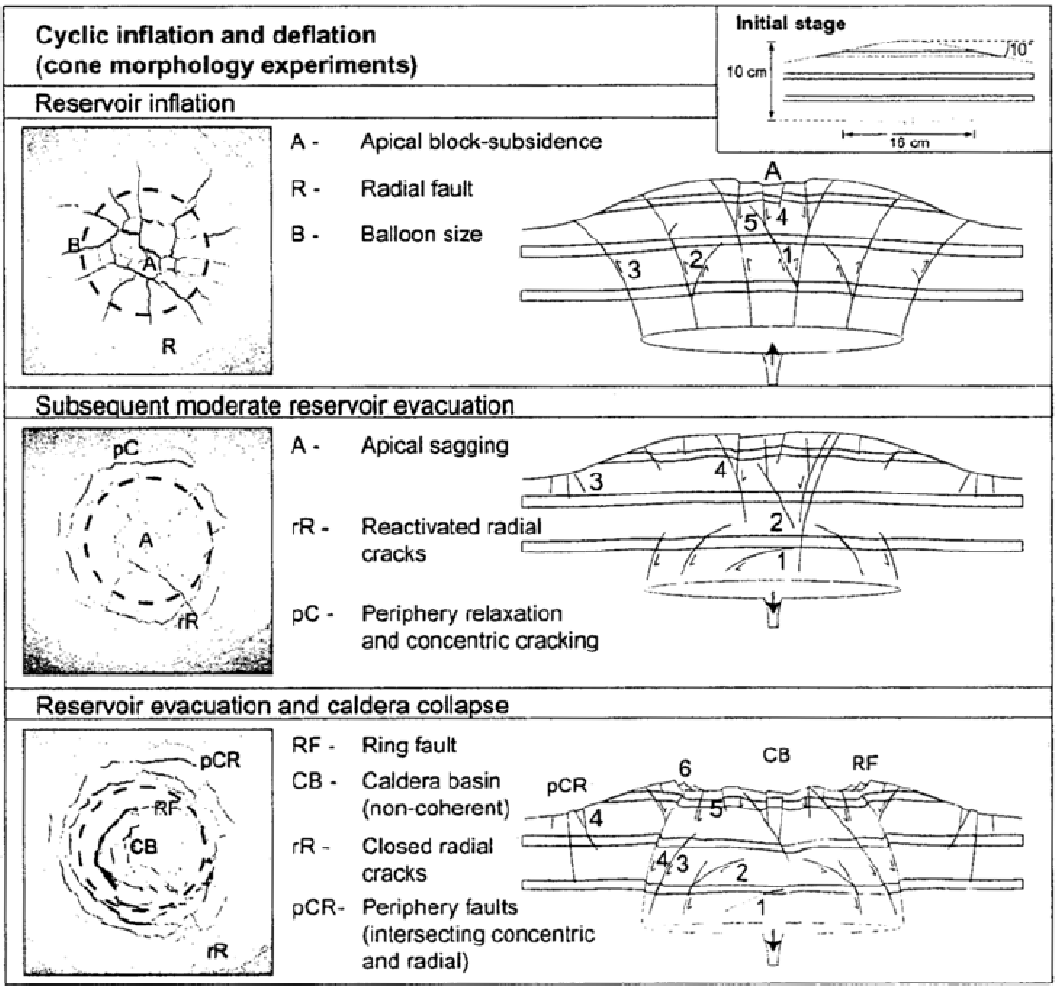

Figure 2.3. Analogue modelling of caldera collapse simulated by an inflating/deflating balloon placed inside a brittle overburden (from Walter and Troll, 2001).

Underpressure mechanisms made large use of various silicone putties sinking into sand layers, or balloon deflating into brittle materials (e.g. sand, flour). This approach is so far the most applied to reproduce caldera collapse processes (Komuro, 1987; Martì et al., 1994; Roche et al., 2000, Fig.2.4; Acocella et al., 2000; 2001b; Walter and Troll, 2001; Troll et al., 2002; Kennedy et al., 2004; Lavallèe et al., 2004; Geyer et al., 2006), as it offers easiness of the modelling procedure and reproducibility of results. Analogue models using the underpressure mechanism have been also used to investigate the role of regional stress and inherited structures on caldera collapse evolution (e.g., Cailleau et al., 2003; Acocella et al., 2004; Holohan et al., 2005, 2008, 2013).

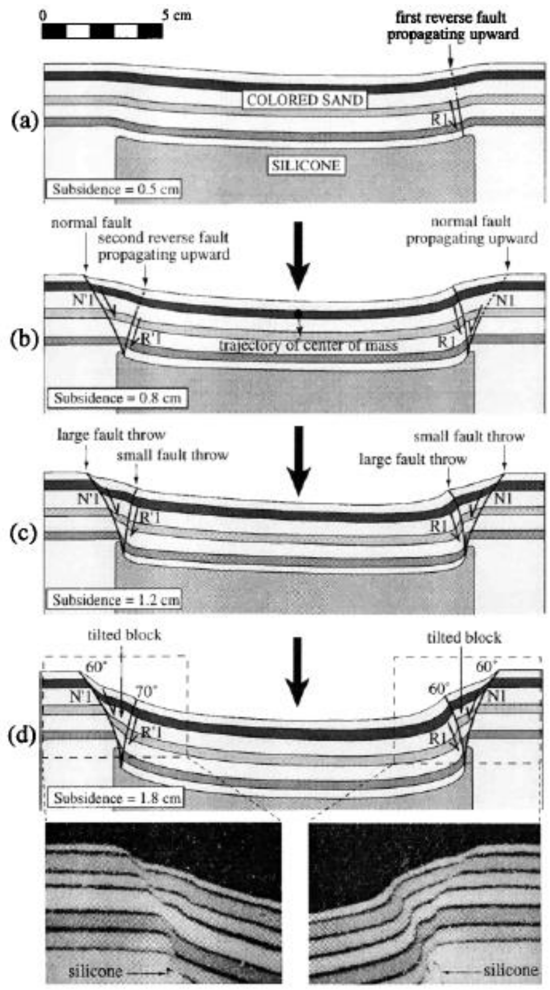

Figure 2.4. Caldera collapse obtained applying the underpressure mechanism. Silicon putty placed below a brittle overburden is forced to sink generating caldera collapse (from Roche et al., 2000).

Among specific results, all these analogue models pointed to general agreement about the first-order characteristics of the process. Acocella (2007) proposed a model for caldera collapse implying the formation of early outward-dipping reverse faults followed by the development of inward-dipping normal faults (Fig. 2.5).

In detail, once the magma chamber experienced underpressure (likely due to magma eruption or depletion induced by magma migration) a first stage (Fig. 2.5a) involving down-sagging at surface, implies inward tilting of the incipient caldera boundaries, followed by a second stage (Fig. 2.5b) of outward-dipping reverse fault development. In a third stage (Fig. 2.5c) the down-sagging migrates in the peripheral area around the collapsing caldera, to afterward develop (fourth stage; Fig. 2.5d) inward-dipping normal faults. This model of evolution is largely accepted and constitutes a starting point for our modelling and investigation.

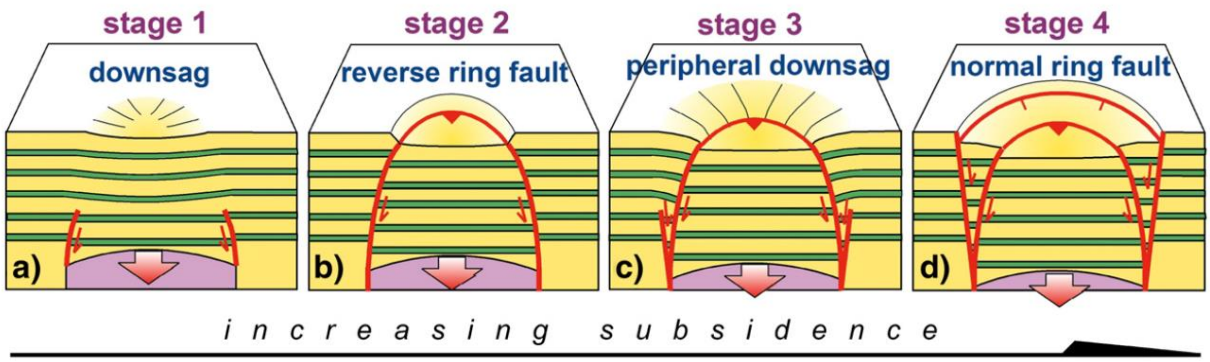

Figure 2.5. Evolutionary model for caldera collapse development, as proposed by Acocella (2007). Stages 1 to 4 describe the formation of incipient caldera to mature collapse through the formation of early outward-dipping reverse faults and subsequent inward-dipping normal faults.

2.3 Modelling strategy

2.3.1 Series D3.6-1: Symmetric/asymmetric caldera collapse

Series D3.6-1 was designed to investigate caldera collapse processes from a general point of view, in order to better understand the possible evolution of the Los Humeros and Acoculco volcanic systems. The basic setup of this series was designed similar to the setup of models described in Series D3.5-2a, which is presented in Deliverable D3.5 and some of those models can be considered part of Series D3.6-1 (e.g., Model 17). Models of series D3.6-1investigated the processes involving symmetric caldera collapse and their setup was afterward varied to reproduce and compare asymmetric models with the natural prototypes. Specifically, asymmetric collapse was induced by tilting slightly the top of the analogue magma chamber, generating in this way a differential vertical stress over its surface due to non-uniform overburden thickness above the analogue magma. Furthermore, the effect of different overburden thickness was tested both on symmetric and asymmetric setup.

2.3.2 Series D3.6-2: Role of pre-caldera volcano-related topography

Series D3.6-2 was designed to test the role of a pre-caldera volcano related topography on caldera collapse processes. In order to test this aspect, we have reproduced in our model a conical volcano edifice, placed at various positions with respect to the analogue caldera to parametrically test its influence. The volcano edifice was reproduced pouring a constant amount of Qz-Kfeld sand mixture (see Section2.4.1) into a circular frame (Fig. 2.6a) located on the model surface, which was afterward removed (Fig. 2.6b) to let the sand mixture flow and create a symmetric cone (Fig. 2.6c). By using a standard frame of 7.5 cm in diameter and

205 g of sand mixture, we obtained a symmetric cone with diameter (at the base) of ~13-14 cm and a height of ~2 cm, that correctly scale the possible dimensions of a real volcano (13-14 km in diameter and 2 km in height).

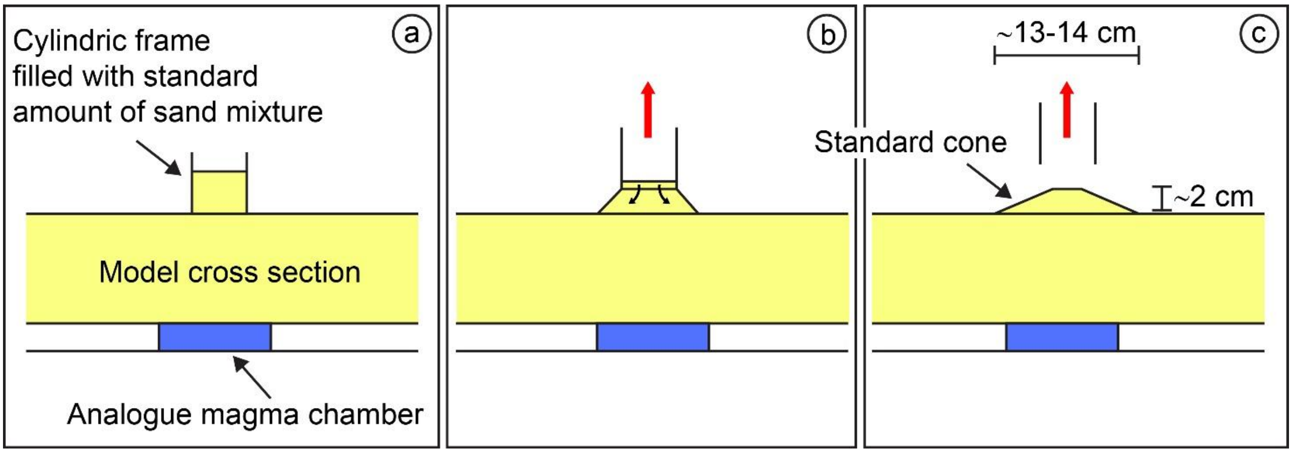

Figure 2.6. Modelling strategy and procedure adopted to build up standard cones simulating a volcano topography on top of an analogue magma chamber of experimental Series D3.6-2. The topography was a symmetric cone with ~13-14 diameter (at the base) and a height of ~2 cm.

During the building procedure of Series D3.6-2 models, we also introduced artificial discontinuities simulating inherited fabrics, to test the coupled effect of existing tectonic structures and the presence of a volcano-related topography. The discontinuities were introduced both in the substrate and overburden according to the procedure described in Section 2.4.1

2.3.3 Series D3.6-3: Caldera resurgence and interaction with pre-existing structures (both regional inherited fabrics and caldera collapse faults)

Experimental series D3.6-3 aimed at investigating the resurgence processes occurring in collapsed calderas. To this aim, we have applied resurgence to experimental setups employed in the other experimental series that are shown both in this report (i.e., Series D3.6-1, D3.6-2 and D3.6-3) and in Deliverable D3.5 (i.e., experimental Series D3.5-2 and subseries). Resurgence was obtained by reinjecting an analogue magma inside the model by means of a tube introduced from the bottom of the model, once the collapsing phase of the model was terminated. Specific aim of this series was to test how broad (i.e., piston-like) or localized caldera resurgence may interact with the caldera faults and/or with inherited faults whose presence has been suggested by the results of WP4 of GEMex Project. Since no clear evidence for a broad or localized resurgence were available for the Los Humeros and Acoculco caldera systems, we have investigated both possibilities, in order to evaluate which of the two may apply better to the natural study case.

Furthermore, in this series we have also tested the interaction of resurgence and asymmetric (trapdoor) collapsed caldera systems, together with the coupled effect of tectonics, which is represented by the presence of inherited (and possibly reactivated) faults. The letter structures were introduced in specific models following the approach described in Section 2.4.1.

2.3.4 Series D3.6-4: combined effects of compressional and extensional tectonics structures and magmatic processes on the Los Humeros Volcanic Complex (LHVC)

The experimental strategy considers and analyses in conjunction the most important geological factors contributing to the structure of the LHVC and geothermal field, as identified by Norini et al. (2019). The aim is to analyse the combined effects of tectonic and magmatic processes on the LHVC prototype volcano and test the hypotheses on the origin and geometry of the secondary permeability within the geothermal reservoir. The modelled geological factors are as follows:

a) Inherited tectonic deformation of the basement. The structural analysis of the LHVC and surrounding basement (Norini et al., 2019) suggests that two different orders of inherited regional tectonic structures played a role in the evolution of the magma feeding system, caldera collapses and post-caldera deformations of LHVC. These regional systems are the Mexican Fold and Thrust Belt (MFTB) compressive structures and the Trans-Mexican Volcanic Belt (TMVB) normal faults and extensional fractures (Fig. 2.7). Both tectonic systems were generated under a regional NE-SW trending σ_{hmax} and postdate the LHVC activity;

b) Deformation induced by caldera collapse. After emplacement of the LHVC magma chamber, the collapse of the Los Humeros and Los Potreros calderas occurred along caldera ring faults with semi-circular asymmetric plan view shapes and some rectilinear strands (Fig. 2.7) (Norini et al., 2015, 2019; Carrasco-Núñez et al., 2017);

c) Post-caldera phase magma intrusion and deformation. In the post-caldera phase, several monogenetic volcanic centres have been emplaced within the caldera complex (Fig. 2.7). Also, resurgence of the Los Potreros caldera floor induced local deformations in the crust (Norini et al., 2015, 2019). Faults with different geometry and kinematic displace volcanic deposits in the centre of the caldera, showing a marked decrease in fault scarps height and displacements toward the caldera rims (Fig. 1.6). These faults delimit distinct resurgence sectors uplifted and tilted by resurgence and doming of the topographic surface. Both post-caldera monogenetic volcanoes and volcanotectonic deformation may be associated with the emplacement of magmatic intrusions below the Los Potreros caldera and a local radial stress field overwhelming the regional stress field (Norini et al., 2015, 2019).

The analogue modelling has been designed to reproduce the above mentioned geological processes and investigate the possible interplay between the inherited tectonic structures in the basement and the evolution of the caldera complex, considering that:

- The south-eastern sector of the Los Humeros caldera morphological rim is rectilinear and roughly parallel to the NE-SW-striking TMVB normal faults and regional σ_{hmax} (Fig. 2.7). Also, the south-western sector of the same caldera rim is roughly parallel to the NW-SE-striking MFTB compressive structures (Fig. 2.7). This geometry indicates that caldera ring faults may have partly reactivated inherited tectonic structures in the basement as weak planes for the collapse of the magma chamber roof;
- The NNW-SSE Maxtaloya-Los Humeros fault swarm delimiting the resurgence area is parallel to the MFTB inherited structures, while the NE-SW Arroyo Grande fault and parallel fault strands have the same strike of the TMVB normal faults and regional σ_{hmax} (Fig. 1.6). This geometric link suggests the possibility that the main volcanotectonic features in the Los Potreros caldera floor have been formed by reactivation of inherited weak planes generated by regional tectonics in the LHVC basement;
- The permeability in the reservoir is mainly secondary and related to the damage zone of resurgence faults delimiting uplifted and tilted sectors of the caldera floor (Norini et al., 2019).

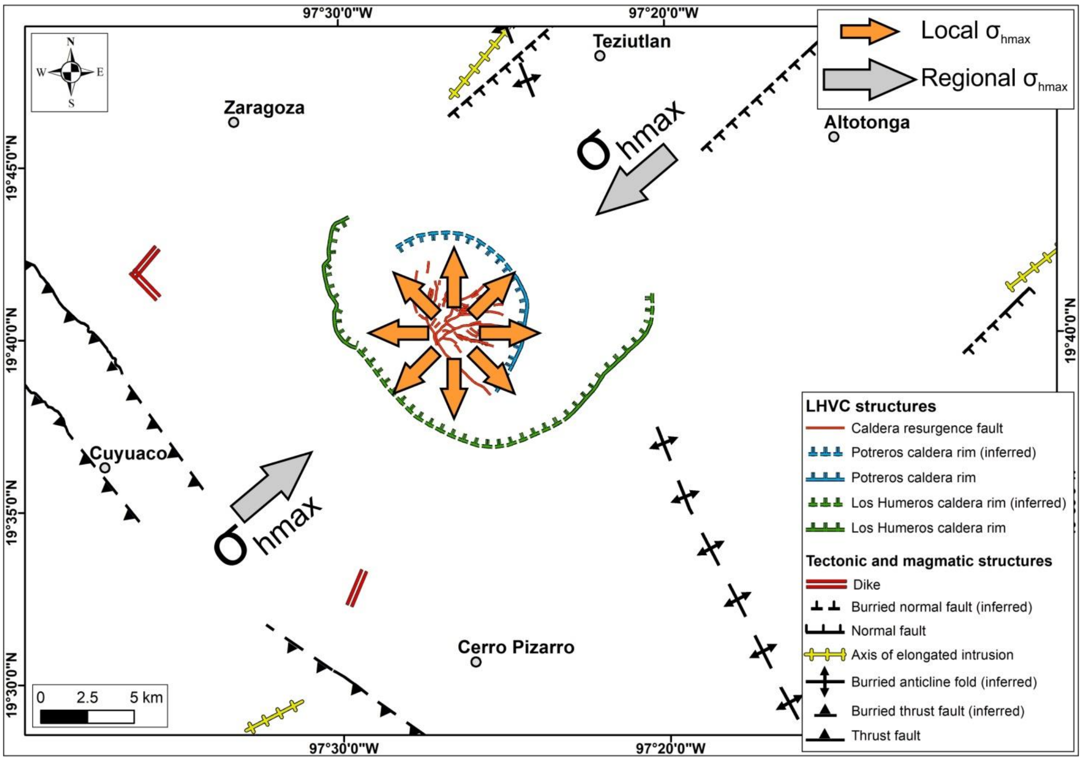

Figure 2.7 simplified structural map of the LHVC area with the main tectonic and volcanotectonic structures and the regional and local stress fields used as a base to set-up the analogue modelling (Norini et al., 2019).

2.3.5 Series D3.6-5: Shallow intra-caldera intrusions

Based on the findings of Lucci et al. (2019, in review), we perform an experimental series of analogue models addressing the potential role of shallow intrusions (< 3km) at Los Humeros as a source of deformation in the caldera floor. Nine experiments were undertaken simulating the ascent of a viscous intrusion in a brittle overburden to test existing relationships between the depth of intrusion and the observed surface deformation.

2.4 Analogue modelling procedure of Series D3.6-1, D3.6-2 and D3.6-3

2.4.1 Material, setup and scaling

Caldera collapse has been modelled by different authors using various approaches, such as rigid “piston-driven” collapse (e.g., Acocella et al., 2000; Roche et al., 2000), with clear advantages for model development and reproducibility. Nonetheless, other approaches - e.g. “balloon-collapse”, where an inflated balloon is deflated inside a sand pack, or depletion of a magma-analogue reservoir - have been also employed (see Acocella, 2007, and reference therein). In our experiments, we followed the latter approach, building a circular magma-analogue chamber below a sand-pack mimicking the brittle overburden. In detail, a circular magma chamber (build with wet chalk poured in a standard silicon mould; 12 cm in diameter and 2 cm thick) was placed at the base of a 6 cm-thick sand pack. Coloured millimetre-sand horizons were sieved with a regular vertical spacing of 1 cm during the building of the model, and used as passive markers to visualise internal deformation once the models were cut. Each model was built in a Plexiglas box and the analogue magma chamber was drained from a central circular hole placed at its base. The amount of drained analogue magma was constantly monitored in order to extract only the desired volume. The magma analogue was simulated with pure vegetable Polyglycerine-3 and Polyglycerine-10 (PG3 and PG10, see Montanari et al., 2017b), while the sedimentary cover consisted of a blend of Quartz sand (Fontainebleau sand, provided by Sibelco Italia S.p.A.) and Potassic-feldspar sand (K-feldspar superfine sand, produced by AKW Kaolin) mixed with a 70:30 proportion in weight (Montanari et al., 2017a). To reproduce caldera collapse, we used frozen PG3 to avoid the introduction of differential vertical stress acting over the analogue magma surface during pouring of the sand mixture. Once the model was built, we waited at least 2 hours before starting the deformation, in order to allow PG3 defrosting. This operation was conducted at controlled ambient temperature (25°C) to guarantee a uniform PG3 rheology for all the performed models. Undesired differential surface deformation during the defrosting procedure was also prevented by verifying horizontality of the model with a spirit level, and afterwards tested acquiring DEMs of model surface at the end of the defrosting procedure. The obtained high resolution DEMs have indeed the ability to catch incipient deformation, invisible to the naked eye. Thanks to this test, we can exclude undesired differential surface deformation before caldera collapse onset. For comparison, during caldera collapse, the 65% of the initial magma-analogue (PG3) was drained out in all experiments to guarantee the same conditions. As described in Deliverable D3.5, we used a basic experimental setup represented by a circular magma chamber and an undeformed overburden, to simply reproduce caldera collapse. Depending on the model, we have varied the shape of the analogue magma chamber by artificially imposing one or two straight sides, simulating pre-existing fault discontinuities. Afterwards, depending on the model, the sand package was pre-deformed by introducing various artificial discontinuities in different positions to simulate inherited fabrics within the analogue brittle crust. Discontinuities in the overburden were obtained by cutting through the sand with a "discontinuity apparatus" (DA), which allows to cut perfectly straight into the sand pack through a knife fixed onto an adjustable glide allowing to vary the cut depth. This operation re-orients particles, generating a sharp and narrow millimetre-scale discontinuity zone that can easily focus the deformation during model development, if favourably oriented with respect to the local stress field. At the end of deformation, target models were soaked in water and frozen for 12 hours, in order to properly consolidate and allow the sectioning of models. This procedure allows to visualise in detail the internal deformation of the caldera fault pattern. Reproducibility of results has been checked by replicating the models several times.

Furthermore, specific series of models were designed to investigate caldera resurgence (i.e., Series D3.6-3) that was obtained by reinjecting analogue magma inside the collapsed caldera. The intrusion rates of analogue magma varied from 20 to 80 cm/h depending on the model. Detailed aspects of the adopted experimental setup for this series are reported in Section 2.4.4, where the experimental series is described.

All the models were scaled down to nature (Ramberg, 1981) following the assumptions and procedure reported in Montanari et al. (2017a). We set a length scaling ratio l* (l* being the ratio l_m/l_n, where l_m is the length in the model and l_n is the length in nature) of 10^{-5}, so that one centimetre in the model scales to 1 kilometre in nature. This scaling value is a proper ratio to investigate model structure at the resolution of interest. Models were run in a natural gravity field, so that g* - this parameter being the scaling ratio between g_m (gravitational acceleration in the model) and g_n (gravitational acceleration in nature) - is equal to 1. The use of Qz/K-feld sand mixture with 70:30 proportion in weight led to a material density (ρ_m) of ~1550 kg m^{-3}, implying a scaling ratio for density ρ^* of ~0.57, considering a natural rock density (ρ_n) of ~2700 kg m^{-3}, while the coefficient of internal friction (μ) requires to be equal for both the analogue material and the natural rock, ($\mu^* \sim 1$) (Table 2-1). A similar density ratio can be considered for a natural magma and the PG3 analogue magma, since PG3 density is $\rho_m \sim 1190$ kg m^{-3}, and ρ_n ~2500-2200 kg m^{-3}, which is the density of an andesitic to rhyolitic magma at ~1000 C° (e.g., Murase & McBirney, 1973) (Table 2-1). The presence of a basaltic/andesitic magma characterises, in fact, the Los Humeros/Los Potreros volcanic complex (Carrasco-Núñez et al., 2017b). However, it is worth noting that these models are not dynamically scaled to natural conditions, since inertial forces are significant in caldera collapse processes and cannot be ignored (see Ramberg, 1981). Regardless, these models can still give valuable hints regarding the kind of structures accommodating caldera collapse as well as the chronology of deformation, as proven by the several analogue modelling studies carried out on this topic (see above Section 2.2).

	Parameter	Model	Nature	Model/Nature ratio
Qz-Kfeld sand mixture (70:30 % in weight) (simulates the Upper Crust - UC)	Density "ρ" (kg m^{-3})	1550	~2700	ρ *=~0.57
	Internal friction coefficient	0.83-1.1	0.85-1	μ*~ 1
	Cohesion "c" (Pa)	10	~$1x10^{7}$	$c^*=10^{-6}$
	Thickness "h" (m)	0.01	1000	$h^*=10^{-5}$
PG3	Density "ρ" (kg m^{-3})	1190	2500-2200	0.48-0.54
	Viscosity "η" (Pa s)	17	$\sim 4 \times 10^{12}$ - $\sim 4 \times 10^{15}$	$4.25x10^{-12}$~4×10^{-15}
PG10	Density "ρ" (kg m^{-3})	1200	2500-2200	0.48-0.54
		450	$\sim 4 \times 10^{12}$ - $\sim 4 \times 10^{15}$	$1.25x10^{-10}$~1.25×10^{-13}
Length "l" (m)		0.01	1000	$l^*=10^{-5}$
Gravity "g" (m s-2)		9.81	9.81	g*=1
Stress "σ" (Pa)				$\sigma^*=5.7x10^{-6}$

Table 2-1. Scaling ratios for the analogue models of Series D3.5-2. The asterisk (*) denotes the ratio between the model and nature for a given parameter. Characteristics of the granular material represented by the Qz-Kfeld sand mixture (70:30 proportion % in weight are from Montanari et al., 2017a). The range for the internal friction coefficients is calculated considering the "peak friction" and "stable friction" values of the granular mixture. Characteristic for Poly-glycerine PG3 from Montanari et al. (2017b)

Caldera collapse may be strictly related to tectonic structures, as likely is the case of the Los Humeros and Acoculco volcanic systems. The studies carried out in the frame of Work Package 4 (WP4) of GEMex Project have highlighted the presence (and the possible influence) of inherited as well as intra-caldera faults both at Los Humeros and Acoculco systems. Furthermore, several studies during time have highlighted this aspect, suggesting the possible presence of inherited faults outside and possibly inside the caldera (Campos-Enriquez & Garduño-Monroy, 1987; López-Hernández al., 2009; Carrasco-Núñez et al., 2017b; García-Palomo et al., 2018; Avellán et al., 2018) that might have influenced the evolution of both Los Humeros and Acoculco volcanic systems (Fig. 2.8).

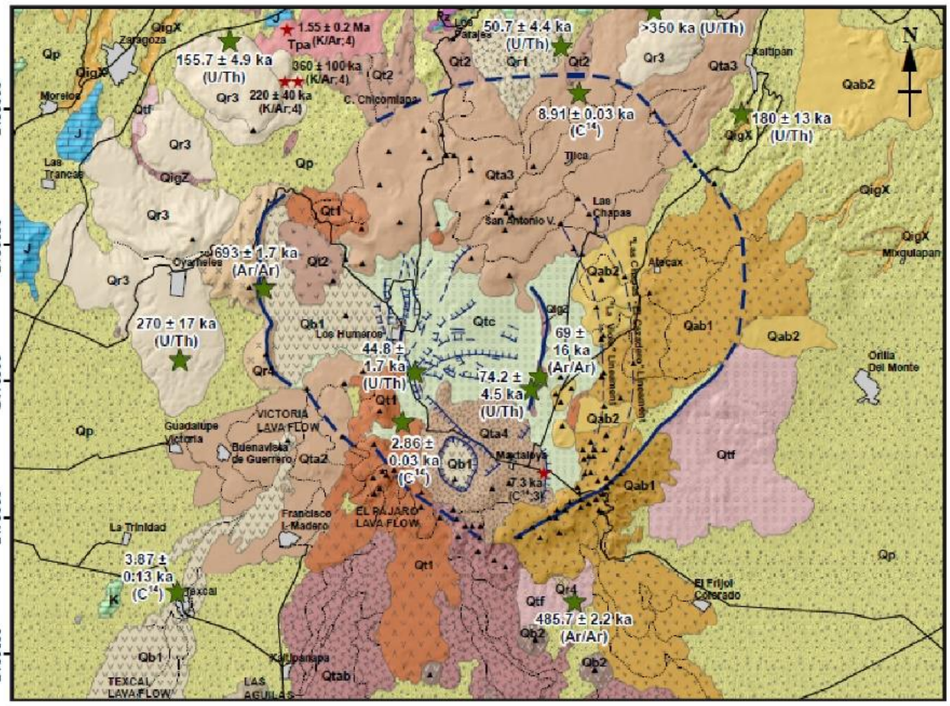

Figure 2.8. Geological map of Los Humeros showing caldera rectilinear ring fault at the south-western and south-eastern margins (from Carrasco-Núñez et al., 2017b).

Task 3.3 has largely investigated this issue in various experimental series reported in Deliverable D3.5. As stated earlier, in Series D3.6-2 and D3.6-3 we aim to investigate the coupled effect of inherited fabrics and volcano-related topography (Series D3.6-2) and caldera resurgence (Series D3.5-3), and thus we have modified accordingly the model setup used for Series D3.5-2. We therefore describe here below the two different approaches used to reproduce inherited fabrics in the models of these series.

As for models belonging to Series D3.5-2 described in deliverable D3.5, we have simulated discontinuities with the following methods.

The first approach simulates an analogue magma chamber delimited by one or two fault discontinuities. Therefore, we have designed the magma chamber with rectilinear and vertical (90°) sides (Fig. 2.9). With a second approach we then introduced artificial discontinuities in the brittle overburden (i.e., the sand mixture package), the latter being simulated by the granular material. In particular, a "discontinuity apparatus" (DA; Fig. 2.10) consisting of a gliding and reclinable knife allowed us to "cut" into the sand creating weak discontinuities zones.

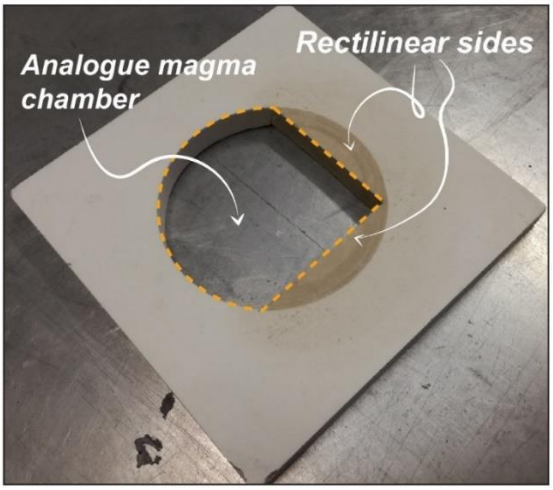

Figure 2.9. Setup used in Series D3.6-2 and D3.6-3 to simulate the analogue magma chamber bordered by rectilinear sides that were introduced to modify the circular shape of the standard analogue magma chamber. These two straight sides simulate the inherited faults that may have influenced the caldera collapse process, and possibly interacted with the pre-caldera volcano topography.

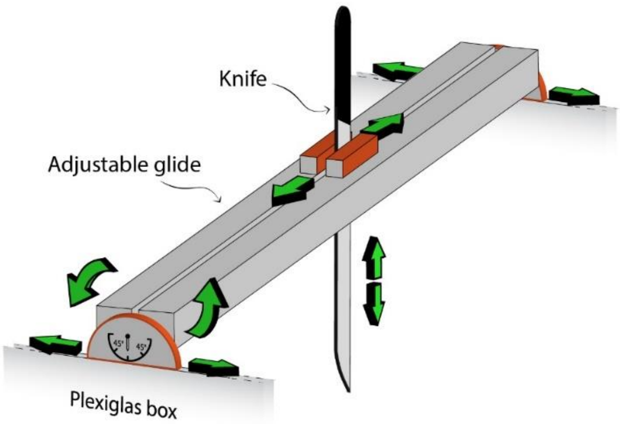

Figure 2.10. Schematic cartoon showing the "discontinuity apparatus" (DA) employed to cut artificial discontinuities into the brittle overburden in models of Series D3.6-2. The gliding knife is adjustable in terms of depth and angle and in this experimental series was used to cut vertical discontinuities interacting with the collapse of a volcanic edifice.

Depending on model setup, we coupled the two approaches to create artificial discontinuities extending from the substrate (i.e., bounding the analogue magma chamber) upsection to the surface. A combination of discontinuities was thus tested in specific models to investigate, for instance, the possible interaction between inherited faults in the presence of a volcano-related topography or broad/localized caldera resurgence.

2.4.2 Description of the experimental series D3.6-1

Models belonging to sub-series D3.6-1 were performed to investigate caldera collapse processes. The basic (standard) setup consists of a circular analogue magma chamber (12 cm in diameter and 2 in thickness) placed at the centre of a Plexiglas box (Fig 2.11). The borders of the chamber were designed vertical, and the extrusion point for the analogue magma is placed at the exact centre of the analogue magma chamber, which is filled with frozen PG3. Six sand-mixture layers, each 1 cm-thick, interbedded with coloured millimetre-markers, were poured and levelled to mimic the volcano-sedimentary overburden sequence. 65% of analogue magma was drained out through an extrusion tube in order to achieve the caldera collapse.

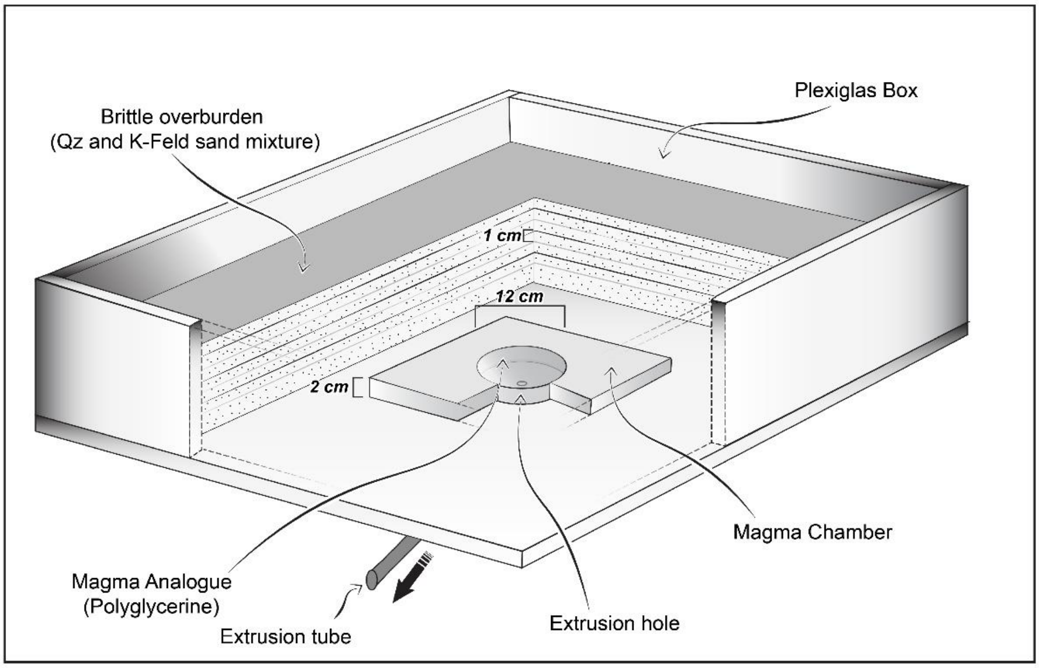

Figure 2.11. Standard setup for Series D3.6-1. A circular analogue magma chamber (12 cm in diameter and 2 in thickness) is placed at the centre of a Plexiglas box. The analogue magma chamber, which is filled with an analogue magma material (Polyglicerine-3 or Polyglicerine-10). The polyglycerine is drained out from a hole placed at the bottom of the analogue magma chamber to obtain the collapse of the brittle overburden. The latter consists of a 6 cm-thick sand-mixture package made up of 1 cm-thick layers separated by thin coloured markers. This basic setup has been modified in other series of models to test the influence of various parameters on caldera collapse processes.

Variation to this basic setup were introduced to investigate:

a) influence of overburden thickness
b) asymmetric collapse
c) tilting of the magma chamber roof

Series D3.6-1 consists of thirteen models, of which we show here six. The specific setup of these models are summarized in Figure 2.12.

Model-17 was developed with a standard setup and thus represents the “reference model” (Fig. 2.11). The other models show some variation with respect to the basic setup. In general, in order to test its influence on model evolution, only a single parameter has been modified in each model. Reference Model-17 is also shown in Deliverable D3.5 as reference model for Series D3.5-2 (specifically Series D3.5-2a), which focused on the first-order structural pattern. In the current Series D3.6-1 we use Model-17 as a reference for a comparison with smaller and secondary structures that may be of interest for the study of Los Humeros and Acoculco systems.

In this series we report three models (Model-7, Model-8 and Model-9) that have been afterward deformed by reinjection. Therefore, the final stages of deformation (i.e., the “reinjection phase”) is shown in (and considered part of) Series D3.6-3, while the initial phase of deformation (i.e., the “collapse phase”) is shown here as a part of Series D3.6-1. Despite model numbering, that was kept as original, models are shown in a rational order, reflecting logical variation to the setup, according to Figure 2.12.

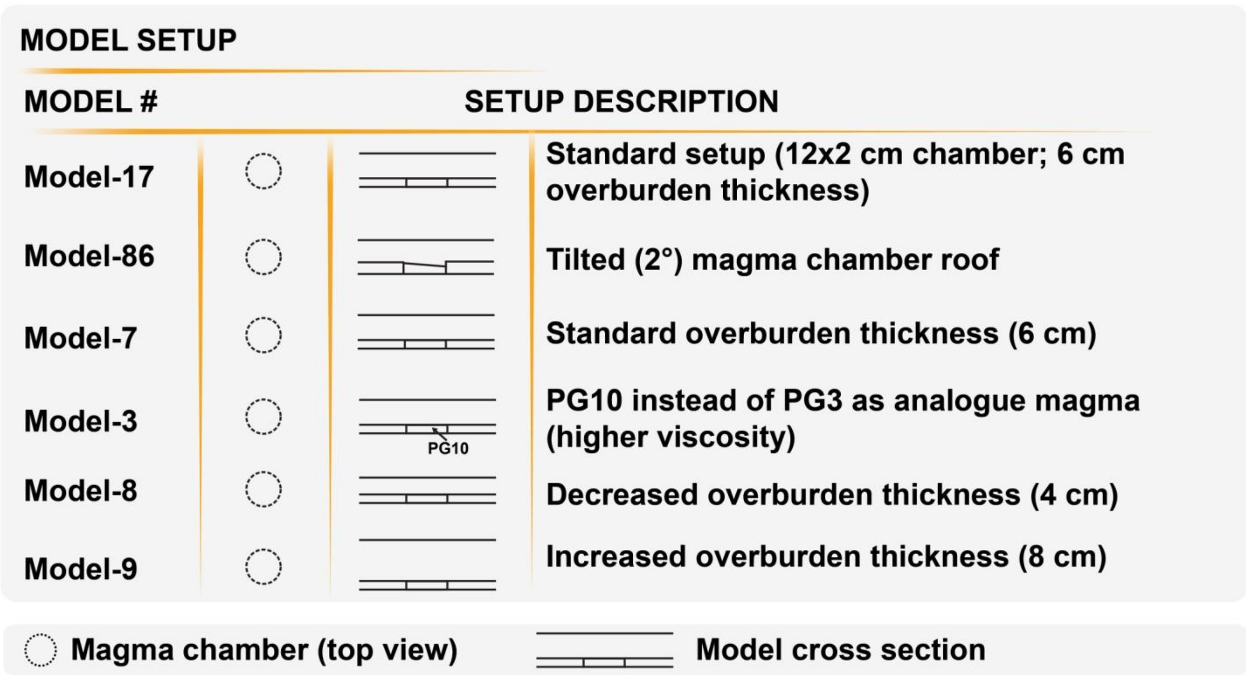

Figure 2.12. Schematic model setups for Series D3.6-1. Schematic top view and cross section of each presented model is shown, together with a simplified description of the main parameters varied in each setup. Model-17 is taken as reference model, having a standard setup (for details, see text).

2.4.3 Description of the experimental series D3.6-2

Experimental series D3.6-2 aims to investigate the role of a volcano-related topography on caldera collapse processes. Despite the volcano edifice at the Los Humeros and Acoculco has been mostly obliterated by caldera eruptions and erosion processes, the presence of a pre-caldera volcanic topography may have exerted some influence on the caldera collapse and therefore on the resulting structural pattern. Following this hypothesis, we have tested the influence of a volcanic cone placed at various positions with respect to an underlying analogue magma chamber in 9 analogue models. These models (Model-33 and Model 41 to Model-48) have tested the role of (i) a central volcano (i.e., centred on the analogue magma chamber), (ii) an eccentric volcano (i.e., located partly above the analogue magma chamber), and finally (iii) an external volcano (i.e., completely external to the analogue magma chamber). Furthermore, the results of Series D3.5-2 of Deliverable D3.5, suggest that inherited tectonic structures may play an important role in caldera collapse process. We have thus coupled the setup of these models with that of Series D3.5-2b,c models. Accordingly, we have introduced one or two artificial discontinuities bounding the analogue magma chamber, represented by rectilinear side(s) together with discontinuities in the overburden by cutting through the sand pack with the discontinuity apparatus (DA) to obtain the setup depicted in Figure 2.13 (see procedure described in Section 2.4.1).

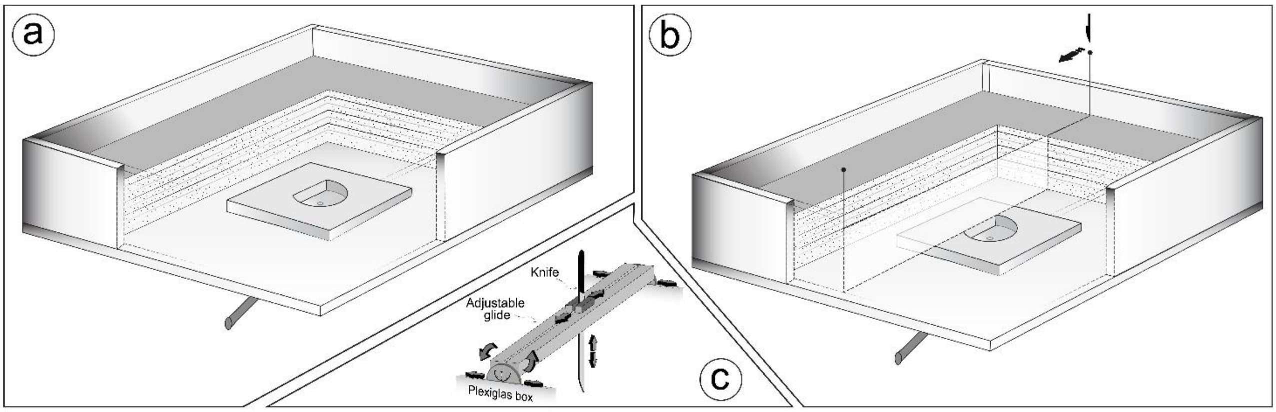

Figure 2.13. (a) Model setups showing a rectilinear side of the analogue magma chamber simulating the presence of a fault bounding the magma chamber. (b) Model setup showing a rectilinear discontinuity bounding the analogue magma chamber in continuity with a sand pre-cut introduced in the overlying brittle overburden through the discontinuity apparatus shown in (c).

The schematic setup of models carried out in Series D3.6-2 are shown below in Figure 2.14.

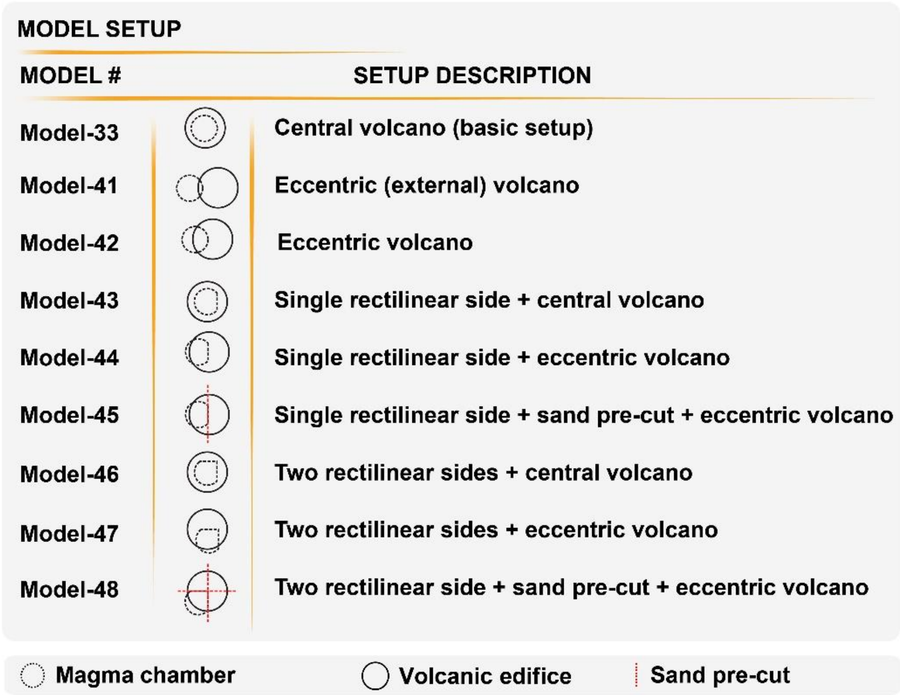

Figure 2.14. Schematic model setups for Series D3.6-2. Schematic top view and cross section of each presented model is shown, together with a simplified description of the main parameters of the setup.

2.4.4 Description of the experimental series D3.6-3

Series D3.6-3 aims at investigating the influence of caldera collapse and subsequent resurgence on the resulting structural pattern. We have thus applied caldera resurgence to the basic setup (see Fig. 2.11) by re-injecting an analogue magma (Polyglicerine-3 or Polyglicerine-10) into the collapsed model caldera system. Principal aims of this experimental series were to test:

a) The effect of “piston like” resurgence (i.e., broad resurgence of the entire collapsed caldera) on a symmetric/asymmetric collapsed caldera
b) The effect of localized resurgence at selected positions inside the collapsed caldera
c) The coupled effect of resurgence and presence of inherited faults (possibly reactivated during caldera collapse and/or resurgence).

The models belonging to this series (twenty-two, of which ten shown) are subdivided into three sub-series according to the above mentioned aims. Therefore, in sub-series D3.6-3a we show models presenting a piston-like resurgence, both symmetric and asymmetric, in sub-series D3.6-3b we report models presenting localized resurgence, and finally in sub-series D3.6-3c we present models investigating the effect of resurgence coupled with the role of inherited discontinuities. The schematic setup of models belonging to the three subseries are shown in Figure 2.15 (Series D3.6-3a), Figure 2.16 (Series D3.6-3b) and Figure 2.17 (Series D3.6-3c).

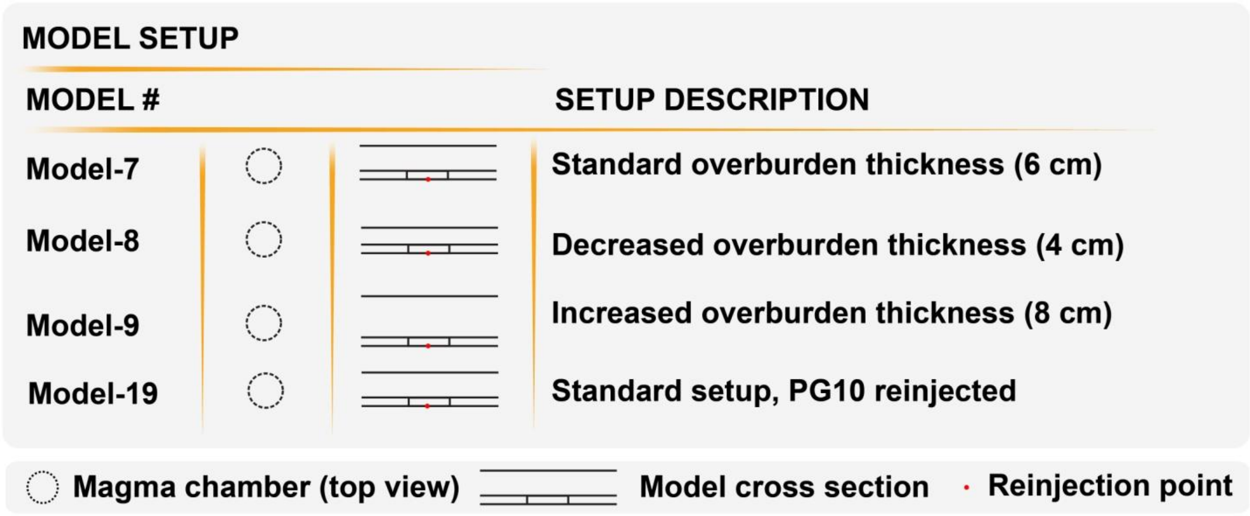

Figure 2.15. Schematic model setups for Series D3.6-3a. Schematic top view and cross section of each presented model is shown, together with a simplified description of the main parameters of the setup.

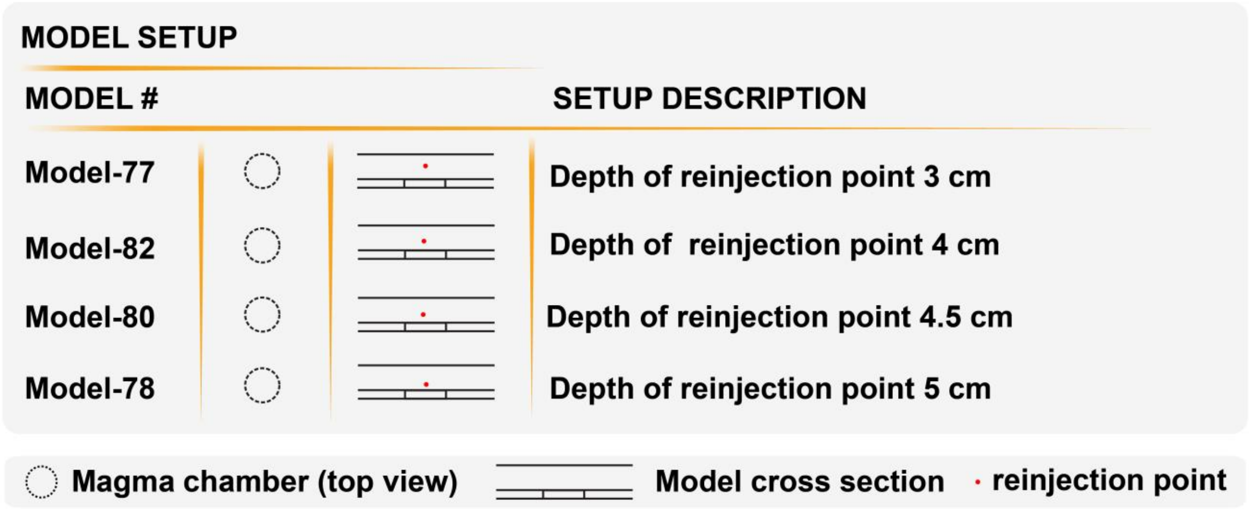

Figure 2.16. Schematic model setups for Series D3.6-3b. Schematic top view and cross section of each presented model is shown, together with a simplified description of the main parameters of the setup.

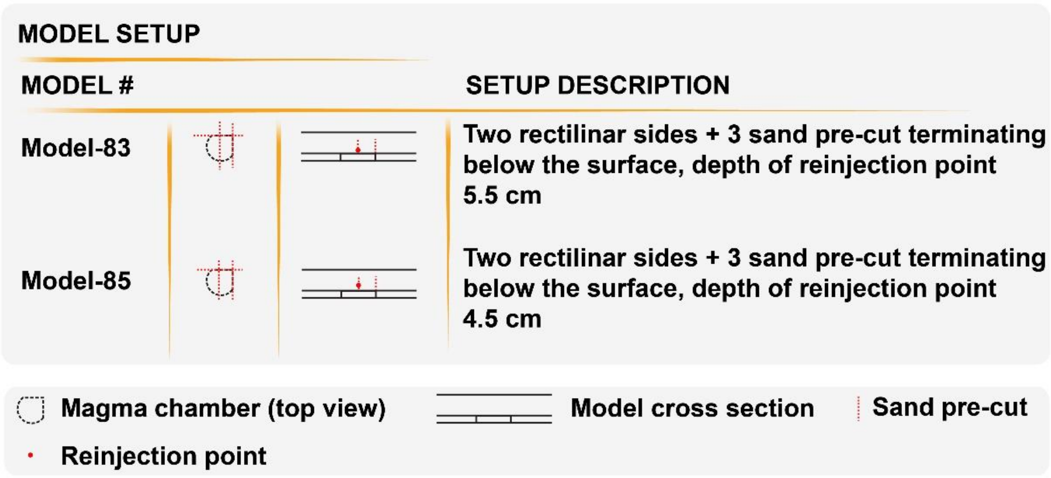

Figure 2.17. Schematic model setups for Series D3.6-3c. Schematic top view and cross section of each presented model is shown, together with a simplified description of the main parameters of the setup.

2.5 Analogue modelling procedure of Series D3.6-4

2.5.1 Series D3.6-4: Material, setup and scaling

The role of the geological factors has been tested using a new modelling apparatus built to reproduce the combined effects of tectonic deformations, caldera collapse and magmatic intrusions in a single scaled experimental set. This apparatus has been designed from the previous apparati used in Norini et al. (2008) and Norini and Acocella (2011), to deform the scaled model by tectonic forces and magmatic pressure.

Standard experimental materials with well-known rheology have been used in the experimental modelling. The LHVC and basement rocks consisted of a mixture of granular materials (e.g. Galland et al., 2006; Norini and Acocella, 2011). The magma analogue in the LHVC magma chamber driving caldera collapse has been simulated with pure vegetable polyglycerine (e.g. Montanari et al., 2017b). The magma driving caldera resurgence has been simulated with molten vegetable oil (e.g. Galland et al., 2006; Norini and Acocella, 2011).

The experimental apparatus consists of a 40 x 60 cm sand box filled with a 7 cm-thick pack of granular material. One of the vertical side plate of the sand box is fastened to a screw jack. Rotation of the screw induces horizontal movement of the vertical plate simulating compressive tectonic of the MFTB. Another perpendicular vertical side plate is attached to a basal thin rubber sheet underling the granular material. The opposite side of the rubber sheet is fixed to the model base. The side plate is fastened to a screw jack, whose rotation induces horizontal movement and gradual extension of the rubber sheet simulating the extensional tectonics associated with post-MFTB magmatism and TMVB activity. As in the LHVC natural prototype, the extension direction in the model is perpendicular to the compression one. The LHVC pre-caldera magma chamber driving caldera collapse has been modelled by a 2 cm-thick polyglycerine layer confined in a vertical cylinder with a diameter of 12 cm sinking below the granular material pack through a descending piston. A circular hole has been previously cut in the basal rubber sheet, allowing direct contact between the sinking polyglycerine and the granular material pack. Emplacement of post-caldera magma driving resurgence of the caldera floor has been simulated injecting molten vegetable oil at a known rate in the granular material with a peristaltic pump through a 4 mm diameter tube. This tube is mounted coaxially with the 12 cm-large piston and cylinder and stands just above the polyglycerine layer. This set-up allows newly-generated post-caldera intrusion geometries (molten vegetable oil propagating in the granular material), not constrained by the pre-caldera magma reservoir (polyglycerine layer confined by cylinder).

2.1. Scaling procedure for LHVC and basement rocks

Model parameters have to be geometrically, cinematically and dynamically scaled, in order to ensure similarities between natural prototypes and experimental results (Hubbert, 1937; Ramberg, 1981). The main forces to consider for correct scaling are body forces due to gravity, and stresses. The dimensionless ratio Π_1 between these forces can be defined as

$$\Pi_1 = \frac{\rho \text{ g l}}{\sigma_t},$$

where ρ is the rock density, g is the gravity, l is the linear dimension, and σ_t is the tectonic stress. The ratio Π_1 must be similar in nature and in the model for the scaling of the analogue experiment to be correct. Thus, the stress ratio σ_t* between model and nature can be calculated from

$$\sigma_t^* \approx \rho^* \text{ g}^* \text{ l}^*,$$

where ρ* is the density ratio, g* is the gravity ratio, and l* is the length ratio between model and nature. The experiments are conducted in the Earth's field of gravity. Consequently, the model/nature ratio for the gravitational acceleration g* is unity. The natural prototype is a volcano with collapse calderas diameter of in the order of ~9-18 km (Carrasco-Núñez et al., 2017; Norini et al., 2019). The experimental piston simulating caldera collapse has a diameter of 12 cm and the resulting length ratio l* is in the order of 1×10^{-5} (1 cm in the experiments corresponds to ∼1 km in nature). The mean density of rocks in the LHVC and basement is assumed to be 2.6 g/cm^3. The granular material used to simulate the volcano and its basement above the magma chamber has a density of ∼1.4 g/cm^3, which imposes a density ratio between model and nature of ρ* ∼ 0.5. Therefore, the dimensionless stress ratio σ_t* between the brittle analogue model and the natural prototype is ∼10^{-5}. For the rocks of the volcanic edifice and basement, we assume a linear Mohr- Coulomb failure criterion, where the parameters are the cohesion C (10^6 to 10^7 Pa) and the angle of internal friction φ (∼35°) (Byerlee, 1978). As the cohesion has the dimension of stress, the ratio for cohesion C* must be in the same range as σ_t* (10^{-5}). This requires the use of a material with C of 10 to 100 Pa. The granular material used in the analogue modelling consisted of a mixture of 80% silica sand (SS) and 20% crushed silica powder (SP) with a cohesion C ∼60 Pa and tensile strength of ∼20 Pa (Norini and Acocella, 2011), so that the ratio between shear strength and tensile strength is 3:1 and the model is correctly scaled (Table 1).

2.2. Scaling procedure for LHVC magmas

The simulation of a material whose rheology is time dependant, such as magma, has to take into account the viscosities and the related strain rates, velocities, and timescales. The viscous stresses in the model are properly scaled if $\sigma_t* \sim \sigma_v*$, where σ_v* is the viscous stress ratio between model and nature. To scale the analogue models, the viscosity ratio of magma η* in model and nature has been used to calculate the corresponding strain rate ratio *e** according to $\sigma_t* \approx \sigma_v* \approx \eta* e*$. The strain rate ratio *e**, being measured in s^{-1}, is the inverse of the time ratio t* and, being multiplied for the length ratio l* allows defining the velocity ratio V* (Merle and Vendeville, 1995). In the LHVC experimental modelling both the length ratio l* and the stress ratio σ_t* are on the order of 10^{-5}.

The LHVC ignimbrites mainly have rhyodacitic to rhyolitic composition (Carrasco-Núñez et al., 2017). The mean magma viscosity driving LHVC caldera collapse is assumed to be in the order of $\sim 10^{10}$ Pa s. To scale the model, we assume a velocity ratio V* of $\sim 10^{-2}$ (1 cm/s in the model corresponds to 1 m/s in nature during the caldera collapse). The analogue of this magma in the LHVC magma chamber has been simulated with pure vegetable Polyglycerine-10 (PG10) with viscosity of 450 Pa s, resulting in a σ_v* of $\sim 10^{-5}$, with the same magnitude of the stress ratio σ_t*.

In the LHVC post-caldera phase, resurgence occurred simultaneously with the emplacement of basaltic-andesitic lava flows, rhyolitic domes and andesitic-rhyolitic pyroclastic fall deposits (Carrasco-Núñez et al., 2017). The mean magma viscosity driving resurgence of the caldera floor is assumed to be in the order of $\sim 10^6$ Pa s. Molten vegetable oil has been used to simulate the emplacement of post-caldera magma driving resurgence of the caldera floor. The intrusion of the molten oil in the granular material with a ∼20 Pa tensile strength ensures propagation of the magma analogue through hydrofractures (Galland et al., 2006). The vegetable oil is solid at room temperature and melts to nearly Newtonian fluid with density of ∼0.9 g/cm^3 when the temperature rises above 30°C. The oil is injected at the base of the model with a rate of 4×10^{-2} m/s. When the oil propagates the model, the intrusion velocity lowers to about 10^{-3} m/s. Considering that medium/low- viscosity intrusions in nature propagate at ∼0.1 m/s, the velocity ratio V* is $\sim 10^{-2}$ (Spence and Turcotte, 1985; Battaglia and Bachelery, 2003; Roman et al., 2004). The oil is intruded when at 35°C, with a viscosity of $\sim 2 \times 10^{-2}$ Pa s, resulting in a σ_v* of $\sim 10^{-5}$, with the same magnitude of the stress ratio σ_t*.

2.5.2 Description of the experimental series D3.6-4

The analogue modelling consisted of 5 steps:

1) In step 1 the sand pack is deformed by the moving plate simulating compression of the MFTB. Shortening of MFTB has been estimated to be 20-30% approaching the front of the fold belt (e.g. Fitz-Diaz et al., 2017). The original length of 40 cm of the experimental model has been reduced to 30 cm with a movement of the vertical plate by 10 cm, corresponding to a shortening of 25%;

2) In step 2, the extensional tectonic phase associated with the TMVB emplacement has been reproduced by the horizontal extension of the basal rubber sheet by 5 cm, to generate NE-SW normal faults in the previously thrusted sand pack;

3) In step 3, a new < 2 cm-thick layer of granular material has been poured on the deformed model, to reproduce the emplacement of the most recent TMVB and LHVC volcanic units sealing and postdating the tectonic faults generated in the first two steps;

4) In step 4, caldera collapse has been generated by 2 cm vertical sinking of the piston and polyglycerine layer simulating the magma chamber roof;

5) In step 5, caldera resurgence has been reproduced by intrusion in the granular material of molten vegetable oil. The intrusion has been stopped when the oil reached the model surface.

2.6 Analogue modelling procedure of Series D3.6-5

2.6.1 Series D3.6-5: Material, setup and scaling and description of the experimental series

The experimental set-up (Fig. 2.18) consists of a 31 × 31 cm glass box filled with a sand pack (crust analogue) of variable thickness (T, of 10, 30 and 50 mm, respectively). The experiments involve both a layered (5 experiments) and a non-layered (4 experiments) overburden. The layering was imposed using a non-cohesive marine sand below a layer of crushed silica sand (grain size = 40-200 μm, cohesion = 300 Pa), fixing the thickness ratio of the two layers (Tu/Tl) to 1, to simulate the stratigraphy in Los Potreros (stiffer post caldera lava flows above softer and less cohesive ignimbrite deposits emplaced during the caldera collapse stage). At the base of the sand pack, a piston, controlled by a motor, pushes upward the silicone (magma analogue) placed inside a cylinder 8 cm in diameter. The injection rate is fixed for all the experiments to 2 mm/hr and each experiment was stopped at the onset of the silicone extrusion. Both sand and silicone physical properties are listed in Table 1. At the end of each experiment, the surface has been covered with sand to preserve their final topography and were wetted with water for cutting in sections to appreciate the subsurface deformation. Such sections were used to measure the mean dip of the apical graben faults (θ) induced by the rising silicone. A digital camera monitored the top view deformation of each experiment at 0.02 fps and a laser scanner, placed next to the camera, provided high-resolution data (maximum error ± 0.5 mm) of the vertical displacement that was used to measure in detail the geometrical features of the deformation i.e. dome diameter (Ld), apical graben width (Lg) and dome flank mean dip (α). According to the Buckingham-Π theorem (Merle and Borgia 1996 and references therein), our models need 7 independent dimensionless numbers to be properly scaled (i.e. 10 variables minus three dimensions; Table 2-2). Such dimensionless numbers can be defined as the ratios (Π) listed in Table 2-3. Some values of Π5, representing the ratio between the inertial and viscous forces, are very small both in nature and experiments (1.3 × 10-20 and 6.1 × 10-10, respectively), indicating that the inertial forces are negligible with respect to the viscous forces in both cases.

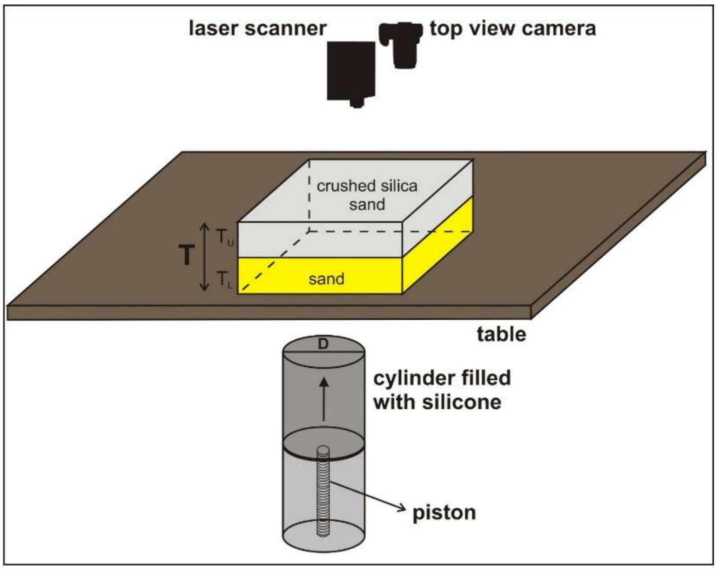

Figure 2.18. Experimental set-up. D = diameter of the cylinder.

Parameter	Definition	Value (experiments)	Value (nature)
T	Thickness of the overburden	3-5 X 10^{-2} m	300-2000 m
L_d	dome diameter	1-1.6 X 10^{-1} m	2000 m
H	Dome height	1.3-2 X 10^{-2} m	100 m
ρ_s	density of brittle overburden	1400 kg/m^3	2800 kg/m^3
ϕ	Angle of internal friction	35°	25-40°
τ_0	Cohesion (brittle overburden)	300 Pa	10^6 Pa
ρ_m	density of intrusive material	1000 kg/m^3	2500 kg/m^3
μ_m	viscosity of intrusive material	10^4 Pa s	10^{15} Pa s
g	Gravity	9.8 m/s^2	9.8 m/s^2
t	Timespan for deformation	2.8-6.5 X 10^4 s	1.9 X 10^{12} s

Table 2-2. Comparison of the geometric and material properties parameters of the experiments and nature.

Dimensionless ratio	Experiments	Nature
$\Pi_1 = T/L_d$	0.2-0.5	0.15–1
$\Pi_2 = H/L_d$	0.08-0.2	0.05-0.1
$\Pi_3 = \rho_s/\rho_m$	1.4	1.12
$\Pi_4 = \phi$	35	25-40
$\Pi_5 = \rho_m H^2/\mu_m t$	6.1 X 10^{-10}	1.3 X 10^{-20}
$\Pi_6 = \rho_m gHt/\mu_m$	1.3 X 10^3	4.6 X 10^3
$\Pi_7 = \rho_s gT/\tau_0$	2.3	8.24

Table 2-3. Definition and values of the dimensionless ratios Π in nature and in the experiments.

2.7 Monitoring and analysis of deformation

2.7.1 Monitoring of 2D and 3D deformation

The 2D model deformation was constantly monitored by automatic acquisition of high-resolution top view photos with 120 seconds time-steps. 3D deformation was quantified using photogrammetric techniques by means of the Agisoft Photoscan® software. To this purpose, we have acquired dedicated high-resolution "all-around" photos of the target model from a pre-determined perspective (Fig. 2.19) in order to obtain a 3D rendering (point dense cloud) of model surface and the interpolated digital elevation model (DEM). The use of markers placed at fixed, and locally geo-referenced positions on the model setup allowed the equal scaling of all obtained DEMs. The zero-reference level for height was arbitrary re-assigned to undeformed portions of each model surface, so that uplift and subsidence developed during model deformation resulted in positive and negative elevation values above and below the reference surface.

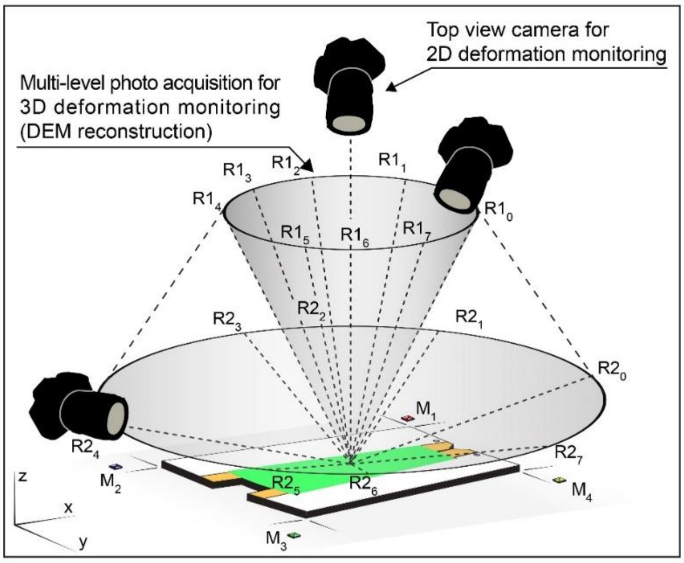

Figure 2.19. Schematic cartoon illustrating the adopted monitoring strategy: a fixed camera acquired high-resolution top-view photos to monitor the 2D deformation, while a moving camera acquired high-resolution photos at pre-determined positions ($R1_0$-$R1_7$ and $R2_0$-$R2_7$), to be used for photogrammetric analysis and DEMs elaboration. The correct scaling of DEMs is warrant by the use of locally geo-referenced markers (M_1-M_4).

3D deformation was also investigated by cutting a pair of sub-orthogonal cross sections through the models, which were taken through a saw after that models were saturated with water and frozen. The model sections were afterward cleaned by razing with a blade. This allowed us to evaluate fault offset and geometry by observation of mm-thick coloured layers introduced during model construction and acting as passive markers of deformation.

2.7.2 Quantitative analysis of deformation

Acquisition of high-resolution photos allowed us to obtain a 3D reconstruction of DEM surfaces. DEMs were elaborated both before the onset of the deformation phase, in order to obtain a reference level to check horizontality, and at the end of deformation. GIS software (QGIS®) were used to visualize, elaborate and make calculation on DEM surfaces.

2D top view photos were shot with time step intervals of 120 seconds to monitor deformation. Furthermore top view photos were used to implement quantitative analysis of model surface. Specifically, top view photos were elaborated to be used for Digital Particle Image Velocimetry Analysis (DPIV) through the *PIVlab* algorithms developed by Thielicke and Stamhuis (2014) available for MATLAB®. DPIV is a common technique for non-invasive, quantitative and qualitative flow visualization. Specifically, the *PIVlab* software analyses image pairs, and then computes particle displacement vectors between the two photographic frames. If the frames are correctly scaled in terms of pixel/meters dimension and time interval, the software can easily provide velocity vectors and derivative parameters, visualized as gradient maps. The obtained maps can then be interrogated in order to produce statistics, velocity (or other parameters) profiles, etc, quantifying the 2D deformation of a target model.

3 Analogue modelling analysis and results

In this section, we present the results of five experimental series, addressing the structural deformation pattern resulting from symmetric/asymmetric caldera collapse, interacting with a pre-caldera volcano-related topography and/or subject to caldera resurgence (both diffuse and localized), coupled with the effect of inherited structures. These issues are reflected by presentation of models, which is subdivided into the experimental series of pertinence, namely:

- *Series D3.6-1: Symmetric/asymmetric caldera collapse*
- *Series D3.6-2: Role of pre-caldera volcano-related topography*
- *Series D3.6-3: Caldera resurgence and interaction with pre-existing structures (both regional inherited fabrics and caldera collapse faults)*

  Series D3.6 is further subdivided into 3 sub-series, reflecting specific aspects, as follow:

  - *Sub-series D3.6-3a: Effect of "piston like" resurgence on symmetric/asymmetric collapsed calderas*
  - *Sub-series D3.6-3b: Effect of localized resurgence on collapsed calderas*
  - *Sub-series D3.6-3c: Effect of resurgence and presence of inherited faults on collapsed calderas*

- *Series D3.6-4: Combined effects of compressional and extensional tectonics structures and magmatic processes on the Los Humeros Volcanic Complex (LHVC)*
- *Series D3.6-5: Shallow-intra-caldera intrusions*

3.1 Series D3.6-1: Symmetric/asymmetric caldera collapse

In this series, we aim to investigate the processes leading to caldera collapse, which may generate symmetric piston-like systems and asymmetric trap-door systems. To this aim, we have performed several analogue models, of which six are shown here below, starting from the reference Model-17 that was built with a standard setup. Afterward, we show models that bear specific variations with respect to the standard setup, in order to test the influence of specific parameters. As mentioned earlier in Section 2.4.2, models are not shown following their progressive numbering, but are organized according to the rationale of series development, in order to logically show results.

Model-8 forms, together with Model-9, a small sub-series investigating the effect of overburden thickness on the evolution of asymmetric/symmetric caldera collapse. After the collapsing phase, once the caldera collapse was obtained, these models were re-injected with PG3 fluid in order to induce caldera resurgence. Therefore, the results of these two models are also shown in sub-series eries-D3.6-3a, which investigates the effect of "piston-like" resurgence.

3.1.1 Model-17

Model-17 constitutes the reference model for caldera collapse, since it was built with a standard setup that was afterward modified according to the requirements of the various experimental series. The standard parameters adopted for this models are represented by a circular analogue magma chamber (with vertical sides), with a diameter of 12 cm and a depth of 2 cm. The analogue magma chamber was filled with PG3 fluid and overlaid by 6 layers of 1 cm-thick sand mixture for a total thickness of 6 cm. Layers were separated by thin (less than 1 mm thick) markers of deformation, represented by sieved coloured K-feldspar sand. Caldera collapse was obtained by draining out the PG3 fluid from a circular hole placed at the bottom of the analogue magma chamber. Specific variations were applied to this standard setup in order to perform the different models.

Model-17 is presented and analysed as reference model also in Deliverable D3.5 (series D3.5-2a) and highlights the first-order correspondence of the caldera collapse evolution with the evolutionary model proposed by Acocella (2007): Model-17 evolution (both plain view and cross section; Fig. 3.1) proceeds as shown in Figure 3.2, developing an early outward-dipping reverse fault system after an initial phase of down-sagging, to further accommodate deformation in the peripheral areas by developing a system of concentric inward-dipping normal faults. For these specific aspects, the reader is referred to Deliverable D3.5.

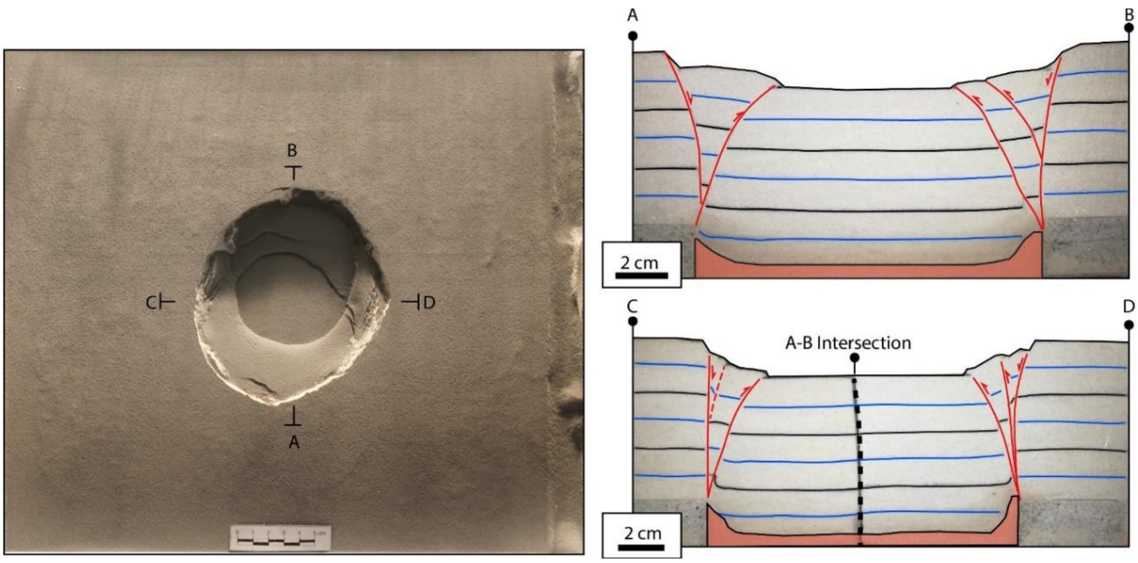

Figure 3.1. Model-17 top view and cross section.

In this series, we use Model-17 to highlight specific structural aspects at a finer-scale, which were not previously highlighted in Series D3.5-2a (due to its aim), particularly the temporal evolution of deformation pattern of faults in plan-view (Figure 3.2). More specifically, the schematic sketch shows incipient down-sagging (Fig. 3.2a and a'), which afterward develops a reverse fault propagating laterally in a counter clockwise direction (Fig. 3.2b and b'). Deformation then shifts toward external areas to develop normal faults that propagate laterally similarly to the previously-formed inner reverse fault (Fig. 3.2c and c'), which afterwards merges with a similar structure developed on the opposite side of the collapsed caldera (Fig. 3.2d and d'). Contemporaneously, yet propagating more slowly, the inner reverse faults continue to develop until they intersect and cross-cut each other to form a 'fish tail'-like fault pattern. Interestingly, the collapsed caldera resulted in a symmetry piston-like caldera system developed through asymmetric steps of faults propagation (Fig. 3.2e and e').

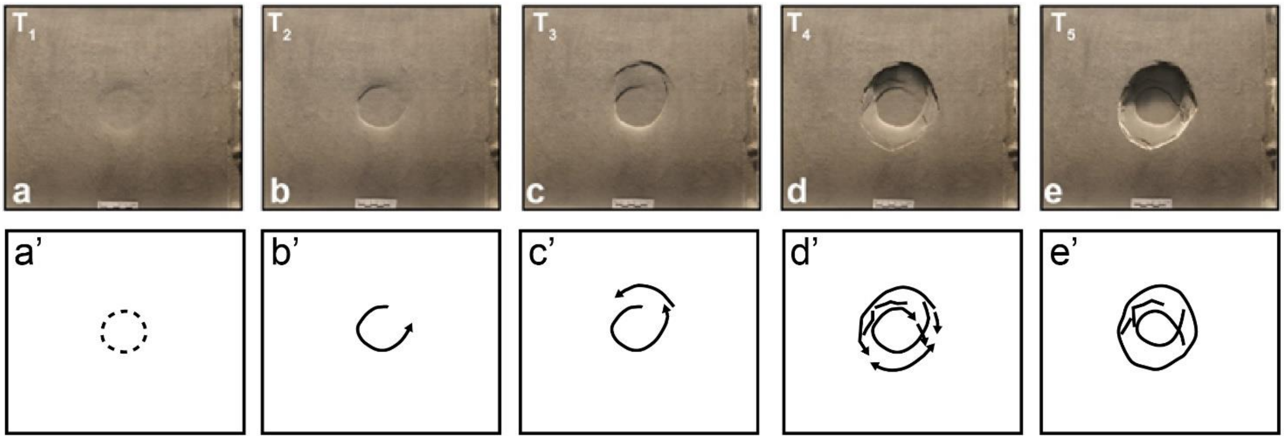

Figure 3.2. Temporal evolution of deformation of Model-17. The schematic sketch shows the direction of propagation throughout time of the main structures (indicated by small black arrows). (a and a') An incipient down-sagging that afterward (b and b') develops a reverse fault propagating laterally in a counter clockwise direction. (c and c'). The deformation shifts toward external areas to develop normal faults laterally propagating as the previously formed inner reverse fault, which subsequently merges with similar structure developed on the opposite side of the collapsed caldera (d and d'). Contemporaneously, yet propagating more slowly, the reverse inner faults continue to grow until they intersect and form a 'fish tail'-like fault pattern. The collapsed caldera (e and e') thus resulted in a symmetry piston-like caldera system, that developed through asymmetric and scattered steps of faults propagation.

Such a transient asymmetric evolution of the collapsed caldera has resulted, at the end of deformation, into a symmetric caldera system, as highlighted by the detailed digital elevation model of model surface (Fig 3.3). The occurrence of transient asymmetric deformation steps is also highlighted by DPIV analysis, showing differential vectors of particle velocity along the main developing structures (Fig. 3.4).

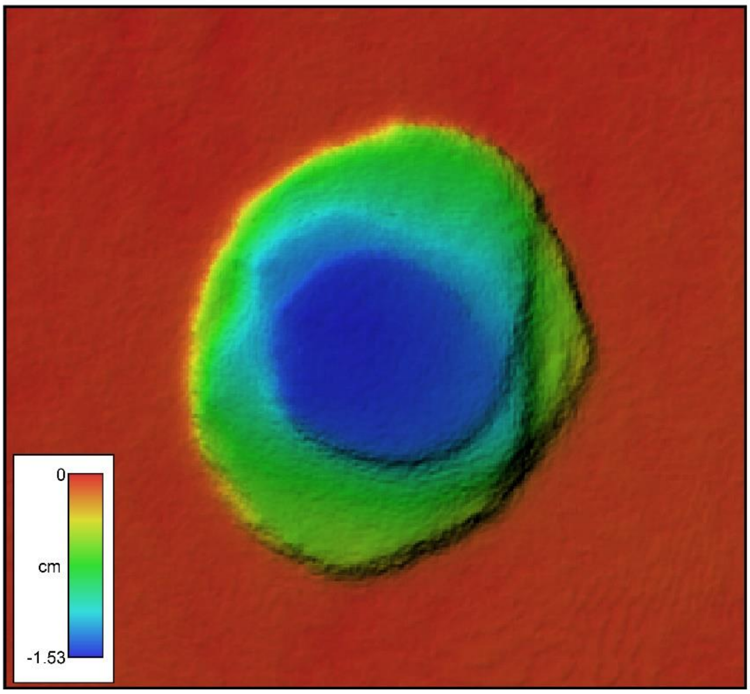

Figure 3.3. Digital elevation model (DEM) of the final stage of caldera collapse for the 'standard' Model-17.

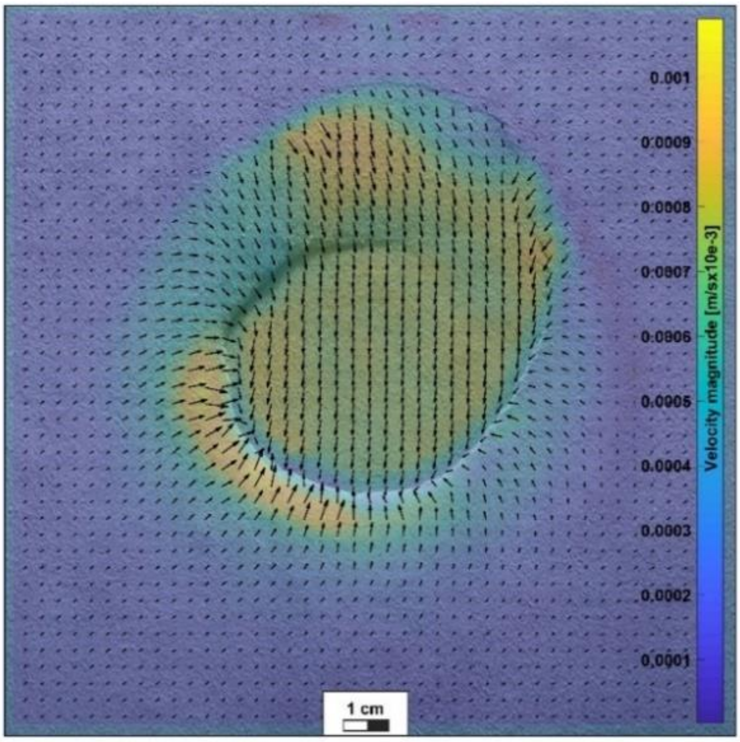

Figure 3.4. DPIV analysis of Model-17 (frames 31-32; time interval between each frame is 120 seconds). Warm colours indicate higher velocities; note that DPIV has the ability to catch only 2D horizontal displacement. DPIV highlights inward movement of particles driven by progressive fault propagation and displacement. Notably, displacement is not uniform along the various fault branches, testifying to transient asymmetric caldera collapse.

3.1.2 Model-86

Model-86 addresses the effects of roof horizontality of an analogue magma chamber. Model-17 was built up with a standard setup and resulted into a symmetric caldera collapse. Nonetheless, some test models showed that, starting from a same standard setup, evolved into asymmetric caldera collapse. To understand the reasons and mechanisms leading to such an asymmetric collapse (i.e., trap-door system), we have tested various hypotheses that could affect model deformation. Considering that the analogue magma chamber and the overlying sand-package were built following a same, standard procedure for all models, factors inducing asymmetry may be associate with:

- differential flow inside the analogue magma chamber
- small tilt of analogue magma surface.

Both conditions are associated with the differential stress applied by the sand overburden on the underlying PG3 glycerine fluid, and both can be used to achieve asymmetric caldera collapse models. More specifically, differential flow inside the analogue magma chamber can result from non-uniform defrosting of PG3/PG10, a problem that was overtaken by allowing complete defrost at ambient temperature (25°C) before the start of model deformation. However, this model set-up is difficult to control for obtaining models experiencing asymmetric caldera collapse.

Instead, the development of asymmetric caldera collapse can be controlled better by introducing a small tilt to the surface of the analogue magma. Differential stress exerted by the overlying brittle overburden can indeed lead to an asymmetric, trap-door caldera. To test this hypothesis, we have performed a specific model built with the same standard setup of Model-17, but imposing a tilt of 2° to the surface PG3 fluid during its freezing (Fig. 3.5).

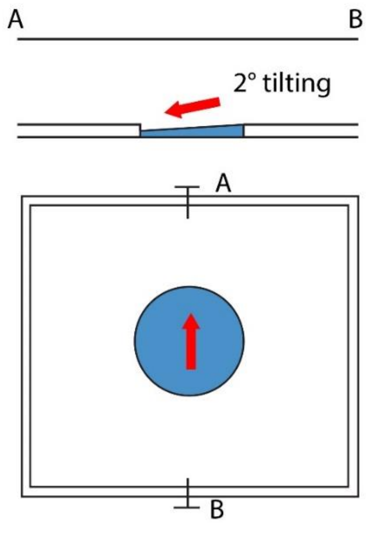

Figure 3.5. Cross section and top view of setup of Model-86. The blue area represents the analogue magma (PG3), that was designed with a roof tilting of 2°. The red arrow indicates the dip direction of the magma chamber roof.

The caldera development followed the pattern of deformation obtained in Model-17, except for the degree of symmetry that characterizes the final collapsed caldera (Fig. 3.6).

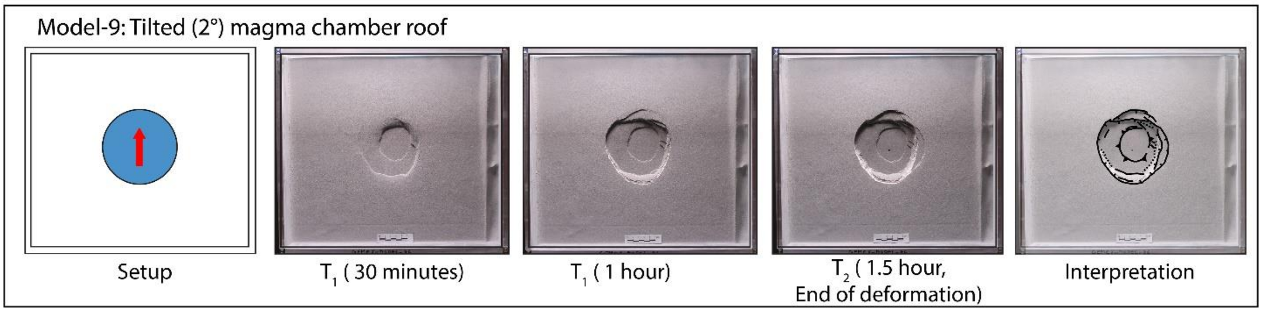

Figure 3.6. Setup, temporal evolution of deformation and schematic top view interpretation of the collapse phase of Model-86.

Both model top view and cross section show that a trap-door system has developed during caldera collapse, with the piston-block tilted toward the area where the analogue magma presented the initial highest thickness (see red arrow in Fig. 3.7), as also highlighted by the digital elevation model in Figure 3.8. This model, therefore, shows that the differential vertical loading can drive the formation of an asymmetric caldera collapse in our models.

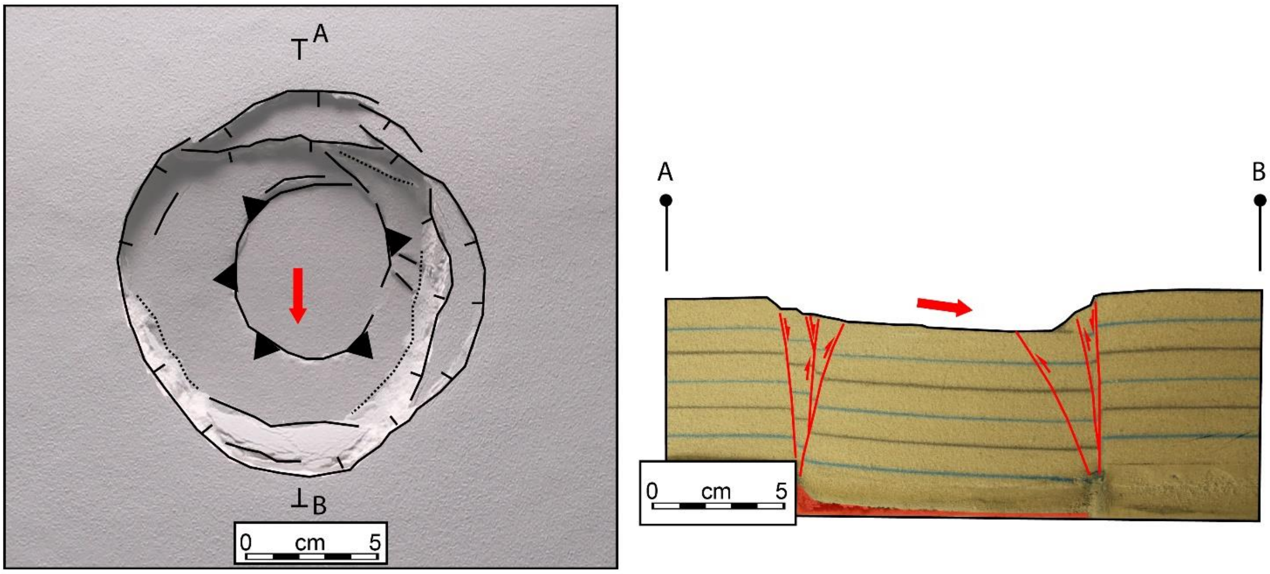

Figure 3.7. Detailed line-drawing interpretation of Model-86 experiencing asymmetric caldera collapse as result of initial differential vertical loading on the analogue magma chamber.

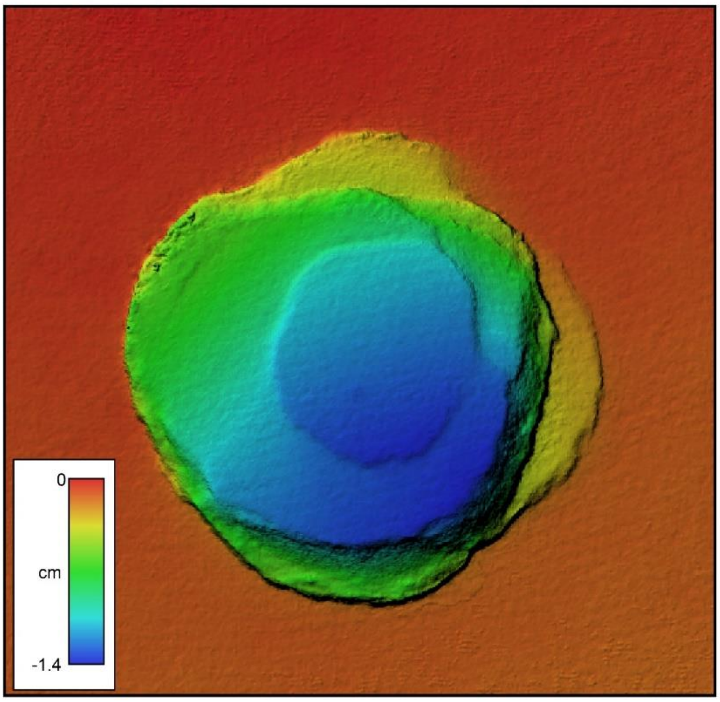

Figure 3.8. Digital Elevation Model (DEM) of the final collapsed caldera reproduced in Model-86, which emphasise the asymmetric (trap-door) caldera collapse.

3.1.3 Model-7

Model-7 was built with a standard setup, identical to Model-86. Despite having a standard setup, Model-7 shows an asymmetric trap-door system (Fig. 3.9), which is more pronounced with respect to Model-86. Model-7 shows a strongly tilted piston block (red arrow in Fig. 3.10 indicates the dip direction), whose deformation is accommodated by the formation of outward dipping normal faults (blue arrows in Fig. 3.10). Furthermore, in this model, a reverse fault dissects the piston (roof) block, likely as a result of differential subsidence/uplift due to the tilting.

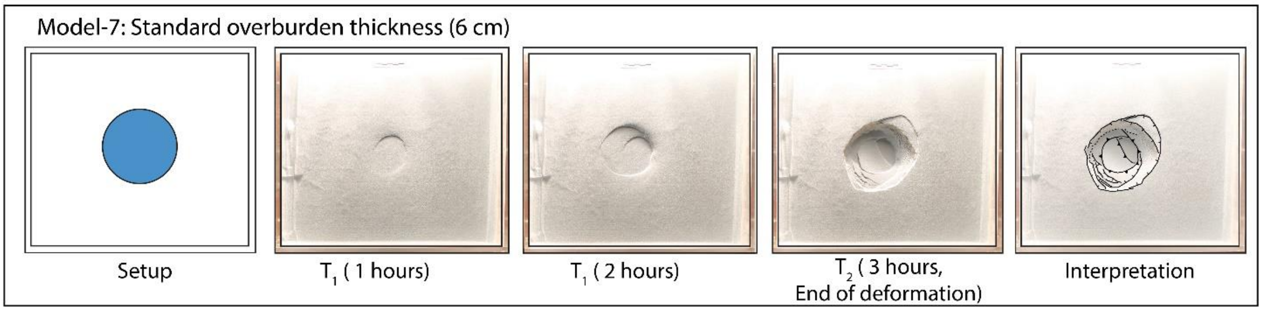

Figure 3.9. Setup, temporal evolution of deformation and schematic top view interpretation of the collapse phase of Model-7.

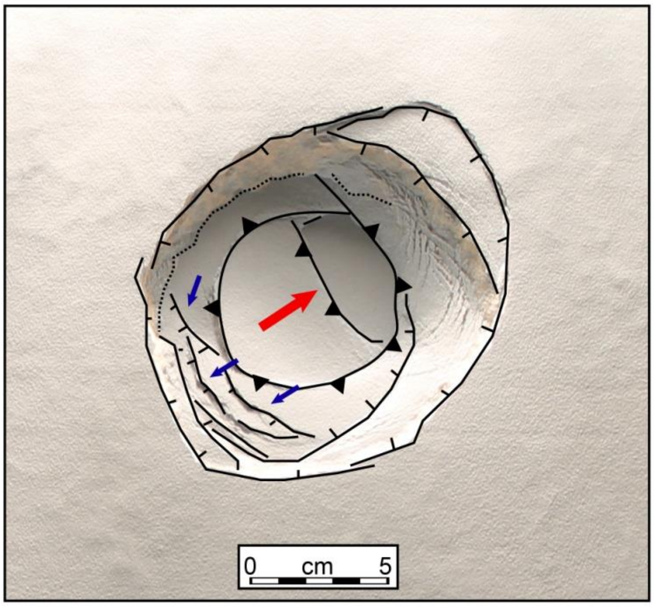

Figure 3.10. Detailed line-drawing interpretation of Model-7. The red arrow indicates the dip direction of the internal piston. Caldera development resulted in a highly asymmetric trap-door system, accommodated by outward dipping normal faults (blue arrows).

3.1.4 Model-3

Model-3 aimed to test the influence of an analogue magma with a higher viscosity than PG3 fluid, simulating a more viscous natural magma (see Tab. 2-1). To this aim, we have introduced Polyglicerine-10 in a circular magma chamber, varying in this way the standard setup of Model-17. The other parameters were left identical to the standard model.

Due to the higher viscosity of PG10, the total model deformation (i.e., the complete caldera collapse) was obtained after 22 hours, the model let deform overnight. Compared to the standard Model-17, despite the longer deformation, the evolution of the structural pattern did not differ significantly, developing an incipient outward-dipping system of reverse faults and, afterward, inward-dipping normal faults (Fig. 3.11).

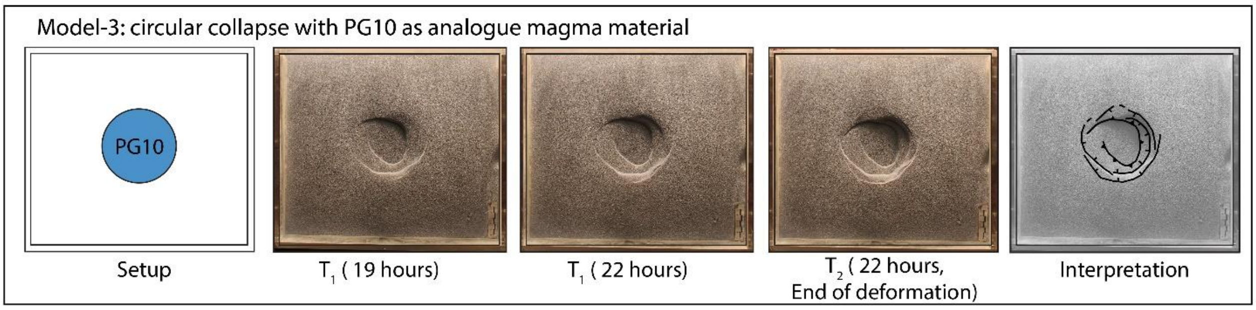

Figure 3.11. Setup, temporal evolution of deformation and schematic top view interpretation of Model-3, which was built using a denser analogue magma (PG10).

Overall, the model resulted in an asymmetric trap-door system, with a highly depressed side and an area of hinge, that did not experience reverse faulting. This asymmetry effect is unlikely to depend on the PG10 glycerine, since a longer time of deformation would favour re-equilibration inside the analogue magma chamber during extrusion.

3.1.5 Model-8

Model-8 tests the influence of a reduced overburden thickness, which has been set at 4 cm, hence 2 cm less than the standard setup (Fig. 3.12). As for Model-3, deformation followed the standard evolution, developing the inner outward-dipping reverse fault system, and subsequent inward-dipping normal faults in the peripheral areas of the collapsing caldera (Fig. 3.12). Nonetheless, this model shows a highly asymmetric structural pattern, the collapsed central piston being strongly tilted. The red arrow in Figure 3.13 indicates the dip direction of the tilted piston block. The rotation, due to differential subsidence originated a series of peculiar structures that are characteristic of models with a well-developed trap-door system.

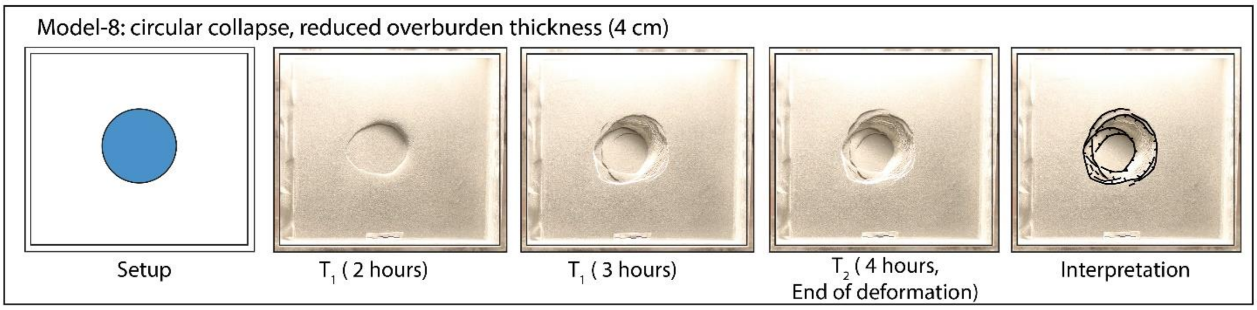

Figure 3.12. Setup, temporal evolution of deformation and schematic top view interpretation of the collapse phase of Model-8.

These structures (blue arrows in Fig. 3.13) are outward-dipping normal faults that accommodate block titling and constitute the hinge of the trap-door system. Notably, these two linking outward-dipping normal faults crosscut the entire caldera depression, linking with the external normal ring faults. Besides, on the most subsided caldera side, a series of radial and intersecting fractures formed during caldera development as a result of the steep fault scarp development. These features are typical of models showing a highly asymmetric trap-door system (Fig. 3.13), and do not show significant difference with respect to Model-86.

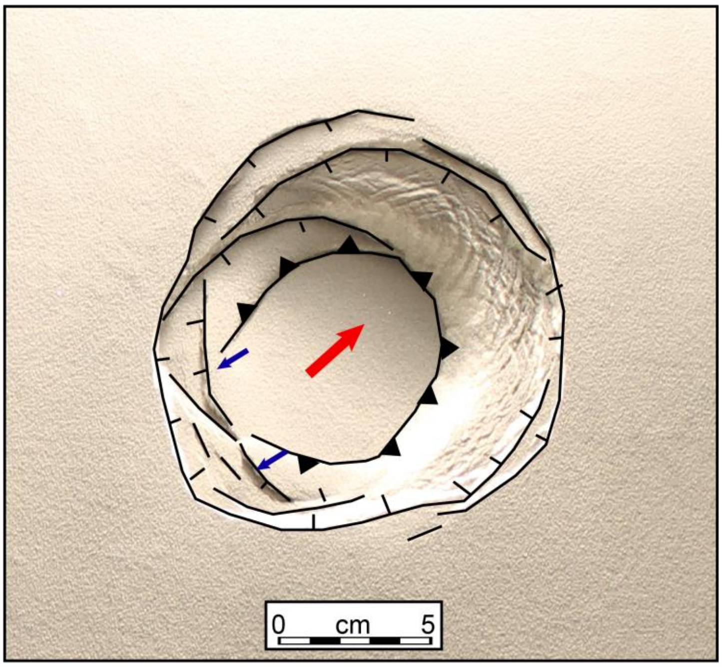

Figure 3.13. Top view interpretation of caldera-collapse related to Model-8, which developed a marked asymmetry, generating a trap-door system. The red arrow indicates the direction of increasing subsidence of central asymmetrically collapsed roof-block that is accommodated by outward dipping normal faults (blue arrows).

3.1.6 Model-9

Model-9 tested the effect of an increased overburden thickness, which has been set at 8 cm, hence 2 cm more than the standard setup (Fig. 3.14). This model experienced a first-order evolution of deformation given by outward-dipping reverse fault at the caldera centre and inward-dipping normal faults in the peripheral area (Fig. 3.14), which is again similar to the 'classical' one. Nevertheless, this model shows some peculiarities, such as an atypical pattern of structures inside the piston (roof) block (Fig.3.15). In particular, the model shows fault branches at the caldera ring propagating both outward (in plain view) and radially; the latter structures may be connected to the increased overburden thickness (Fig. 3.15).

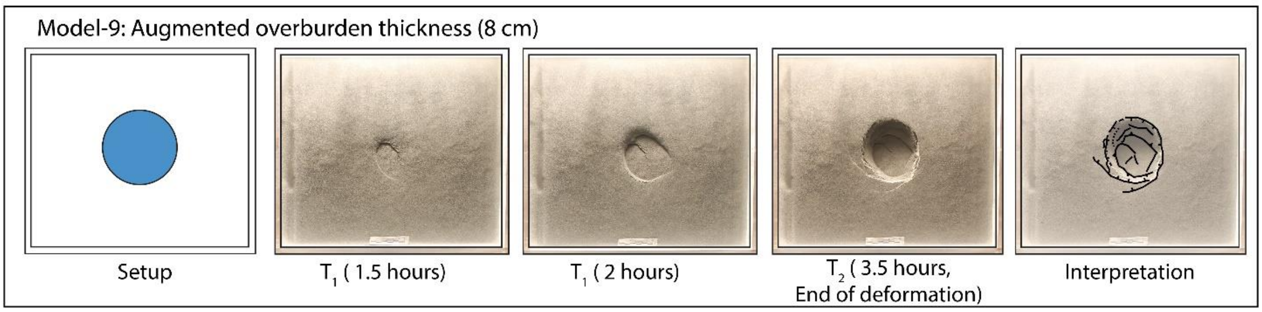

Figure 3.14. Setup, temporal evolution of deformation and schematic top view interpretation of the collapse phase of Model-9.

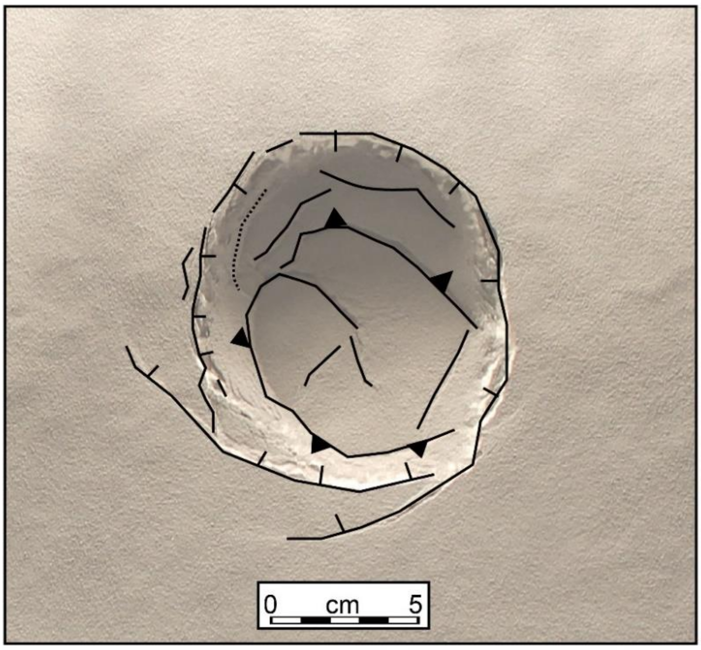

Figure 3.15. Detailed line-drawing interpretation of Model-9.

3.2 Series D3.6-2: Role of pre-caldera volcano-related topography

Series D.3.6-2 is composed of 9 models (all of them shown here below) that aimed at investigating the role of possible pre-caldera, volcano-related topography on caldera collapse processes. To this aim, we have placed a sand-mixture cone, built according to the standard procedure described in Section 2.3.2, placed at various positions with respect to the underlying analogue magma chamber. As done in other experimental series, the geometry of the latter has been varied in order to reproduce and test the effect of inherited discontinuities, both bounding the magma chamber and/or affecting the brittle overburden. In this way, we have tested the coupled role of pre-caldera volcano-related topography and inherited structures. For each model, we show the structural interpretation of model top view and the obtained digital elevation model (DEM).

3.2.1 Model-33

Model-33 is the reference model for Series D3.6-2, and was built with the standard setup of Model-17 (i.e., a circular analogue magma chamber with 6 cm sand mixture overburden), with the addition of an analogue cone simulating a pre-caldera volcano topography. The analogue cone was settled on top of model surface, and centred on the analogue magma chamber (Fig. 3.16). Model deformation proceeded similarly to other models, obtaining caldera collapse by draining the analogue magma out from the analogue magma chamber.

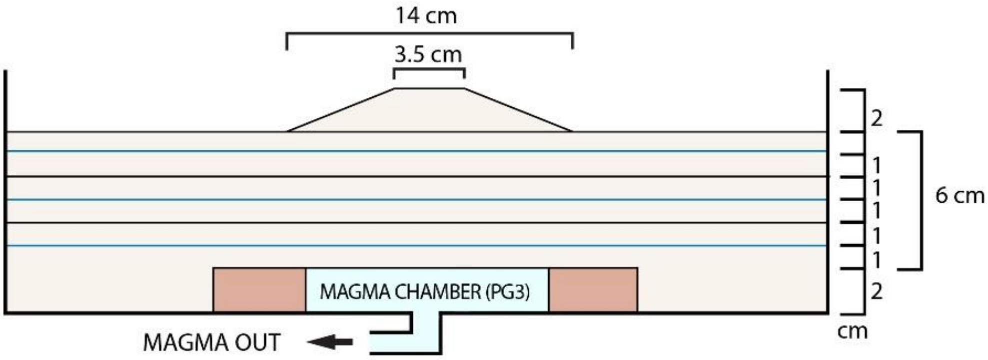

Figure 3.16. Schematic carton showing the setup (in cross section) of Model-33. Above the magma chamber and the overburden (6 cm sand-pile), we placed a standard sand cone mimicking the presence of a pre-caldera volcano. The dimension of the cone (13-14 cm diameter at the base, and 2 cm in height) here shown were reproduced in all models of Series D3.6-2.

Results of modelling show a near-symmetric caldera collapse (Fig. 3.17), as highlighted by the digital elevation model obtained at the end of the deformation phase (Fig. 3.17). Topographic profiles across the model show two topographic steps that correspond to the surficial evidence of the outward-dipping reverse fault system. In particular, on one side of the model the fault is less inclined and emerges at surface in an inner position. Nonetheless, cross sections (Fig. 3.16) show that the caldera collapse did not result in a trap-door system, laying the internal markers of deformation almost horizontal.

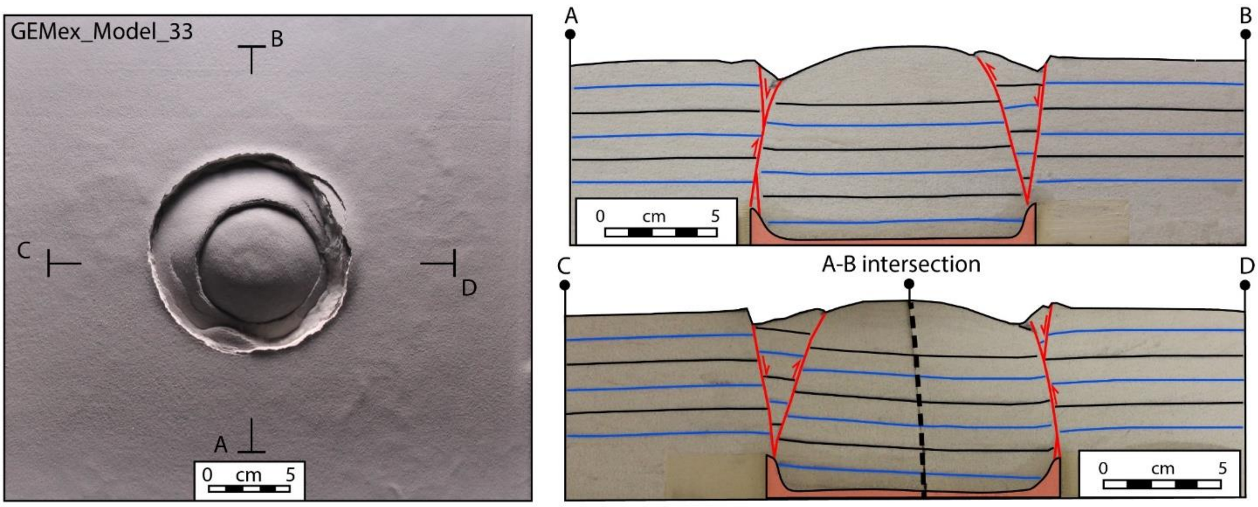

Figure 3.17. Model-33 top view and cross section showing the patter of deformation after caldera collapse. The internal architecture is similar to the standard Model-17 (Series D3.6-1): both internal outward dipping reverse faults and external inward dipping normal faults are visible.

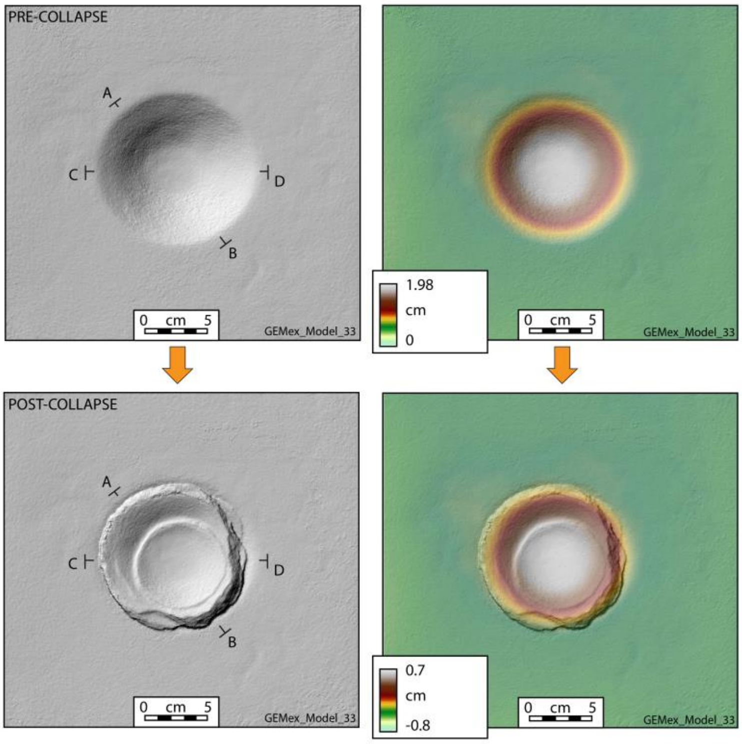

Figure 3.18. Digital elevation models (DEMs) for Model-33. The left panels show the "hillshade relief" for the pre-collapse and post-collapse phases, while panels on the right show the DEMs for the same pre-deformation and post-deformation phases. Note the perfect symmetry of the undeformed cone before caldera collapse, and the near-symmetry of he collapsed caldera.

Topographic profiles (Fig. 3.19) show a model subsidence of about 1.5 cm, and highlight the occurrence of intra-caldera relief related to pre-collapse volcanic-edifice. The overall deformation geometry of Model-33 shows near symmetric collapse, which accounts for the scarce influence of a centred pre-caldera volcano edifice on caldera collapse.

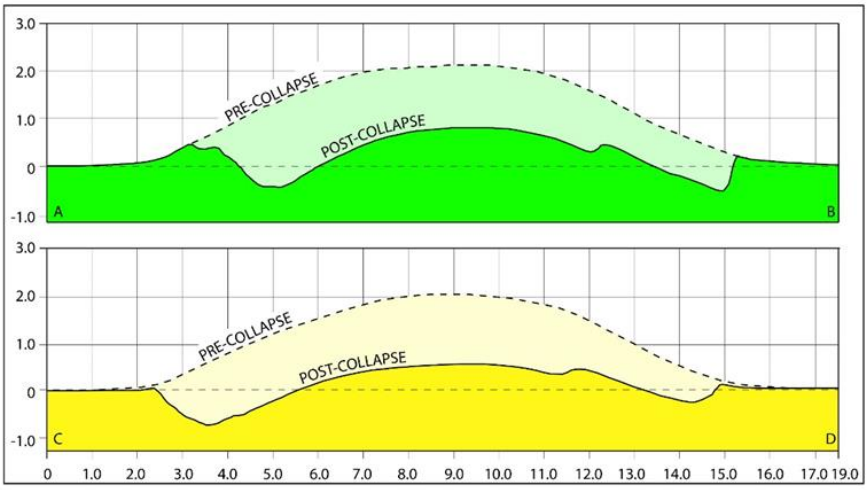

Figure 3.19. Topographic profile across two traces across model Model-33 (see position of trace AB and CD in Fig. 3.18) comparing pre-collapse and post-collapse model topography.

3.2.2 Model-41

Model-41 tested the influence of an eccentric (external) volcanic edifice on the caldera collapse process. The setup of Model-33 was modified by changing the position of the volcano, placing it almost outside the analogue magma chamber. This setup (Fig. 30) resulted in a caldera collapse showing features similar to models built without a volcano edifice. Digital elevation model (Fig. 3.21) shows the symmetry of the resulting collapsed structure with only the inward-dipping fault constituting the ring faults of the caldera system interacting with the eccentric volcano. Part of the volcanic edifice is forced to collapse inside the caldera due to the normal throw of the fault intersecting the volcano flank. The remnant of the volcanic edifice is unaffected by the caldera collapse, as well as caldera development is unaffected by the presence of the volcano.

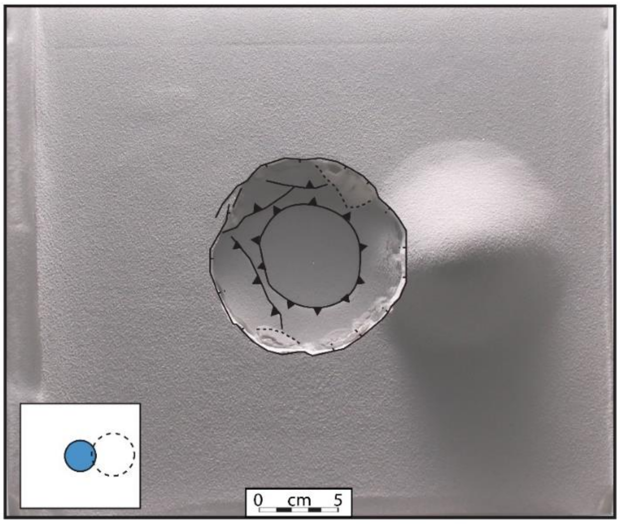

Figure 3.20. Model-41 setup (inset) and top-view with line drawing of interpreted structures.

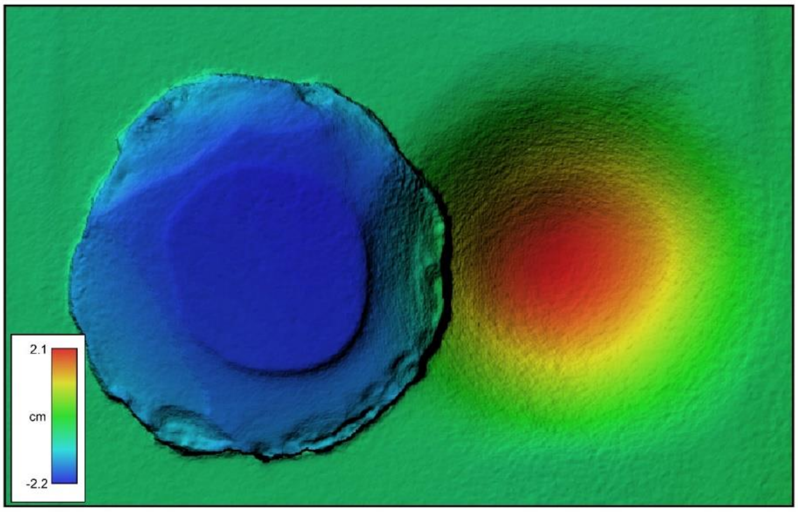

Figure 3.21. Digital elevation model (DEM) of Model-41.

3.2.3 Model-42

Model-42 tested the influence of an external volcano as Model-41, but with less eccentricity: the apex (i.e., its vertical projection) is tangent to the analogue magma border (Fig. 3.22) and the volcano shows a larger overlap with the underlying chamber.

Model deformation resulted in a gentle asymmetric collapse, showing many features similar to asymmetric models of other experimental series. In Model-42 the inner ring of outward-dipping reverse faults is "attracted" by the volcano flank, resulting in an elliptical plan-view geometry. Furthermore, on the volcano flank, the reverse faults link with the inward dipping normal fault responsible for the collapse of the analogue volcano flank. Interestingly, an array of normal faults developed on the opposite side, likely accommodating the tilting of the central piston toward the volcano (red arrow in Fig. 3.22). This behaviour is likely due to the differential vertical stress induced by the volcanic edifice partially overlapping the analogue caldera. The digital elevation model (Fig. 3.23) shows the area close to the collapsed volcano flank as the most subsided within the caldera depression.

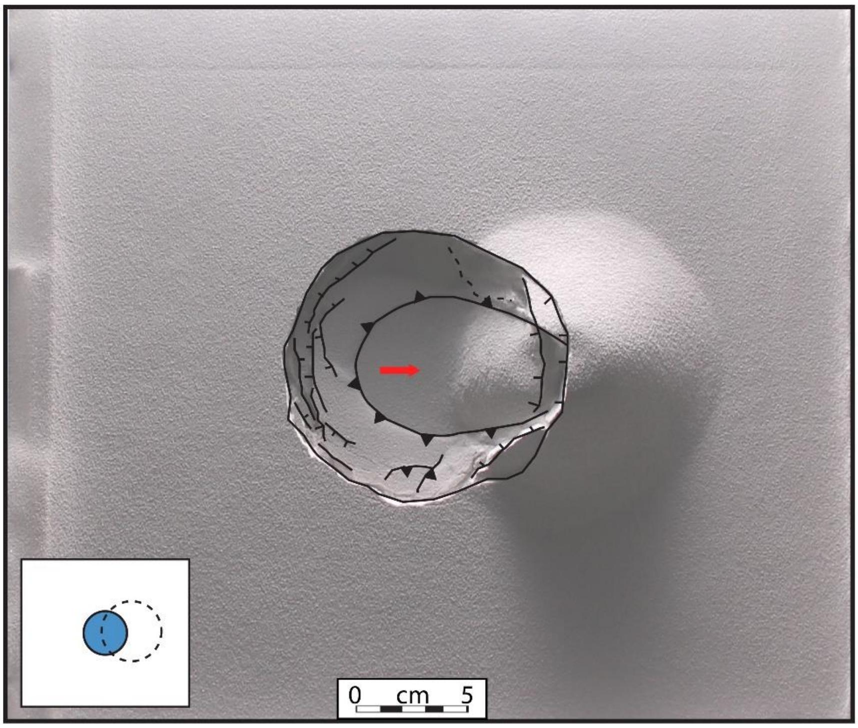

Figure 3.22. Model-42 setup (inset) and top-view with line drawing of interpreted structures.

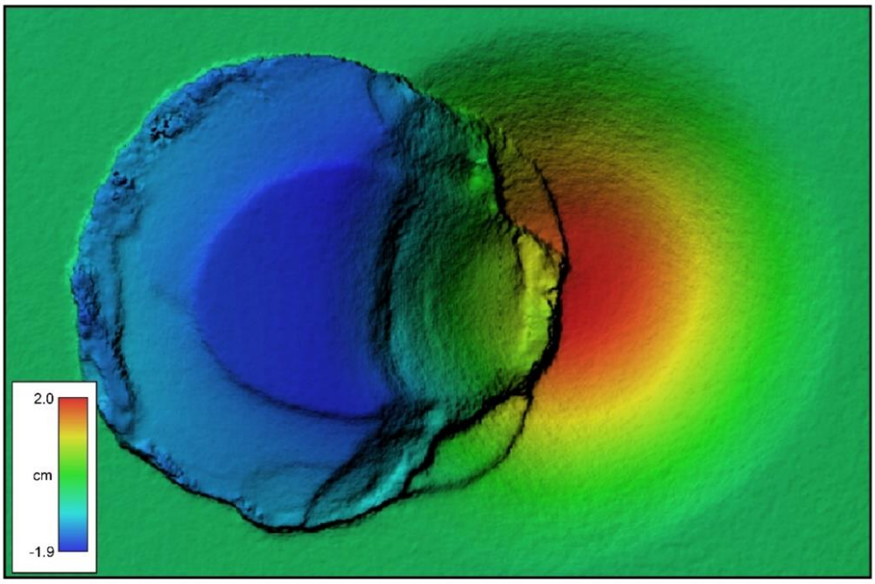

Figure 3.23. Digital elevation model (DEM) of Model-42.

3.2.4 Model-43

In Model-43 we tested the coupled effect of a volcano edifice and structural inherited discontinuities. To this aim, we placed the volcano edifice in a centred position above the analogue magma chamber, which in this specific setup, was designed with a rectilinear side, simulating an inherited fault bounding the magma chamber (according to procedure described in Section 2.4.1).

Model development resulted in a symmetric caldera collapse (i.e., the central piston subsided symmetrically, Figs. 3.24 and 3.25), yet, the fault pattern experienced some modifications due to the presence of an analogue magma chamber with a rectilinear side. As described in Deliverable D3.5 for models of Series D3.5-2c, the presence of this feature (which mimics an inherited discontinuity bounding the magma chamber) affects the development of the reverse and normal fault systems, forcing faults to propagate along a rectilinear trajectory. Therefore, in correspondence of the rectilinear side, the collapsed caldera developed an inner rectilinear reverse fault and an outer rectilinear normal fault segment (Figs. 3.24 and 3.25),

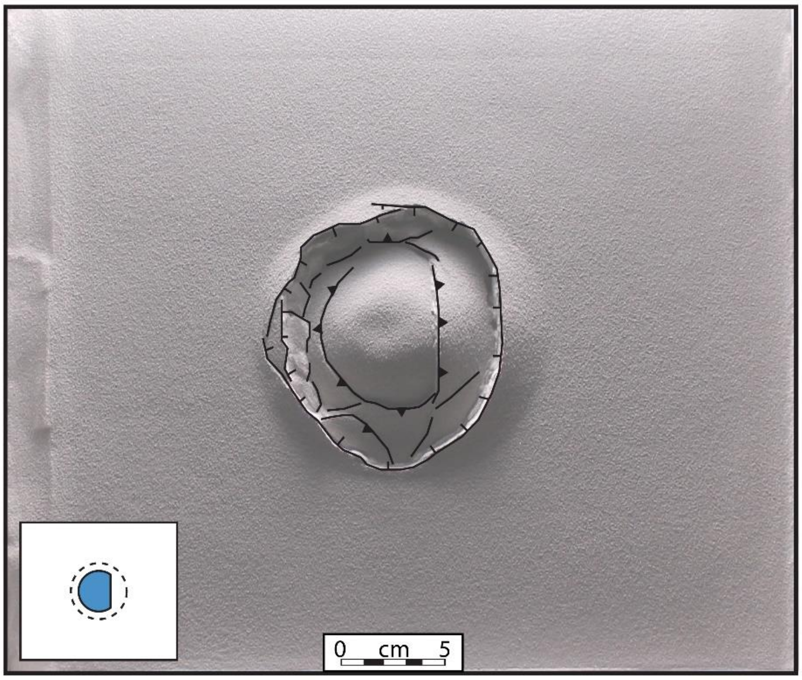

Figure 3.24. Model-43 setup (inset) and top-view, with line drawing of interpreted structures.

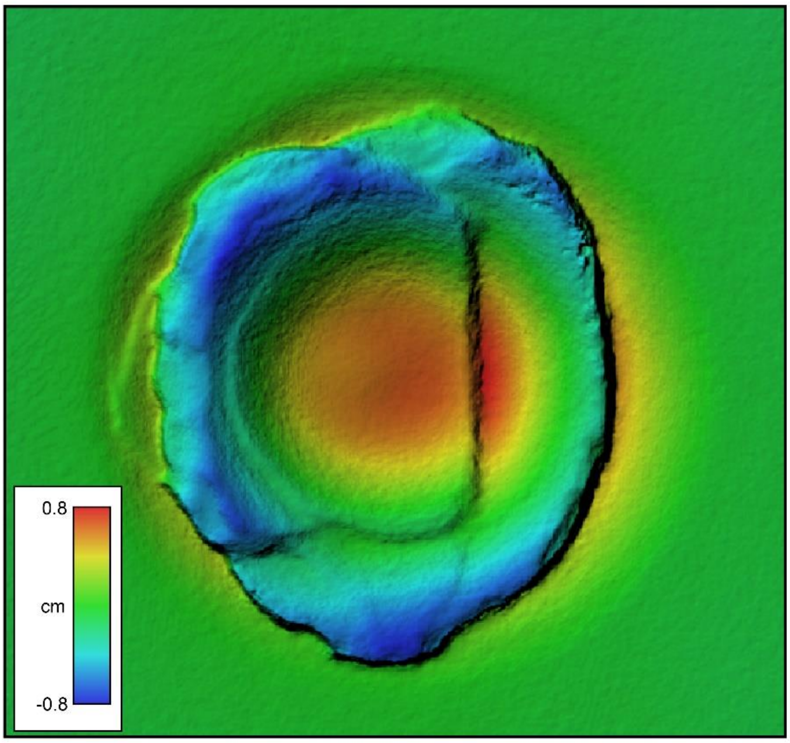

Figure 3.25. Digital elevation model (DEM) of Model-43.

3.2.5 Model-44

Setup of Model-44 was designed similar to Model-43, but with the volcano edifice placed in an eccentric position, with the vertical projection of the volcano apex tangent to the rectilinear side of the analogue magma chamber. The aim of this model is to test the coupled effect of an inherited structure bounding the analogue magma chamber and the presence of an eccentric volcano. The result of the modelling (Fig. 3.26) is not dissimilar to Model-43. Nonetheless, the presence of the eccentric volcanic edifice developed a low degree of asymmetry in the collapse of the central piston (as visible in the DEM, Fig. 3.27), not observed in Model-43. This asymmetry is also manifested by the presence of incipient normal faults on the opposite side of the collapsed volcano flank, as a result of the roof tilting. As in Model-43, rectilinear inner reverse and outer normal faults developed in correspondence of the rectilinear side of the analogue magma chamber (Figs. 3.26 and 3.27).

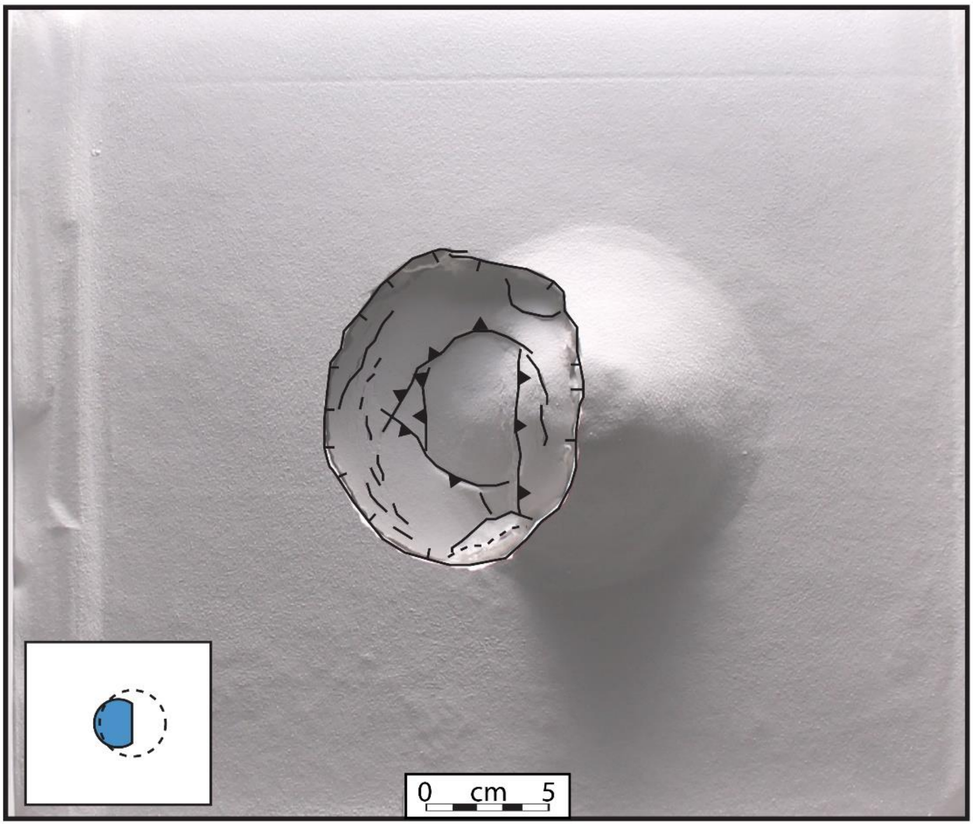

Figure 3.26. Model-44 setup (inset) and top-view with line drawing of interpreted structures.

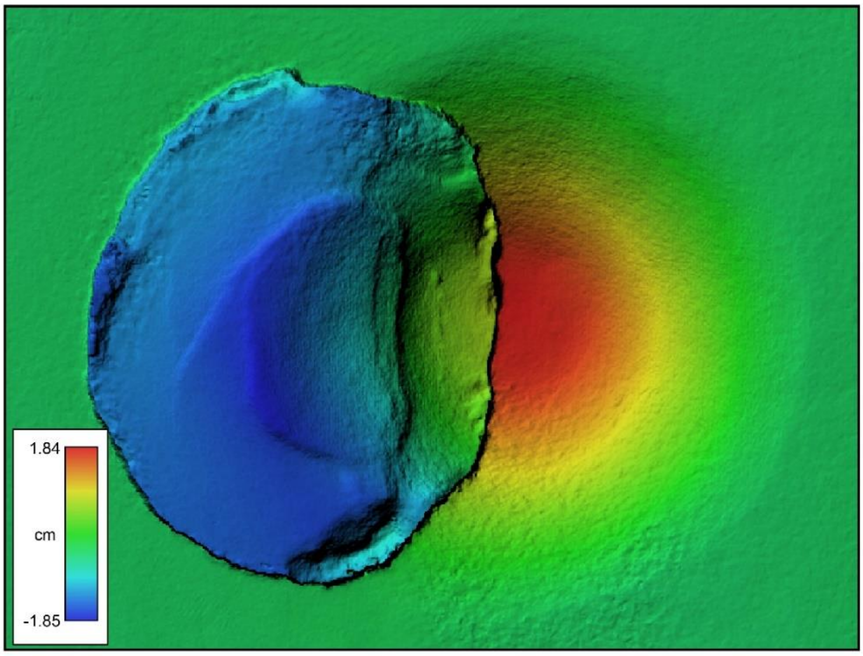

Figure 3.27. Digital elevation model (DEM) of Model-44.

3.2.6 Model-45

Model-45 replicates the setup of Model-44, with the difference that the inherited discontinuity bounding the analogue magma chamber also extend through the overlying overburden sand pack, according to the procedure described in Section 2.4.1.

The deformation pattern resulting from caldera collapse is similar to Model-44, yet with a less marked asymmetry (Fig. 3.28 and 3.29). Furthermore, the role of inherited structures crosscutting the overburden sand package is in agreement with evolution of Series D3.5-2d models described in Deliverable D3.5. In particular, models of Series D3.5-2d showed that a discontinuity bounding the analogue magma chamber and crosscutting the overburden package force the development of a single, high-angle normal fault at the caldera rim, inhibiting the formation of a rectilinear reverse fault belonging to the inner outward-dipping reverse fault system. The deformation pattern of Model-45 thus shows a similar evolution. The external normal faults do not show a perfect rectilinear trace in map view, as a consequence of the interaction between the fault and the volcanic edifice topography.

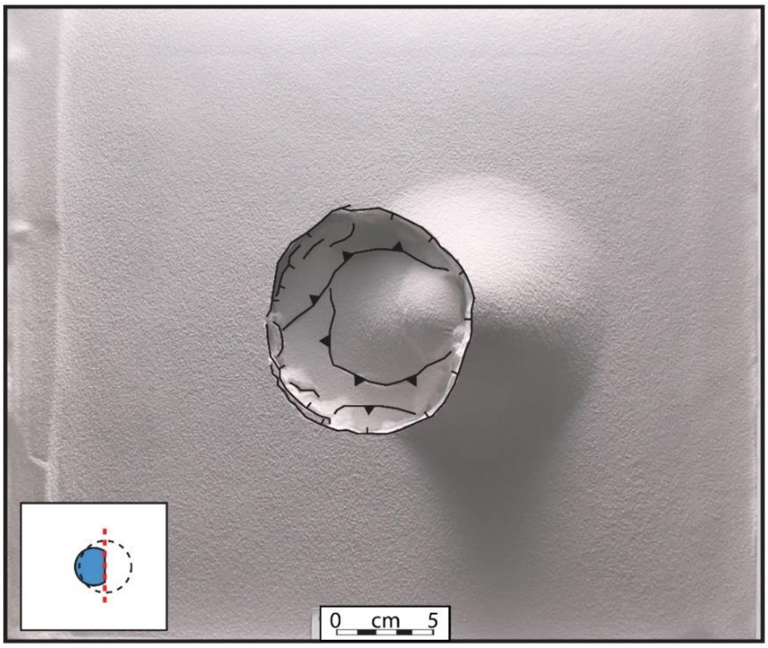

Figure 3.28. Model-45 setup (inset) and top-view with line drawing of interpreted structures. The red dashed line in the setup marks the position of the introduced inherited discontinuity crosscutting the whole overburden.

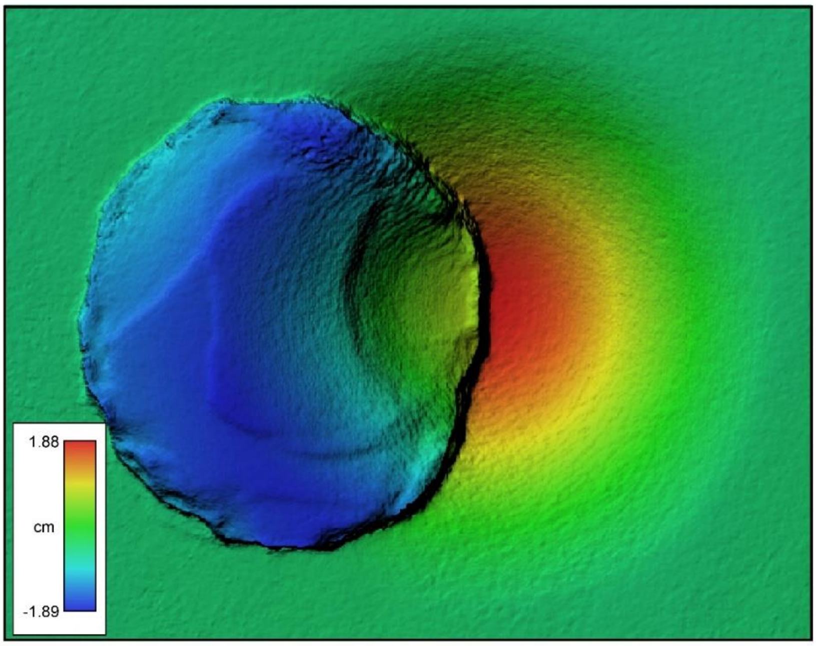

Figure 3.29. Digital elevation model (DEM) of Model-45.

3.2.7 Model-46

Model-46 was setup to investigate the effect of two inherited, orthogonal faults coupled with the presence of a centred volcanic edifice. This model thus differs from Model-43 for the presence of a second discontinuity. Model deformation shows no major variations in comparison to Model-43, as both a rectilinear inner reverse fault and an outer normal fault develop in correspondence of one rectilinear side of the analogue magma chamber (Fig. 3.30 and 31). Conversely, in correspondence of the second rectilinear side, we observe only a rough rectilinear normal fault, the presence of a rectilinear reverse fault being masked by internal caldera deformation. Regardless, this model outcome is consistent with the deformation pattern of the similar Model-43.

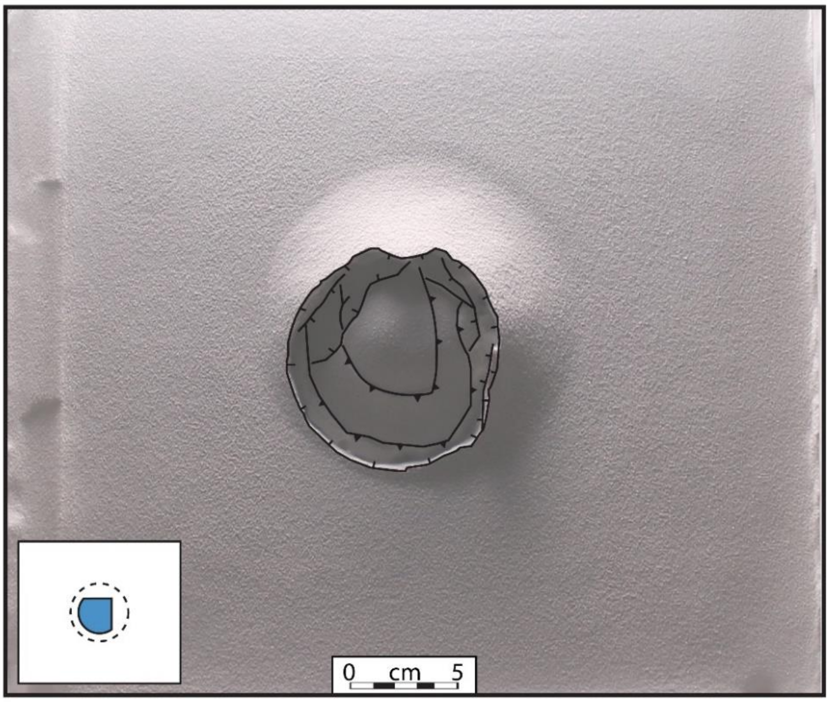

Figure 3.30. Model-46 setup (inset) and top-view with line drawing of interpreted structures.

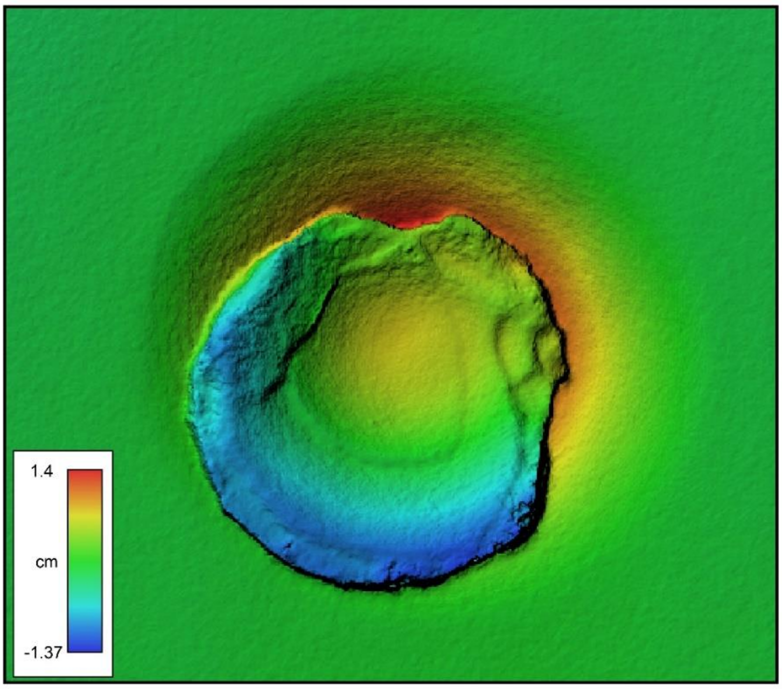

Figure 3.31. Digital elevation model (DEM) of Model-46.

3.2.8 Model-47

Model-47 was setup to test the effect of two inherited, orthogonal discontinuities bounding the analogue magma chamber (similar to Model-46), coupled with the effect of an eccentric volcanic edifice (see setup in Fig. 3.32). In this case, model deformation implied the formation of two external rectilinear normal faults and a more complex internal architecture, likely complicated by the effect of the eccentric volcanic edifice. A rectilinear reverse fault is visible on the right part of the model (red arrow in Fig. 3.33), running parallel to the rectilinear normal fault. The other fault - which is expected to follow the other rectilinear side of the underlying analogue magma chamber - follows instead a trajectory that is oblique to this side of the chamber (yellow arrow in Fig. 3.33). This behaviour is possibly due the interaction of caldera faults with the collapsing flank of the eccentric analogue volcanic edifice.

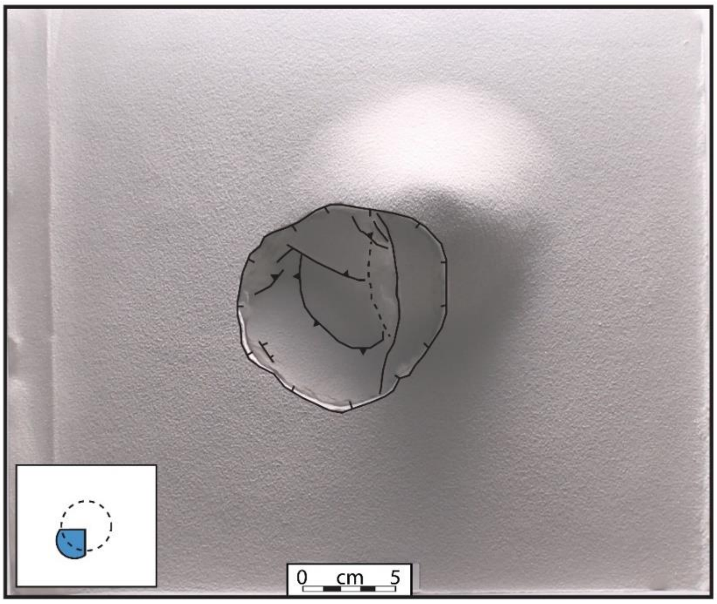

Figure 3.32. Model-47 setup (inset) and top-view with line drawing o of structures.

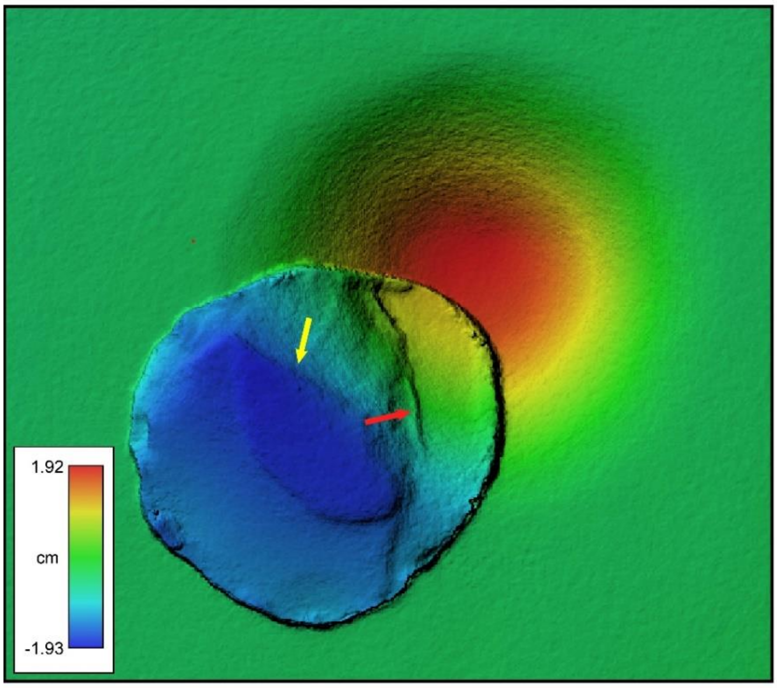

Figure 3.33. Digital elevation model (DEM) of Model-47. Red and yellow arrows indicate structures of interests (see the text for details).

3.2.9 Model-48

Model-48 tested a setup similar to Model-47, with the difference that the two artificial discontinuities crosscut the whole overburden, thereby mimicking inherited faults that bound the analogue magma chamber and extend up to the surface (see procedure described in Section 2.4.1).

Based on the results of Model-45, Model-48 was expected to develop two rectilinear normal faults at the caldera rim, inhibiting the formation of internal rectilinear reverse faults. Model-48 perfectly reproduced such an expected deformation pattern (Fig. 3.34 and 3.35). In addition, Model-48 also developed an asymmetric collapse of the central piston due to the differential vertical load induced by the collapsing volcano flank, which was accommodated by a fault with unclear kinematics. Similar to other models, the asymmetric collapse developed an array of normal faults on the less subsided part of the caldera piston, accommodating the tilting of the internal block.

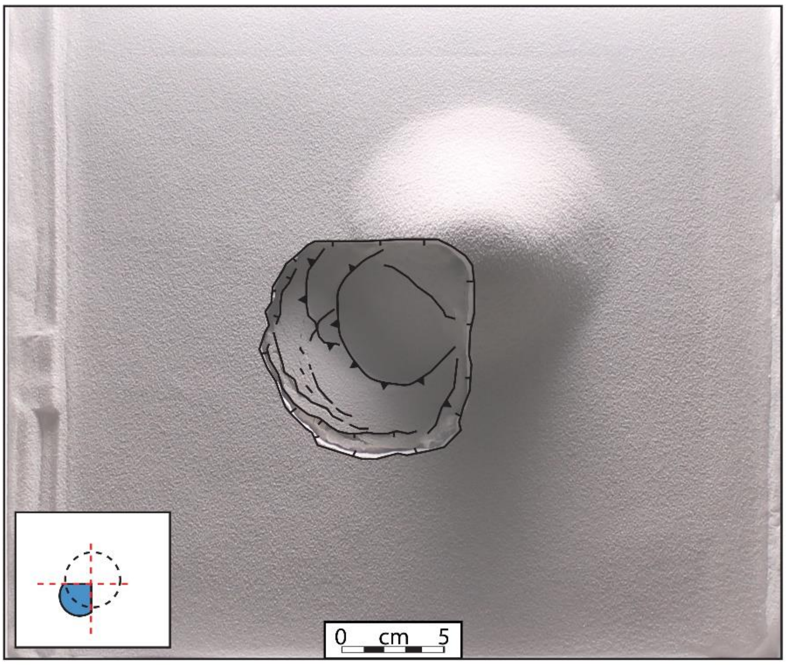

Figure 3.34. Model-48 setup (inset) and top-view with line drawing of interpreted structures. The red dashed lines in the setup mark the position of artificial inherited discontinuities crosscutting the whole overburden.

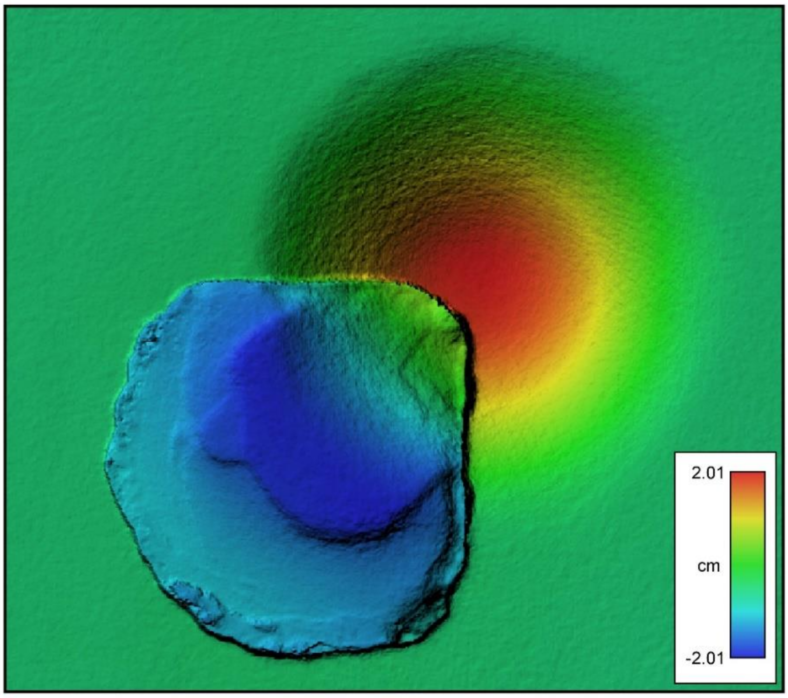

Figure 3.35. Digital elevation model (DEM) of Model-48.

3.3 Series D3.6-3: Caldera resurgence and interaction with pre-existing structures (both regional inherited fabrics and caldera collapse faults)

Series D3.6-3 aims to test caldera resurgence and its interaction with inherited structures. According to this aim, the model are shown below grouped in three specific sub-series:

- Sub-series D3.6-3a: Effect of "piston like" resurgence on symmetric/asymmetric collapsed calderas

- Sub-series D3.6-3b: Effect of localized resurgence on collapsed calderas

- Sub-series D3.6-3c: Effect of resurgence and presence of inherited faults on collapsed calderas

3.3.1 Sub-series D3.6-3a: Effect of "piston like" resurgence on a symmetric/asymmetric collapsed caldera

3.3.1.1 Model-7

Model-7 shows the result of caldera resurgence applied to collapsing phase, which has been previously described in Series D3.6-1. At the end of caldera collapse (Fig. 3.36), the analogue magma (PG3) was re-injected at the base of the model, inside the analogue magma chamber, to induce caldera resurgence. The

Polyglycerine-PG3 slowly flowed below the collapsed roof block (or piston) and induced a uniform, broad (i.e., piston-like) caldera resurgence that affected the structural pattern of the whole model.

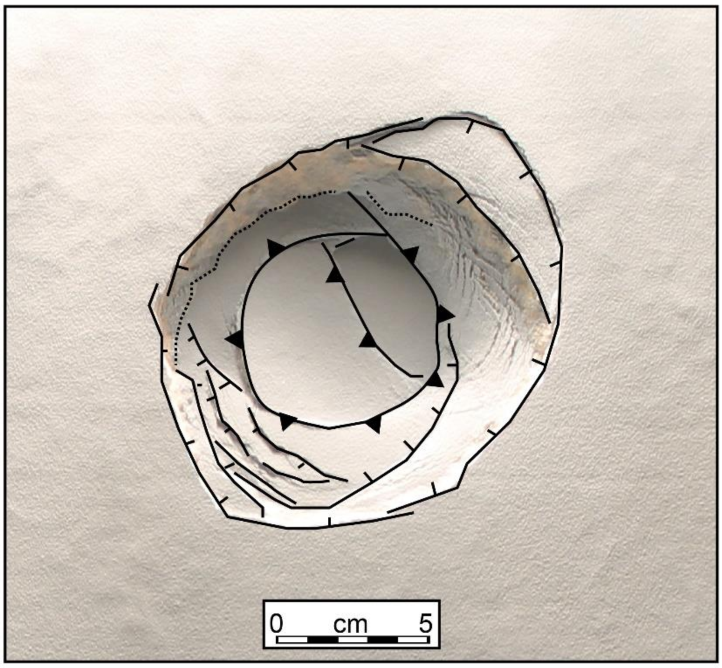

Figure 3.36. Deformation of Model-7 at the end of caldera collapse phase (see Section 3.1). Caldera resurgence was applied after this deformation stage.

The effect of caldera resurgence on Model-7 are shown in Figure 3.36. The interpreted line drawing of structures highlights the presence of both reactivated (inverted) and newly-formed faults. In particular, a new reverse fault crosscuts the central resurgent piston, accommodating deformation. Nonetheless, deformation associated with resurgence is largely accommodated by ring normal faults that were reactivated and partly recovered the extensional throw acquired during caldera collapse. This normal fault system accommodating caldera collapse (described in Section 3.1 for Model-7) is strongly reactivated during caldera resurgence. Interestingly, some normal faults that delimit the central piston increase their vertical normal throw to accommodate rotation and uplift of the roof (trap-door) block, as shown in the model cross section (Fig. 3.37). Evolution of Model-7 indicates that in the case of a trap-door caldera system, a broad piston-like resurgence increases the degree of asymmetry due to differential uplift of the caldera roof block.

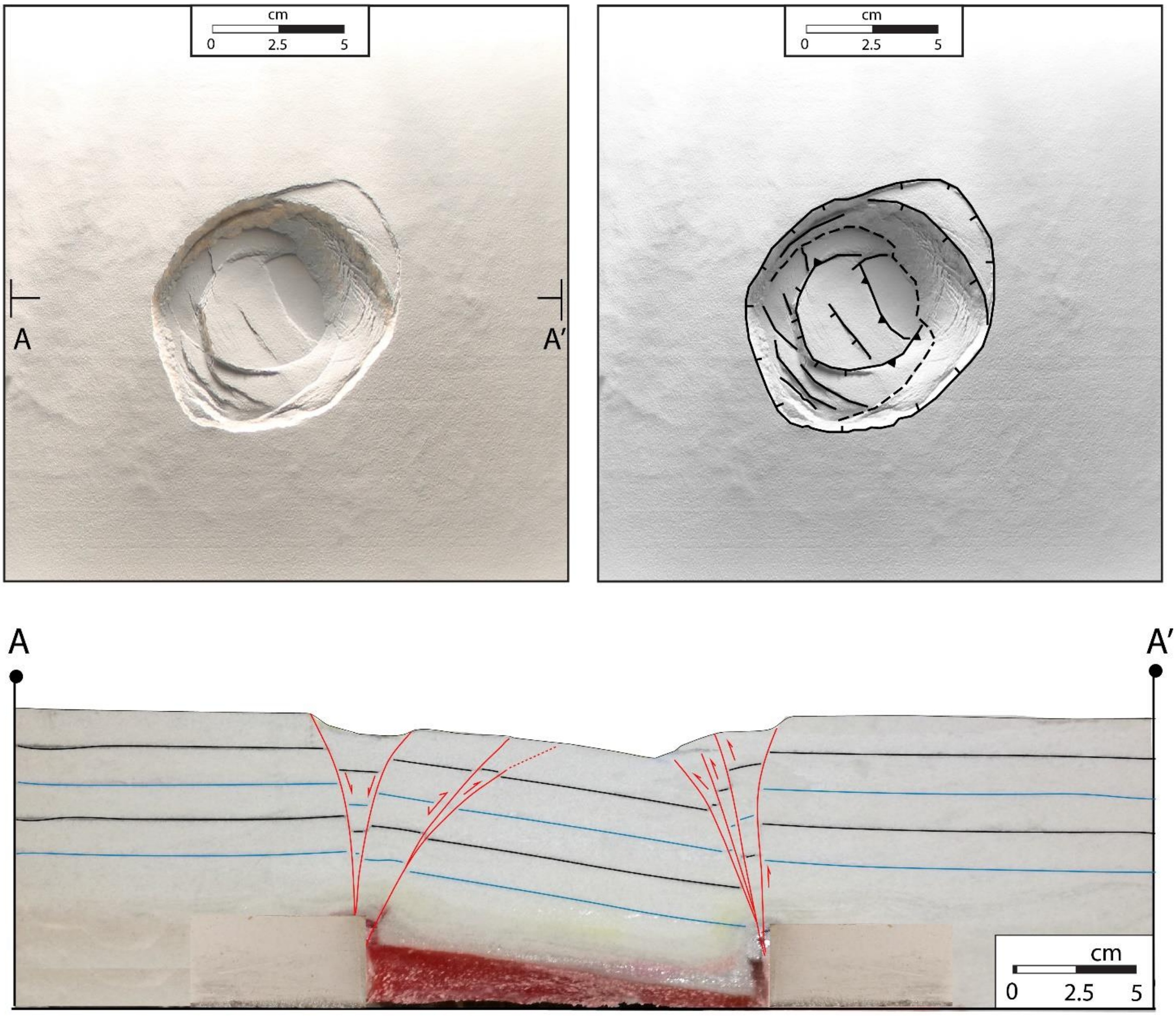

Figure 3.37. Top view of Model-7 at the end of caldera resurgence (left upper panel) with interpretation of structure (right upper panel). The interpreted model cross section (lower panel) shows reactivation of collapse-related structure, and formation of new faults induced by caldera resurgence. The newly re-intruded analogue magma PG3 is the reddish fluid.

3.3.1.2 Model-8

Model-8 tested the effect of a reduced overburden thickness on caldera collapse, and afterward, on caldera resurgence. Therefore, the model was set up with 4 cm of overburden thickness (2 cm less than standard). The collapse phase of Model-8 has been shown earlier in Series D.3.6-1; Figure 3.38 shows the final stage of caldera collapse, as interpreted in Section 3.1. Caldera collapse resulted in a trap-door system showing a structural pattern similar to Model-7, with the normal fault system accommodating deformation.

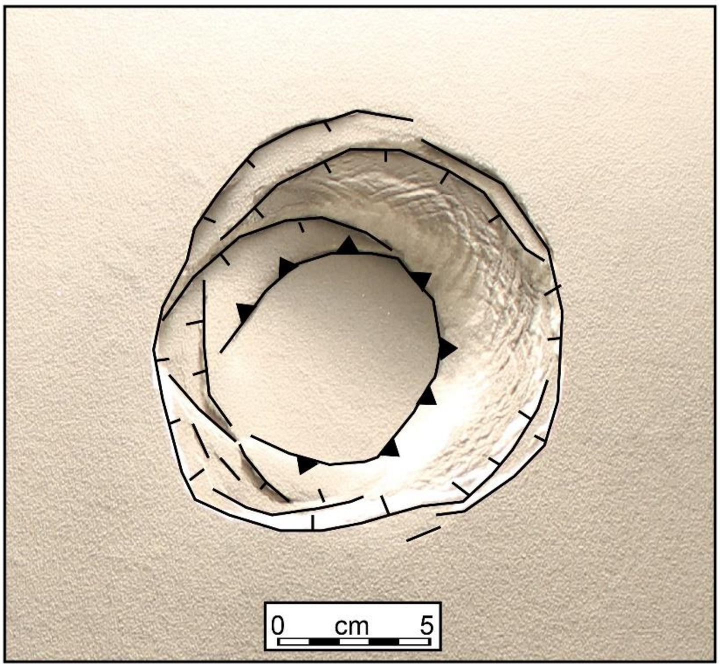

Figure 3.38. Deformation of Model-8 at the end of caldera collapse phase (see Section 3.1).

Intra-caldera resurgence was obtained by intruding an analogue magma (PG3) at the base of Model-8, in order to induce a broad, piston-like resurgence. The central roof block was progressively tilted during caldera resurgence (Fig.3.39). During this process, some ring normal faults were reactivated by the analogue magma re-intrusion, and often regained part of the original vertical throw. The final model outcome depicts a well-developed, piston-like resurgent asymmetric (trap-door) system.

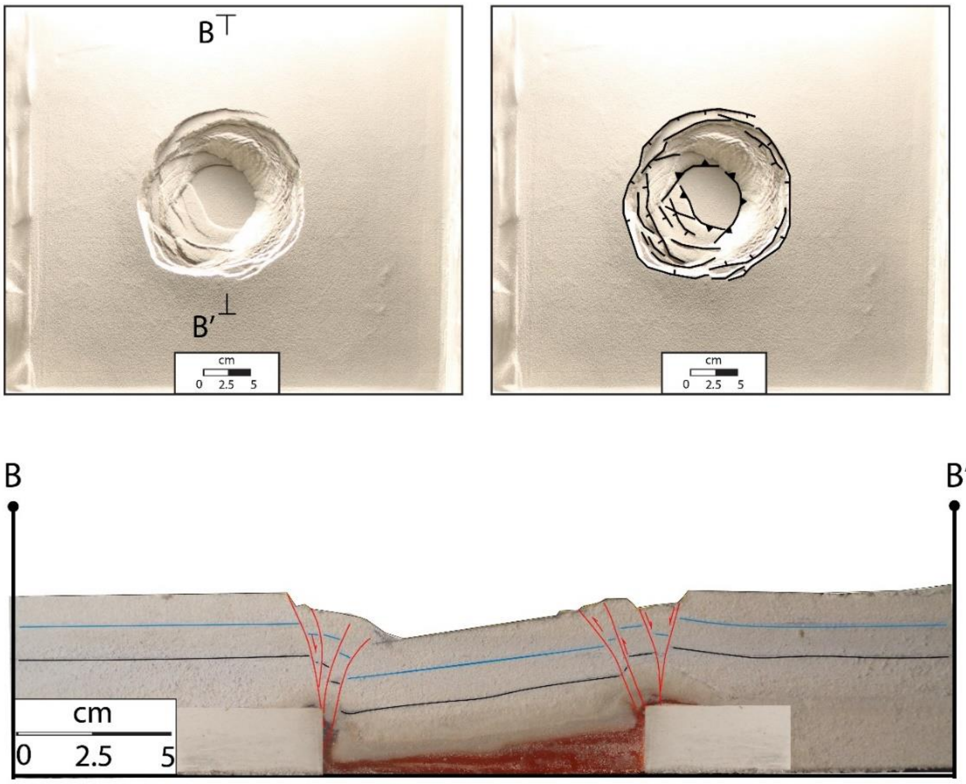

Figure 3.39. Top view of Model-8 after caldera resurgence (left upper panel) with interpretation of the resulting structural pattern (right upper panel). As for Model-7, the interpreted model cross section (lower panel) shows reactivation of collapse-related fault systems accommodating caldera collapse. The newly re-intruded analogue magma PG3 is the reddish fluid.

3.3.1.3 Model-9

Model-9 investigated the influence of a increased overburden thickness on caldera collapse, and afterward, on caldera resurgence. Therefore, the model was set up with 8 cm of overburden thickness (2 cm more than standard). The caldera collapse phase of Model-9 has been shown earlier in Section 3.1. The resulting caldera collapse can be described as symmetric caldera collapse, yet with some peculiarities, such as an atypical pattern of structures inside the piston (roof) block, as well as the occurrence of fault branches at the caldera ring propagating both outward (in plain view) and radially (Fig. 3.40).

As in the previous models of this series, broad caldera resurgence was induced by intruding Polyglycerine PG3 at the base of the analogue magma chamber. In this model, the effect of caldera resurgence simply resulted in the uplift of the central piston, forcing the caldera ring faults to partly recover their original throw, as observable on both model top-view and cross-section (Fig. 3.41). Since the piston block subsided vertically during caldera collapse, the broad caldera resurgence did not originate any new structure, differently to what observed in asymmetric Model-7 and Model-8.

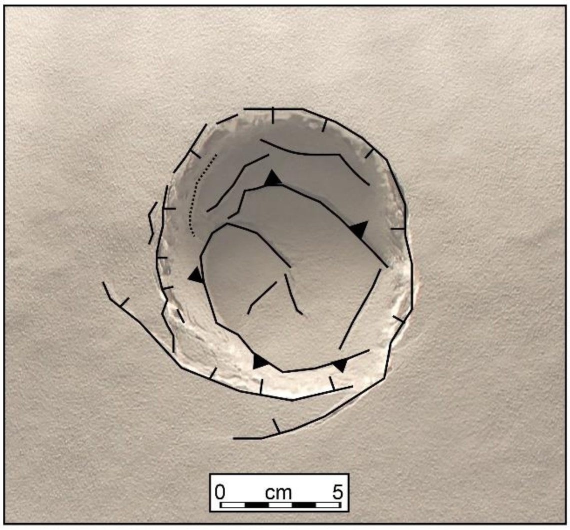

Figure 3.40. Top view interpretation of the structural pattern resulting from caldera collapse of Model-9.

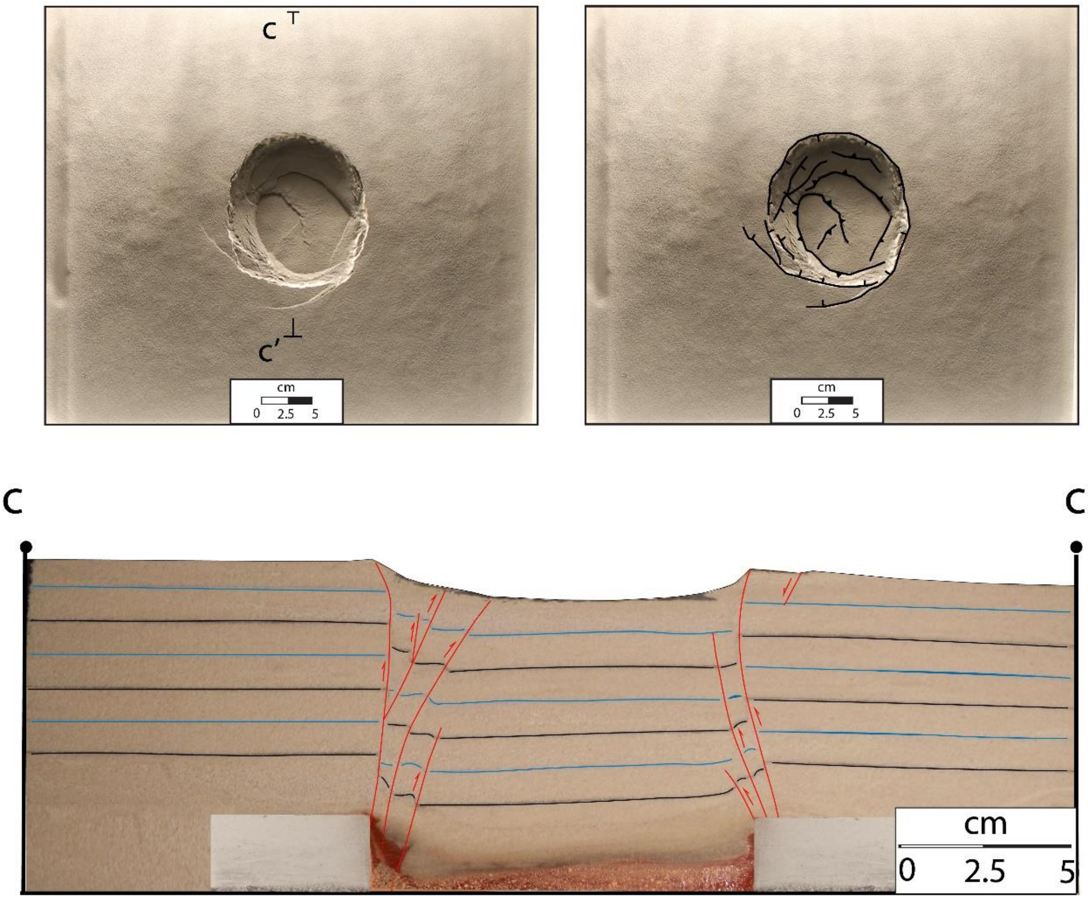

Figure 3.41. Top view of Model-9 after caldera resurgence (left upper panel) with interpretation of the resulting structural pattern (right upper panel). Interpreted model cross section (lower panel) shows reactivation of collapse-related structure and normal fault system accommodating deformation during caldera collapse. The newly re-intruded analogue magma PG3 is the reddish fluid.

3.3.1.4 Model-19

Model-19 differs from previous models of Sub-series D3.6-3a, since it was designed to investigate the influence of a high-viscosity analogue magma re-intruding the collapsed caldera. The results of the first deformation phase (i.e., the collapsing phase) is shown in Figure 3.42, and was obtained by draining out the PG3 fluid from the analogue magma chamber. Model deformation produced a gentle asymmetric caldera collapse, clearly showing the inner outward-dipping ring reverse faults and outer inward-dipping normal faults. Faults in the upper part (top view) of model surface acquire a larger throw, causing the caldera piston block to gently dip toward this direction (red arrow in Fig. 3.42).

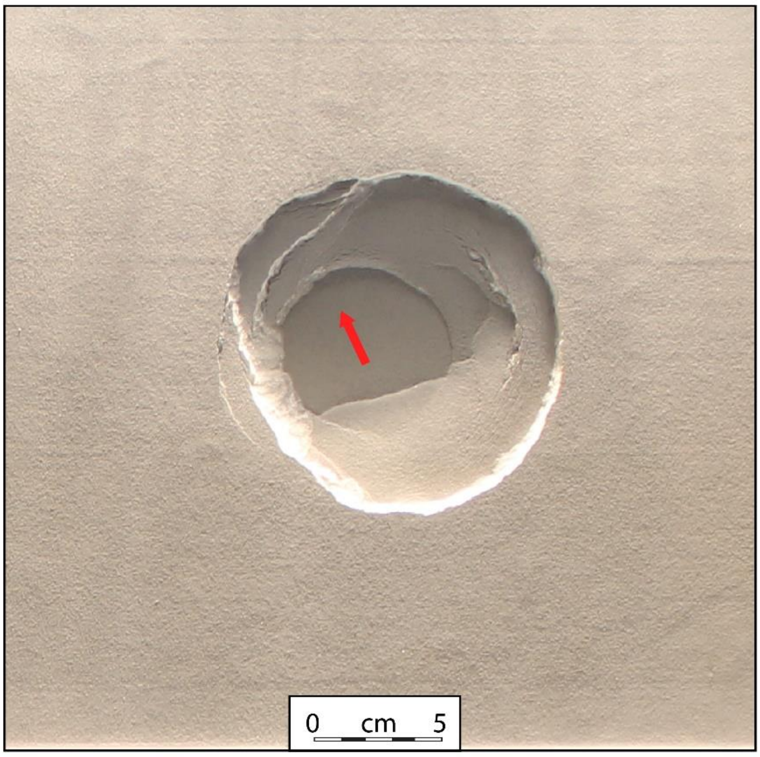

Figure 3.42. Model-19 result of caldera collapse. The red arrow indicates the dip direction of the gentle asymmetric roof block.

Differently to the previous models, in Model-19 we induce piston-like caldera resurgence by re-injecting PG10 fluid, which has a density higher than PG3. Re-intrusion of the analogue magma exploits the collapse-related asymmetry and increases the tilting of the trap-door system (Fig. 3.43). Due to the asymmetric resurgence, the model developed newly-formed faults, which are similar to those previously described for models experiencing trap-door caldera collapse. Model cross section (Fig. 3.43) highlights the intrusion of PG10 in a lateral position, which creates (during progressive upward migration) a gentle doming and consequent tilting of the resurging caldera piston.

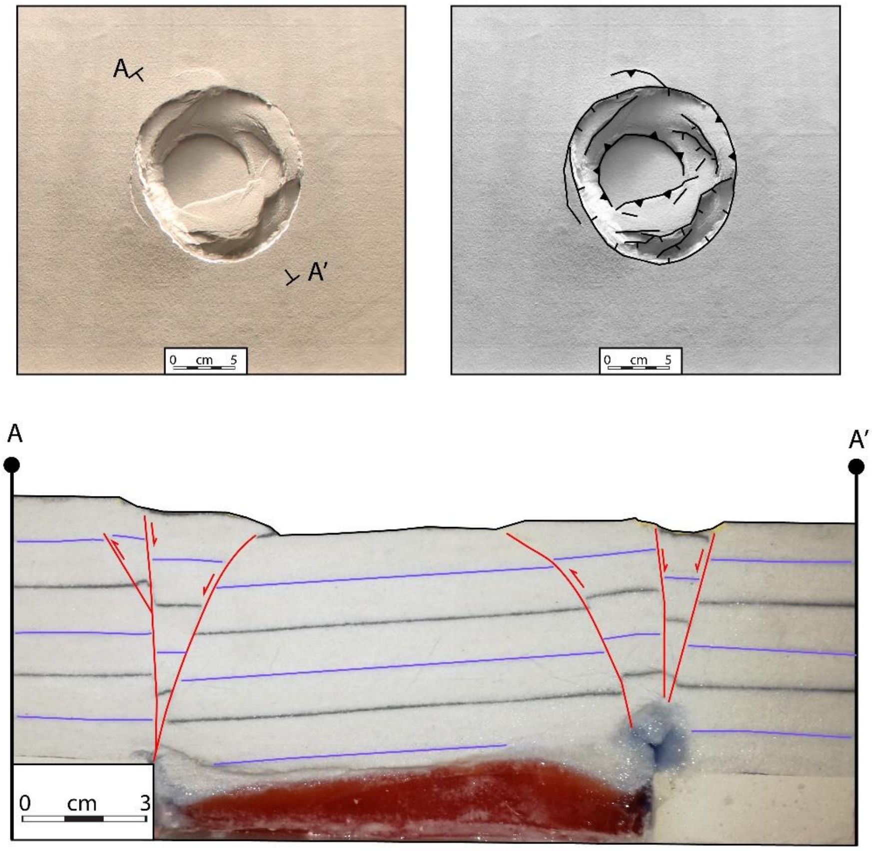

Figure 3.43. Top-view of Model-19 after caldera resurgence (left upper panel) with interpretation of the resulting structural pattern (right upper panel). Interpreted model cross section (central panel) shows reactivation of collapse-related fault systems that accommodate deformation during caldera collapse, that is typical of models showing a trap-door collapse style. The newly re-intruded analogue magma PG3 is the reddish fluid, while the greyish-bluish area represent the residual PG3 used to produce initial caldera collapse and that has been intruded during resurgence.

The final caldera resurgence outcome of Model-19 consists of a tilted trap-door system with a more subsided area, which is highlighted by blue colour in the DEM shown in Fig. 3.44. This area is located in the opposite side with respect to the normal fault system accommodating the upward tilting of the roof block. Finally, another remarkable effect of caldera re-intrusion regards the observation that the re-injected PG10 (in red colour in model cross section of Figure 3.44) causes the residue of original PG3 fluid (coloured in blue) to migrate upward and exploit boundary faults (Fig. 3.43).

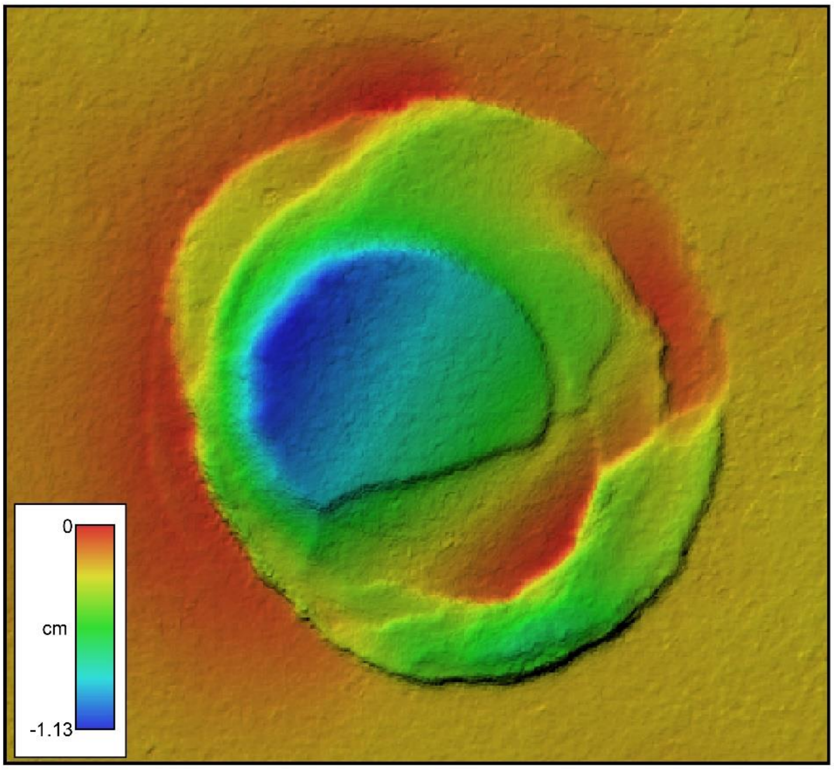

Figure 3.44. Digital elevation model (DEM) of caldera resurgence obtained for Model-19.

3.3.2 Sub-series D3.6-3b: Effect of localized resurgence on collapsed calderas

Models belonging to sub-series D3.6-3b aimed to test the effect of a localized resurgence on the structural pattern of collapsed calderas. To test the conditions at which localized resurgence can be obtained, and the consequent effect on caldera structures, we performed five models with a standard setup (4 of which are shown as the most significant), but with different reinjection depths below the model surface. In particular, we systematically varied the intrusion depth from shallow (3 cm below the model surface) to deep (5 cm below the model surface) over a total overburden thickness of 6 cm. The intrusion rates of analogue magma was kept constant for all models of this series, and settled at 80 cm/h. Re-injection at the desired depth was obtained by introducing a small tube (diameter of 0.4mm) from the base of the model. In order to not perturb the internal architecture acquired during caldera collapse and resurgence, the tube was removed only after the end of model deformation (i.e., when the model was wet, frozen, and then sectioned).

Different depths of intrusion resulted in different resurgence styles and structural patterns, which are systematically described below.

3.3.2.1 Model-77

Model-77 was set up as standard model (circular analogue magma chamber filled with PG3 fluid) and overlaid by a 6 cm thick sand mixture overburden. This model aimed to test the effect of intra-caldera magma re-intrusion at shallow levels, and, therefore, the re-injection point was fixed at 3 cm below the model surface (Fig. 3.45).

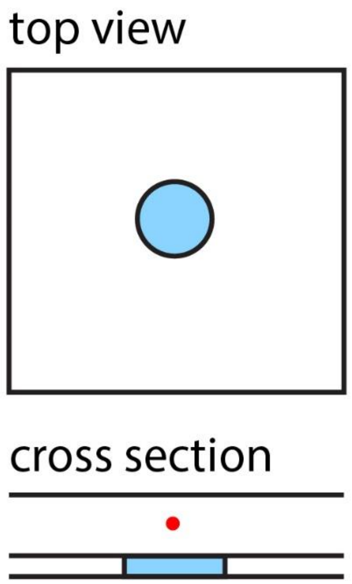

Figure 3.45. Model-77 setup (top view and cross section). A circular analogue magma chamber is placed below a 6cm-thick sand overburden. The red dot indicates the depth of magma reinjection (3 cm below model surface).

PG3 reintrusion induces the analogue magma to migrate upward following a dyke-like trajectory (Fig. 3.46), which firstly induced a superficial bulging (or doming) and then extruded at the model surface (not shown in Fig. 3.46). The original internal collapsed caldera architecture is modified by reintrusion of the analogue magma, which created reverse faults propagating upward consequently to the migration of PG3 fluid. This process resulted in a well-defined, circular surface budging. Digital elevation model (Fig. 3.47) and line-drawing interpretion of top view photos highlight the effect of magma re-intrusion at surface. Interestingly, the resurgent dome is characterised by radial fractures and few major rectilinear faults that accommodate superficial extension. One or more of these faults are the most likely to have facilitated the extrusion at surface of the PG3 analogue magma.

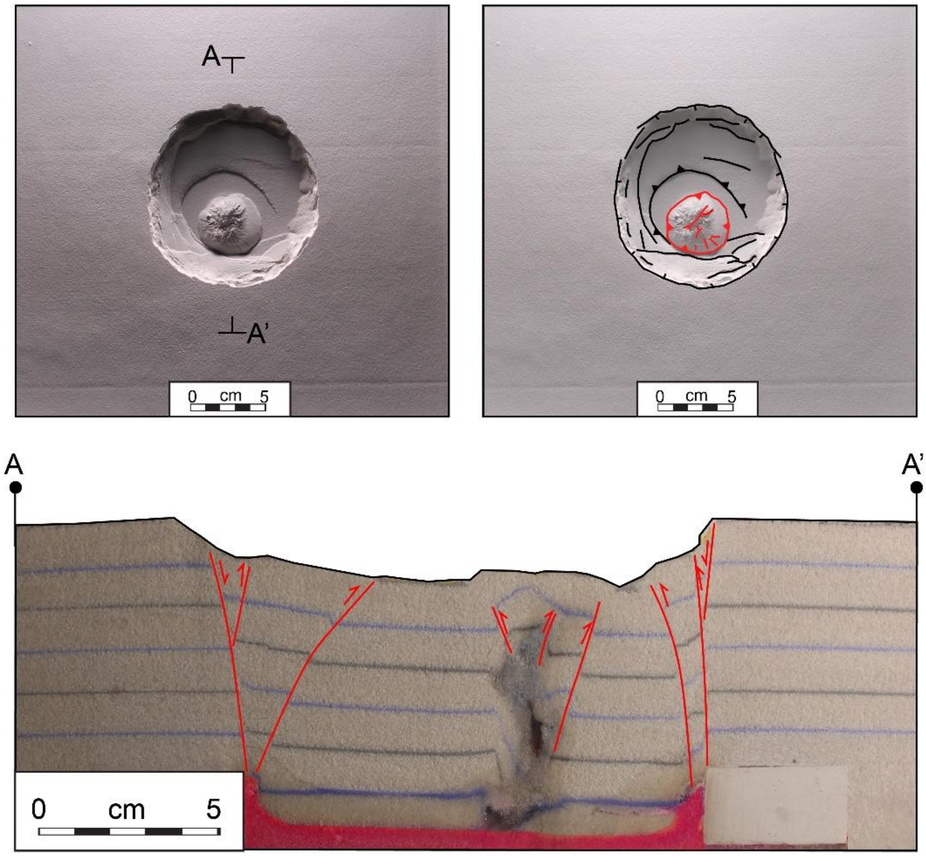

Figure 3.46. Top view of Model-77 after caldera resurgence phase (left upper panel) with interpretation of structures (right upper panel). Such top view photo was taken immediately before the analogue magma extruded at the model surface. Red lines on model top view denotes the newly-formed faults induced by magma re-injection. Interpreted model cross section (lower panel) shows the remnant of analogue magma (PG3 fluid in red) not extruded during the caldera collapse phase, as well as the newly re-intruded magma (PG3, greyish-bluish area) that generated a vertical dyke and a related surface bulging.

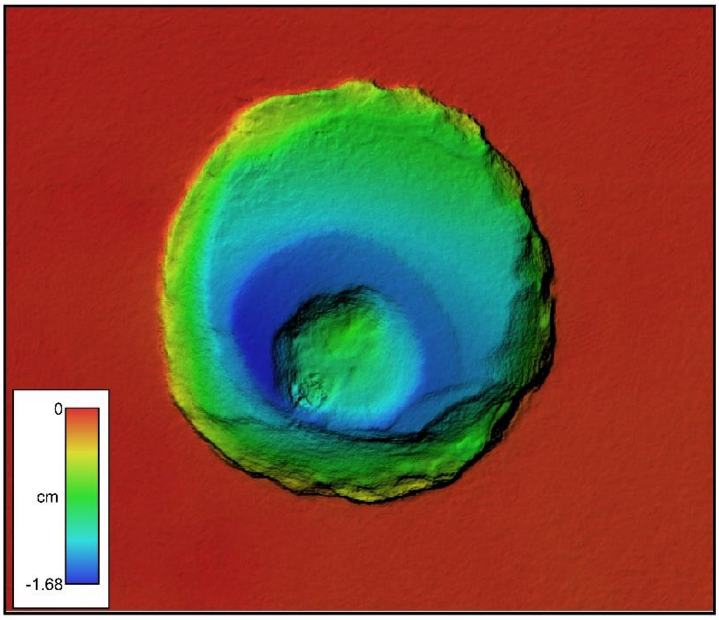

Figure 3.47. Digital elevation model (DEM) of localized caldera resurgence obtained for Model-77.

3.3.2.2 Model-82

Model-82 was designed as Model-77 with a standard setup, but with a reinjection depth of 4 cm below the model surface (i.e., 1 cm deeper than Model-77) (Fig. 3.48)

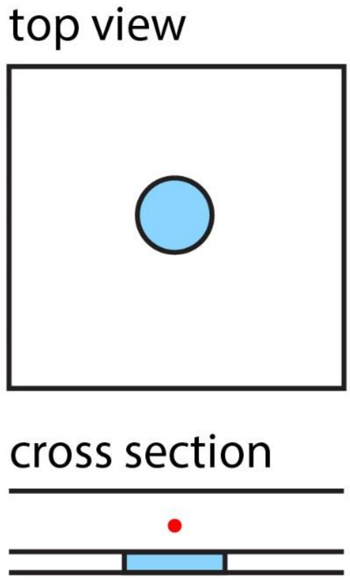

Figure 3.48. Model-82 setup (top view and cross section). A circular analogue magma chamber is placed below a 6 cm-thick sand overburden. The red dot indicates the depth of magma reinjection (4 cm below model surface).

Re-injection of PG3 fluid was applied to Model-82 in order to induce localized intra-caldera resurgence. Model top view and cross section (Fig. 3.49) show that, even at a depth greater than Model-77, re-intrusion in Model 82 caused a similar structural pattern. More specifically, the re-intruded analogue magma caused the formation of a dyke-like structure that induced deformation in the brittle overburden, and created a reverse fault system deforming the model surface. An evident doming is, in fact, well observable on model top-view and digital elevation model (Fig. 3.50), and radial fractures, together with normal faults, accommodate stretching of the dome’s crest. Due to the increased depth of intrusion and the dip of the generated reverse faults, the surface dome shows a larger diameter in comparison to that of Model-77. Furthermore, a larger quantity of analogue magma remains trapped above the point of re-injection, creating a small chamber from which two dikes depart from its boundaries (Fig. 3.49).

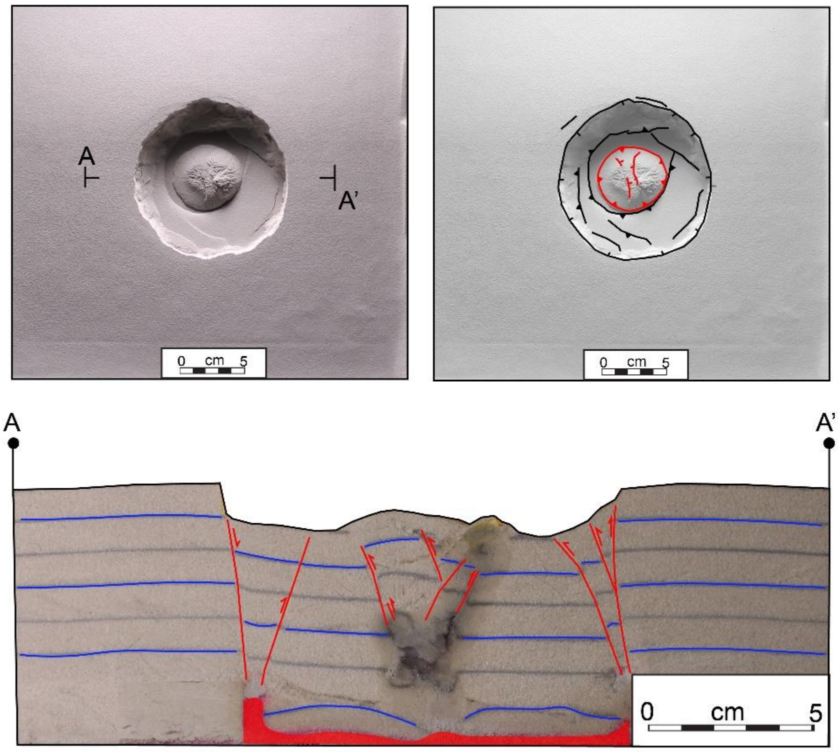

Figure 3.49. Top view of Model-82 after caldera resurgence (left upper panel) with interpretation of the structural pattern (right upper panel). Interpreted model cross section (lower panel) shows the remnant of analogue magma (PG3) not extruded during the caldera collapse phase (highlighted by red transparency), as well as the new re-intruded analogue magma (PG3, greyish areas) that generated a steep dyke and an overlying superficial bulging. Red lines on model top-view denote the newly-formed faults induced by magma re-injection. The top-view photo was taken immediately before the analogue magma extruded at the model surface; extrusion can be instead inferred in the cross section.

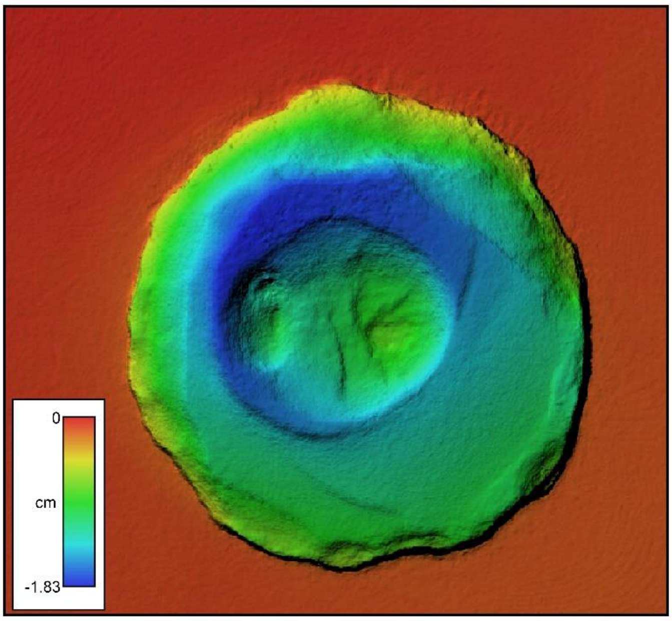

Figure 3.50. Digital elevation model (DEM) of localized caldera resurgence obtained for Model-82.

3.3.2.3 Model-80

Model-80 tested the effect of localized intra-caldera resurgence produced by a deeper intrusion point, which was set at 4.5 cm below the model surface (Fig. 3.51).

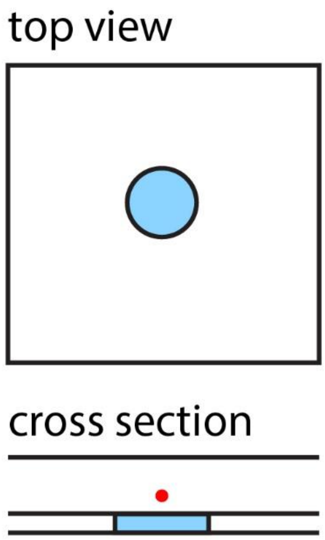

Figure 3.51. Model-80 setup (top view and cross section). A circular analogue magma chamber is placed below a 6 cm-thick sand overburden. The red dot indicates the depth of magma reinjection (4.5 cm below model surface).

Figure 3.52 shows the final stage of caldera resurgence (captured in top-view photo) and model cross section for Model-80. In agreement with a point of reinjection deeper than in Model-77 and Model-82, the resulting surface deformation consists of a larger, and higher resurgent dome (see the DEM in Fig. 3.53). Emplacement of such a newly-formed dome is accommodated by several normal faults generating small grabens on its top. The top-view photo and DEM show, in fact, that the dome is affected by a central area of subsidence, which may accommodate the emplacement of analogue resurgent dome. Specifically, a longer fault crosscuts the entire dome crest and stops the propagation of the smaller normal faults bounding the grabens (see line-drawing on top-view image; Fig. 3.54). The deformation pattern on top of the resurgent dome is thus characterised by a sub-orthogonal fault pattern, with a major fault and other minor faults delimiting different blocks over the dome crest. Notably, resurgent structures (marked in red on top-view photo) interact with caldera collapse-related faults (marked in black on top-view photo), dislocating them (Fig. 3.54).

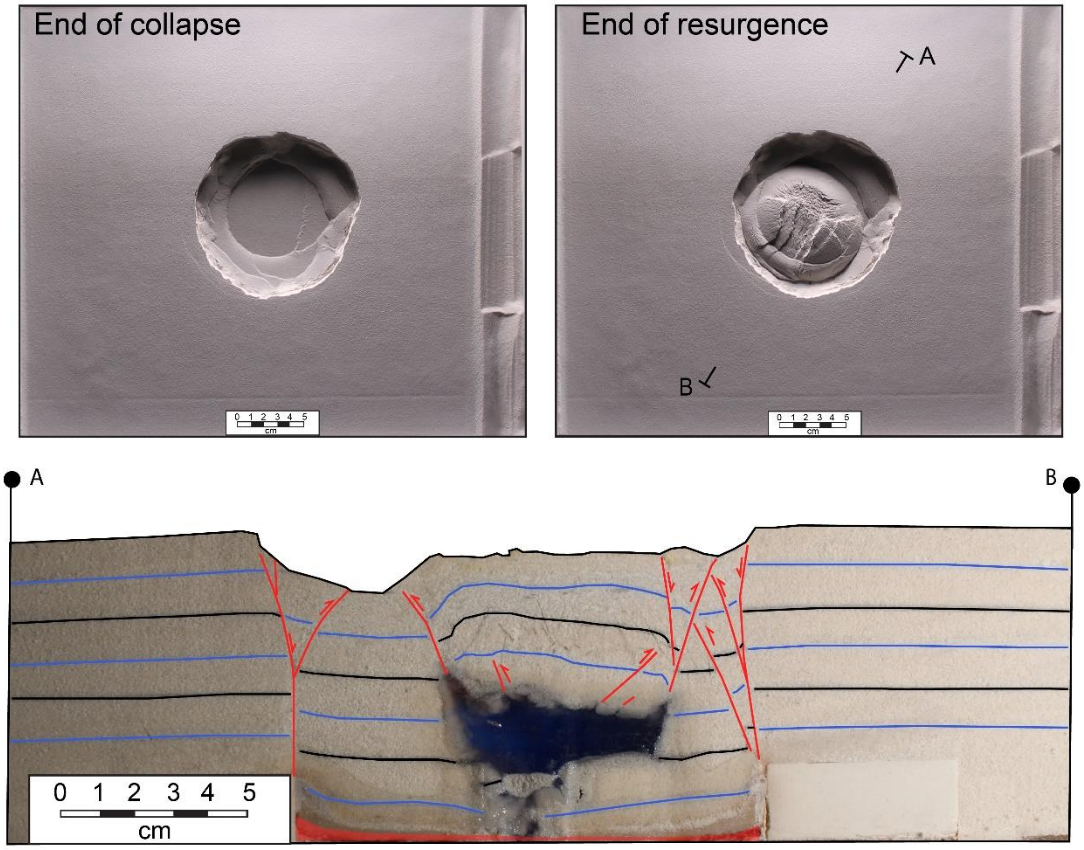

Figure 3.52. Top view of Model-80 after caldera collapse (left upper panel) and localized caldera resurgence (right upper panel). Interpreted model cross section (lower panel) shows the remnant of analogue magma not extruded during the caldera collapse phase (PG3, highlighted by red transparency), as well as the new re-intruded magma (bluish PG3) that generated the sill-like intrusion and superficial doming. Red lines on model top-view denote the newly-formed faults induced by reinjection of analogue magma.

The cross section effectively shows the internal architecture produced by re-intrusion of the analogue magma (blue PG3) and consequent intra-caldera resurgence. A sill-like structure is intruded above the initial point of injection, and propagates laterally to ultimately generate small, steep dike-like structures localising brittle deformation. From the dike apex, in fact, reverse faults propagate upwards reaching the model surface and allowing doming formation. Some smaller analogue dikes nucleate above the central part of the sill intrusion, stopping their ascent at ca. 3 cm below model surface.

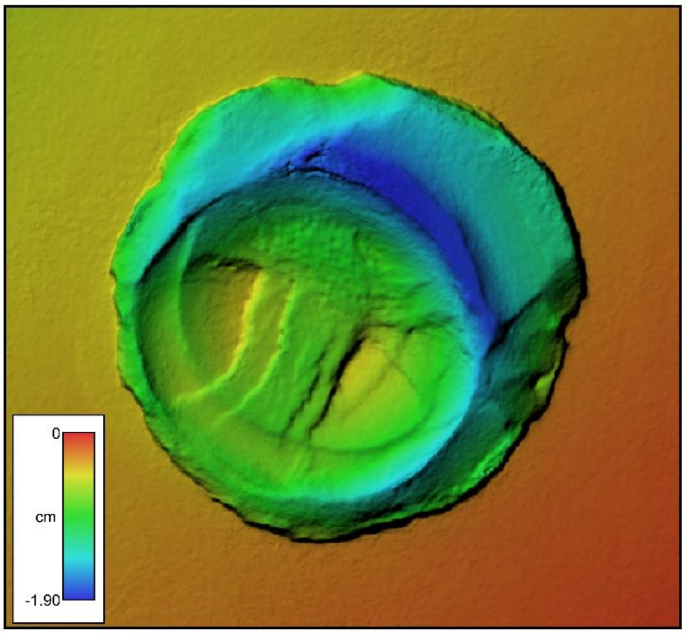

Figure 3.53. Digital elevation model (DEM) of localized caldera resurgence obtained for Model-80.

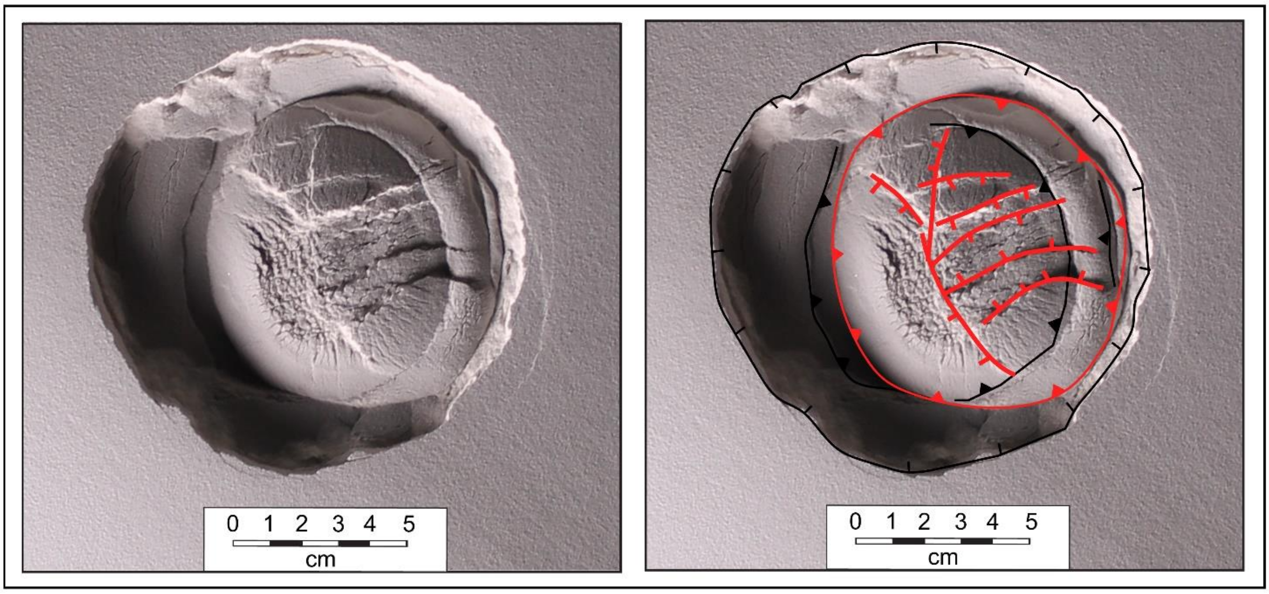

Figure 3.54. Uninterpreted (left panel) and detailed top view line-drawing interpretation (right panel) after caldera resurgence for Model-80. Caldera collapse-related faults (black lines) and resurgence-related faults (red lines) are shown.

3.3.2.4 Model-78

Model-78 is the last model presented for Series D3.6-3c. This model was designed with the deepest reinjection point (5 cm below the model surface; Fig. 3.55), the injection point being placed immediately above the analogue magma chamber.

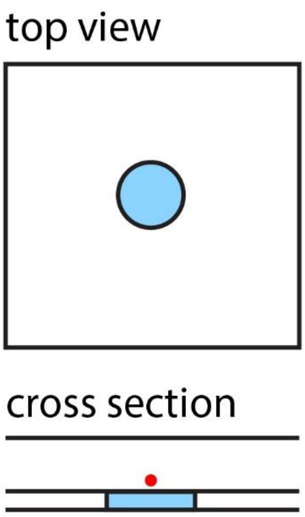

Figure 3.55. Model-78 setup (top view and cross section). A circular analogue magma chamber is placed below a 6 cm-thick sand overburden. The red dot indicates the depth of magma reinjection (5 cm below model surface).

Caldera collapse development followed the classical evolution, resulting in the symmetric collapse evident in the left panel of Figure 3.56. Resurgence was applied after the collapse phase by re-injecting the analogue magma. As visible from the right panel of Figure 3.56, the effect of magma reinjection was a piston-like resurgence instead of the localized resurgence observed in the previous models. The piston-like resurgence forced the external ring faults to recover part of their vertical throw acquired during the caldera collapse phase. This process led to an essential symmetrical uplift of the central caldera piston (Fig. 3.57). The model cross-section shows instead some differences with respect to a typical piston-like resurgence, particularly a moderately dipping sill-like structure at the centre of the resurgent caldera (Fig. 3.56). Part of the intruded analogue magma deformed the internal structure of the caldera piston to form the sill, while some other fluid migrated downward along the injection tube to flow into the former analogue magma chamber. The final model outcome was a broad caldera uplift. This evolution is clearly related to the deep point of reinjection. The overburden load was seemingly too high to allow the intrusion of the analogue magma at shallower levels, which instead flowed laterally into the analogue magma chamber and re-exploited previous caldera-related faults to accommodate resurgence. Accordingly, the DEM does now show evidence of newly-formed faults (Fig. 3.58). Likely, a model with a deeper point of re-injection would cause a simple piston-like resurgence with no sill-like intrusion.

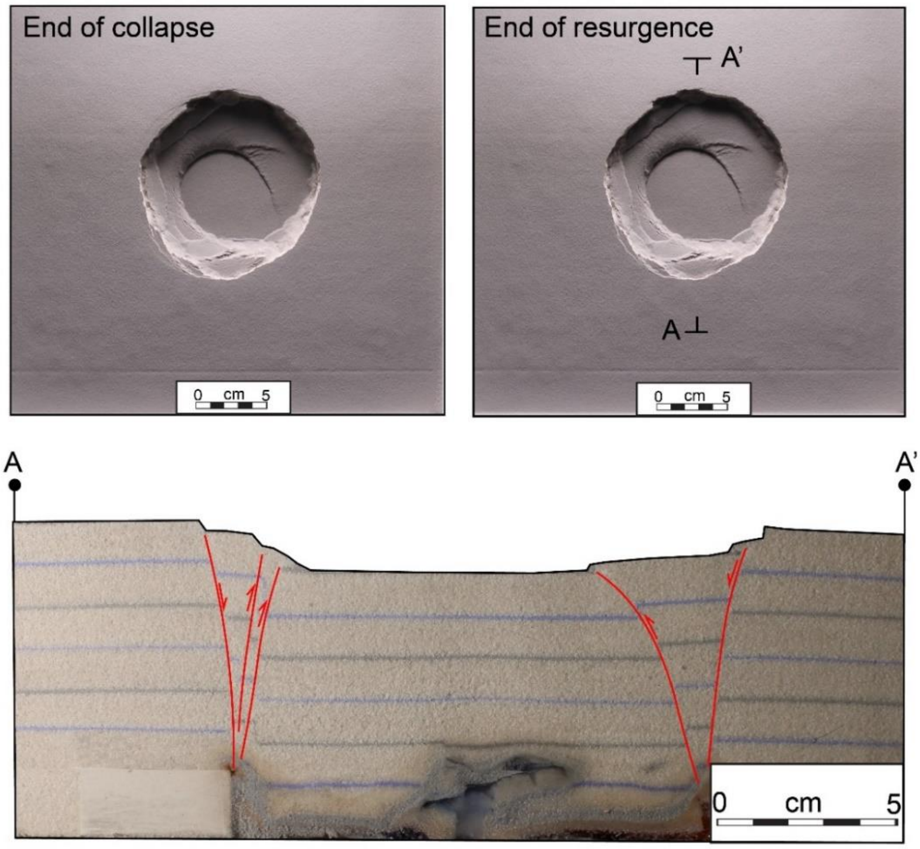

Figure 3.56. Top view of Model-78 after caldera collapse (left upper panel) and localized caldera resurgence (right upper panel). Interpreted model cross section (lower panel) shows re-intruded analogue magma (PG3, greyish area) generating a small sill-like structure.

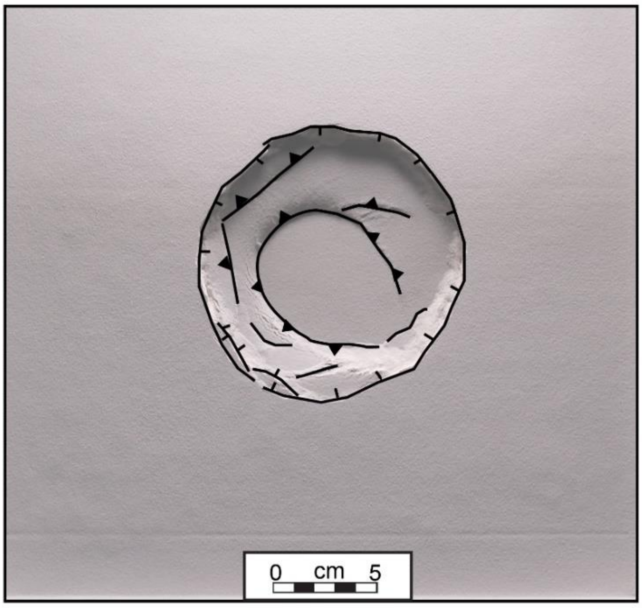

Figure 3.57. Model-78 top view after the end of the resurgent phase. No newly-formed structures are visible and the internal geometry of faults did not experience major modifications, caldera resurgence being almost totally accommodated by the reactivation of ring faults.

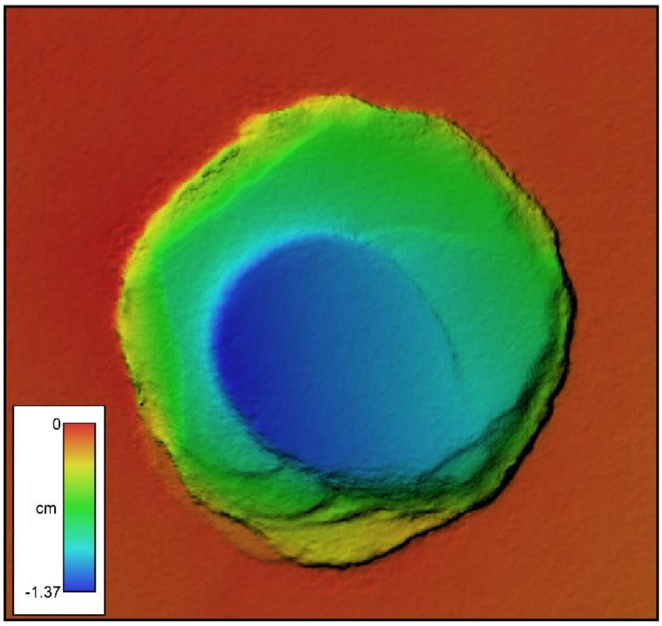

Figure 3.58. Digital elevation model (DEM) of piston-like caldera resurgence obtained for Model-78.

3.3.3 Sub-series D3.6-3c: Effect of resurgence and presence of inherited faults on collapsed calderas

The last sub-series presented below deals with caldera resurgence (both piston-like and localized) and its interaction with inherited structures. We are going to show here the models that have provided insights into the topic addressed by this series.

Model-83 and Model-85 share the same setup of Model-76 that has been previously shown in Series D3.5-2d (Deliverable D3.5), which resulted from the combination of various setups and aimed to test specific hypotheses resulting from the study carried out in the frame of Work Package 4 (Liotta and WP4 Working Group, 2019; see Fig. 1.5). In particular, we aimed to test the hypothesis that the reactivation of inherited structures controlled the collapse of the Los Humeros and Acoculco calderas. These structures represent inherited faults that were supposed to crosscut only the overburden pile beneath the volcano-clastic deposits and lava-flows. Accordingly, we designed a setup with two artificial discontinuities bounding the analogue magma chamber in the substrate and extending upward in the brittle overburden to reach a depth of 2 cm below the model surface. In addition, we placed a third central discontinuity above the analogue magma chamber, reaching again a depth of 2 cm below the model surface. We applied a broad (Model-83) and a localized caldera resurgence (Model-85) to this setup by intruding analogue magma at the base of the model and at a depth of 4.5 cm to test the mutual influence of magma re-injection and inherited faults on caldera resurgence.

3.3.3.1 Model-83

Model-83 was built with the setup described above, and was designed to generate a broad (i.e., piston-like) resurgence by re-intruding analogue magma at the base of the model (6 cm depth below the model surface). The point of injection was then placed in correspondence of the introduced central discontinuity (Fig. 3.59).

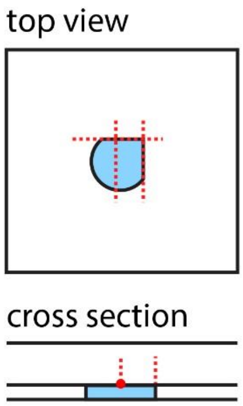

Figure 3.59. Model-83 setup (top view and cross section). A circular analogue magma chamber is placed below a 6 cm-thick sand overburden. The red dot indicates the depth of magma reinjection (6 cm below model surface).

As expected, reinjection of analogue magma caused a piston-like resurgence with a small intrusion at the centre of the caldera piston, in correspondence of the tube inlet. This intrusion is likely an artefact due to presence of the tube and not a real effect of analogue magma migration, which instead flowed into the analogue magma chamber causing piston-like resurgence. In particular, Figure 3.60 shows Model-83 at the end of caldera collapse (left panel) and caldera resurgence (right panel). Caldera resurgence caused only central piston uplift, which was accommodated by reactivation of ring normal faults that recovered part of the vertical throw, and without any evident effect on the caldera centre. Model cross section (Fig. 3.60) does not show significant internal deformation. In particular, no evidence of reactivation of the central discontinuity can be observed in top-view (see also line-drawing interpretation in Fig. 3.61). or in cross section (Fig. 3.60). The high-resolution DEM supports the finding that no displacement can be detected in the central part of model surface (Fig. 3.62), thereby confirming the non reactivation of the central discontinuity.

The two rectilinear artificial discontinuities delimiting the analogue magma chamber, and crosscutting part of the overburden, generated rectilinear caldera sides (as already described for Model-76 of Deliverable

D3.5, Series D3.5-2d) (Fig. X). In Model-83, these faults were exploited by the system to accommodate caldera resurgence.

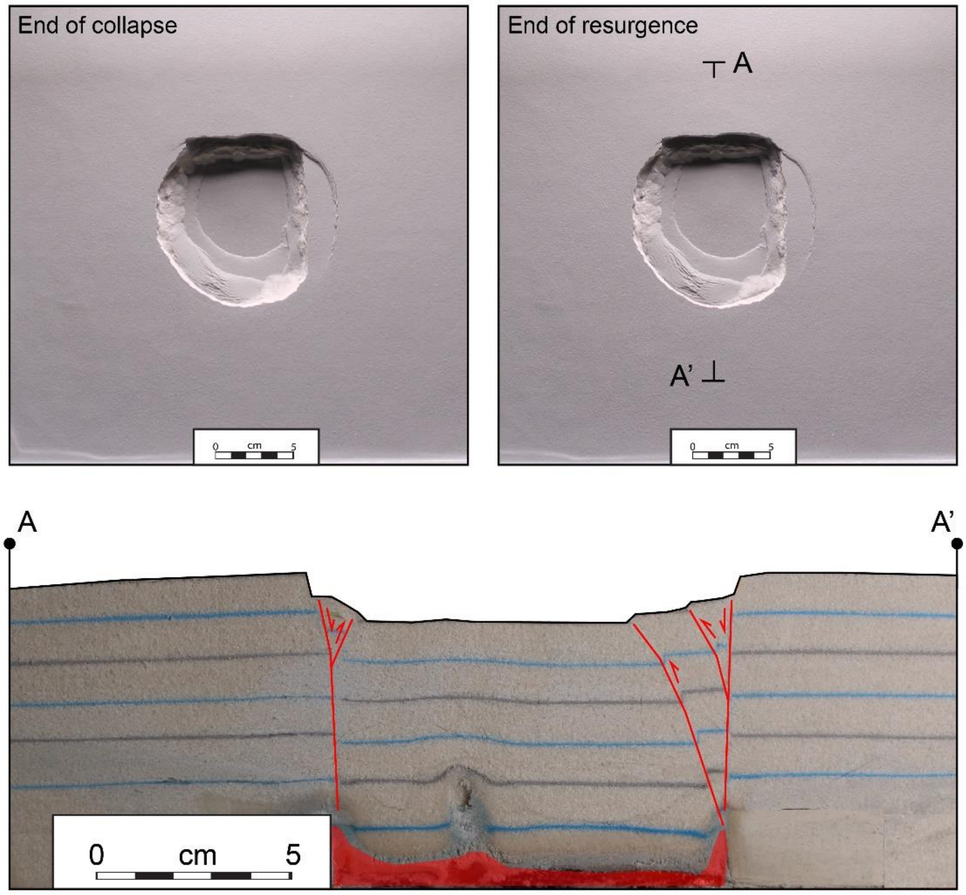

Figure 3.60. Top view of Model-83 after caldera collapse (left upper panel) and broad caldera resurgence (right upper panel). Interpreted model cross section (lower panel) shows the re-intruded analogue magma (PG3, highlighted in red transparency) in the analogue magma chamber.

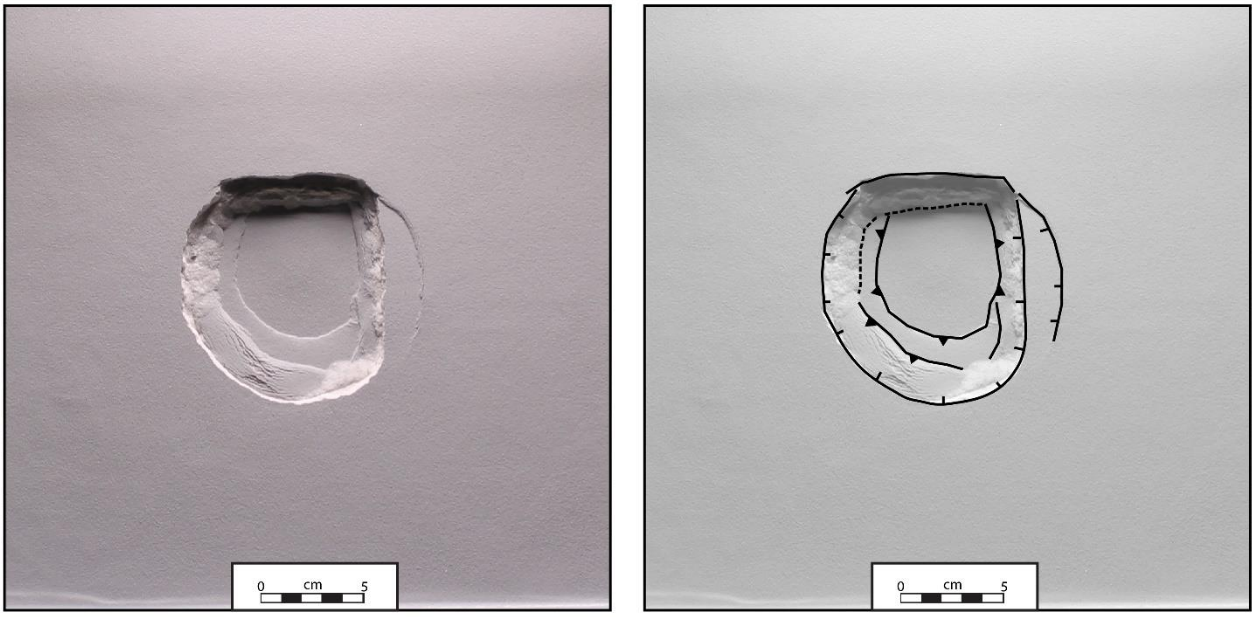

Figure 3.61. Model-83 top-view showing the collapsed caldera after the resurgent phase (left panel), with line-drawing interpretation (right panel).

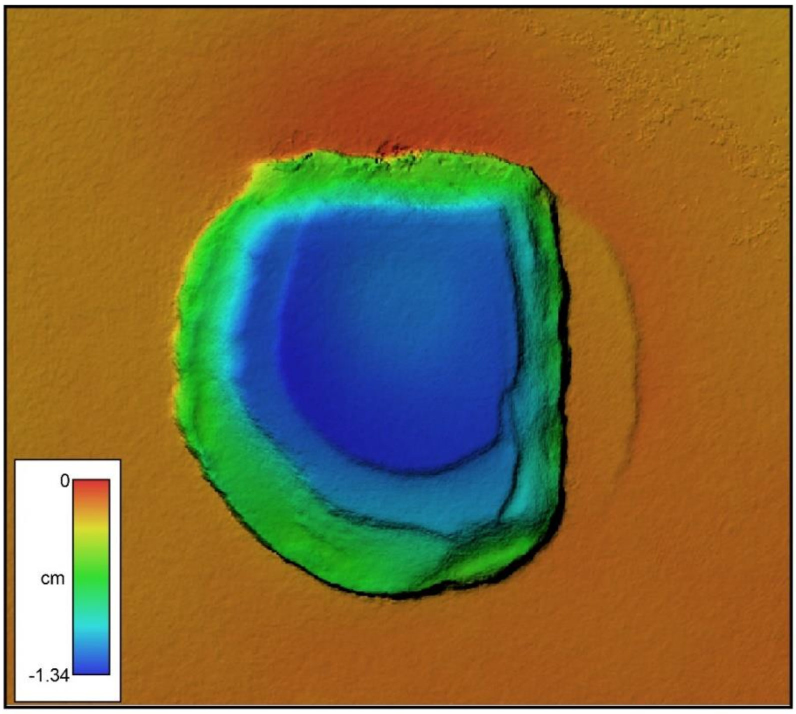

Figure 3.62. Digital elevation model (DEM) of piston-like caldera resurgence obtained for Model-83.

3.3.3.2 Model-85

Model-85 replicates the setup of Model-83 and was used to test the structural setting related to localized resurgence. The depth of reinjection was set at 4.5 cm below the model surface (Fig. 3.63) as in Model-80, which is presented in sub-series D3.6-3b.

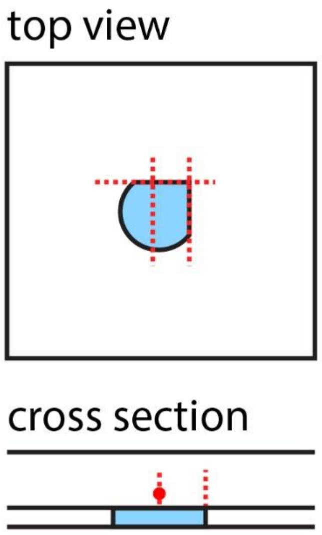

Figure 3.63. Model-85 setup (top view and cross section). A circular analogue magma chamber is placed below a 6 cm-thick sand overburden. The red dot indicates the depth of magma reinjection (4.5 cm below model surface).

As expected from results of previous sub-series D3.6-3b, analogue magma reinjection induced localized caldera resurge at the model centre (Fig. 3.64 and Fig. 3.65), disrupting the internal structural architecture of the model, and forming a small intrusion from which depart reverse faults propagating up to model surface (see cross-section in Fig. 3.64). These faults accommodate the doming visible on model top view and DEM (Figs. 3.64 right panel, Fig. 3.65 and Fig. 3.66). The dome crest is dissected by normal faults that accommodate stretching on its external region. These normal faults define a peculiar sub-orthogonal pattern over the dome (Fig. 3.65). No evidence for the reactivation of the central artificial discontinuity during caldera resurgence has been observed.

As in Model-83, the inherited structures introduced at the caldera boundaries were reactivated during caldera collapse. However, in Model-85 these faults were not exploited to accommodate uplift related to caldera resurgence (as instead occurred in Model-83), but resurgence affected only the central part of the collapsed caldera system (Fig. 3.65).

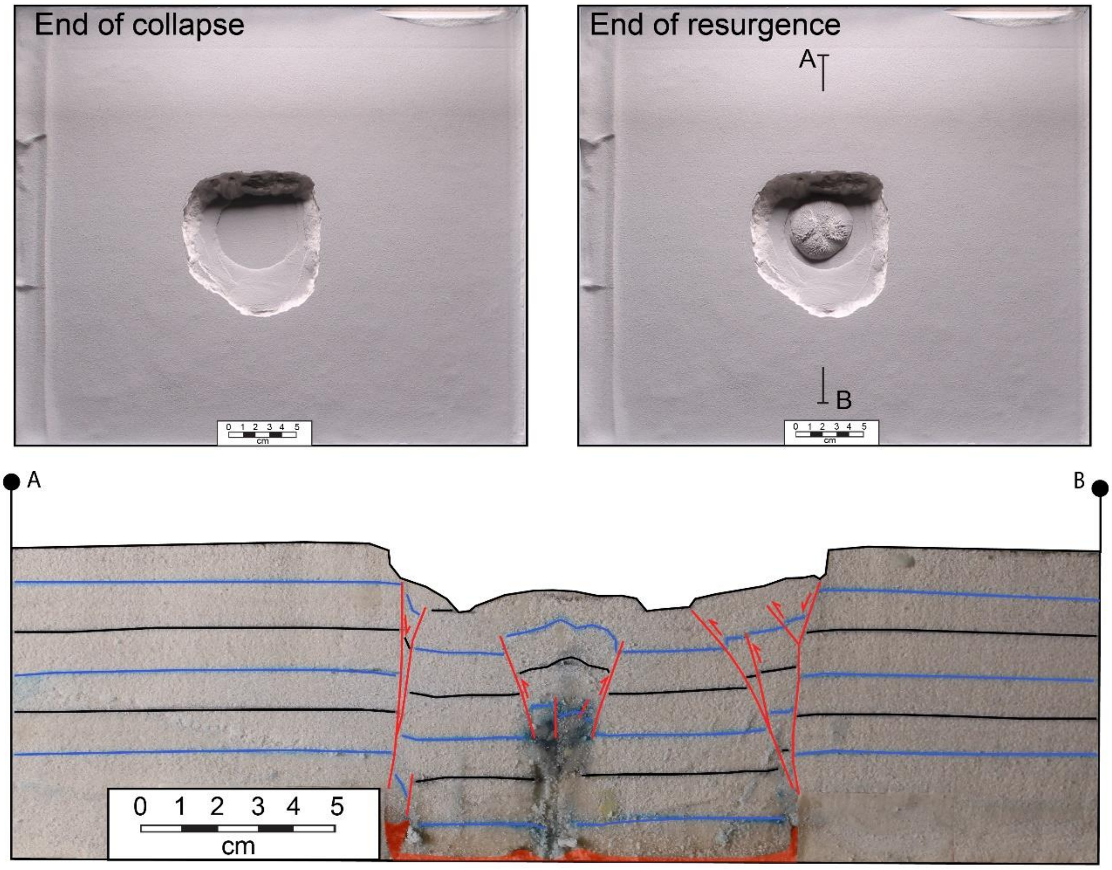

Figure 3.64. Top view of Model-85 after caldera collapse (left upper panel) and localized caldera resurgence (right upper panel). Interpreted model cross section (lower panel) shows the re-intruded analogue magma (PG3, greyish area) and the remnant of analogue magma not extruded during the caldera collapse phase (PG3, highlighted in red transparency).

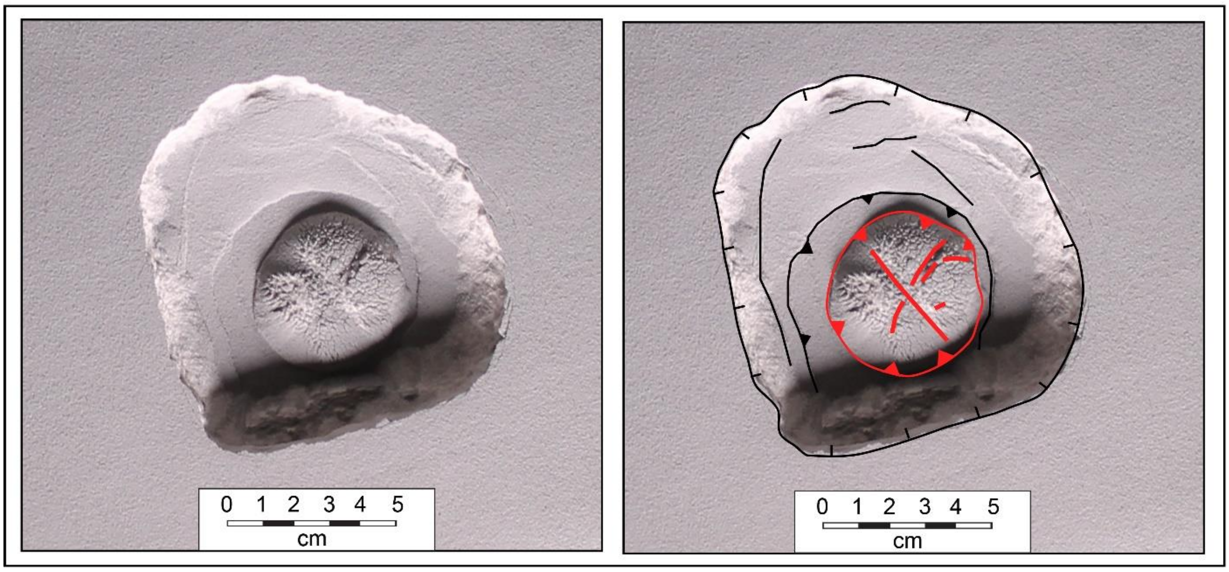

Figure 3.65. Model-85 top-view captured after the resurgence phase (left panel) with line-drawing of interpreted structures (right panel). Red lines mark the faults that developed during caldera resurgence.

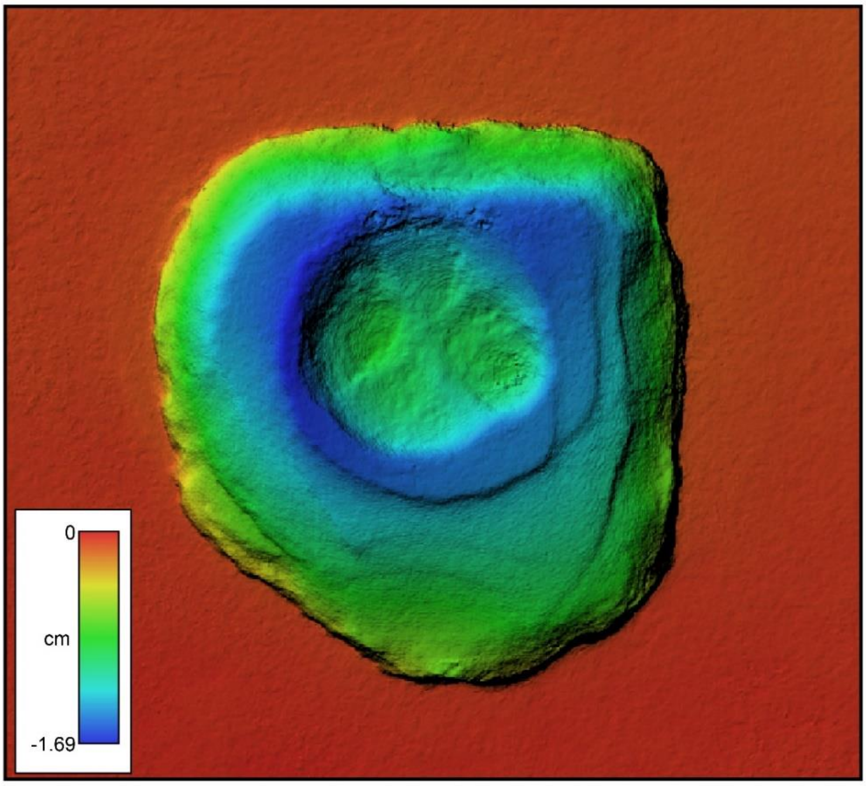

Figure 3.66. Digital elevation model (DEM) of localized caldera resurgence obtained for Model-85.

3.4 Series D3.6-4: Combined effects of compressional and extensional tectonics structures and magmatic processes on the Los Humeros Volcanic Complex (LHVC)

In this series the combined effects of tectonic and magmatic processes on the evolving caldera complex have been analysed. The experimental results have been studied observing both the surface (incremental deformation) and the internal part (final deformation) of the models. Vertical surface variations were measured through digital elevation models (DEMs) from photogrammetric data, to depict uplifting and subsiding areas. In addition, the experiments were photographed to record the structures developed during progressive deformation, with sequential zenithal photographs georeferenced in a GIS. The DEM and photographs of the model have been oriented in the GIS so that the experimental compressive structures are roughly parallel to the NW-SE MFTB thrust faults and folds and the experimental extensional structures are roughly parallel to the TMVB NE-SW normal faults. The model comprised thin markers layers of different colours. Completed experiments were wet and then sliced to reveal the structures within the cone and basement in cross sections. Some of the vertical cross section have been georeferenced in a 3D GIS to visualize structures in three dimensions.

1) In step 1 the sand pack is deformed simulating compression. As expected, the compression generated well developed NW-SE thrust faults in the granular material pack;

2) In step 2 the sand pack has been extended simulating tectonic extension generating normal faults in the already deformed model (Fig. 3.67, 3.68, 3.69);

Figure 3.67. Plan view of the analogue model deformed by compression followed by extension.

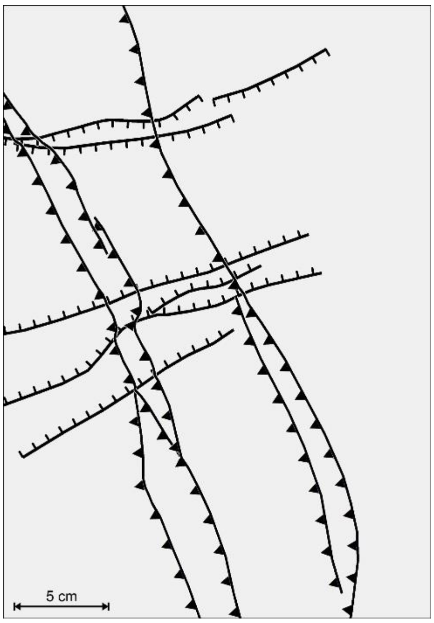

Figure 3.68. Structural sketch map of the analogue model deformed by compression and extension.

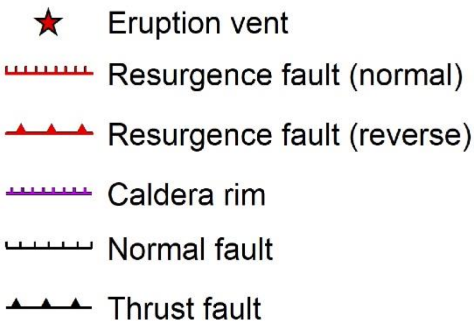

Figure 3.69. Legend for sketch maps of figures 3.68, 3.71, 3.73, 3.74, 3.77.

3) In step 3 the deformed model is covered by a uniform layer of granular material sealing the inactive compressive and extensional faults;

4) In step 4 caldera collapse is simulated. The symmetric circular collapse at depth induced remarkably asymmetric deformation at the model surface. The simulated caldera depression is bordered by multiple caldera rims composed by rectilinear and curvilinear segments. The rectilinear segments connect one with the other at high angle (Fig. 3.70). Most of these rectilinear segments are roughly parallel to the compressive and extensional inherited basement faults (Fig. 3.71). The caldera floor is also asymmetric, dipping NE (Fig. 3.72);

Figure 3.70. Plan view of the analogue model after caldera collapse.

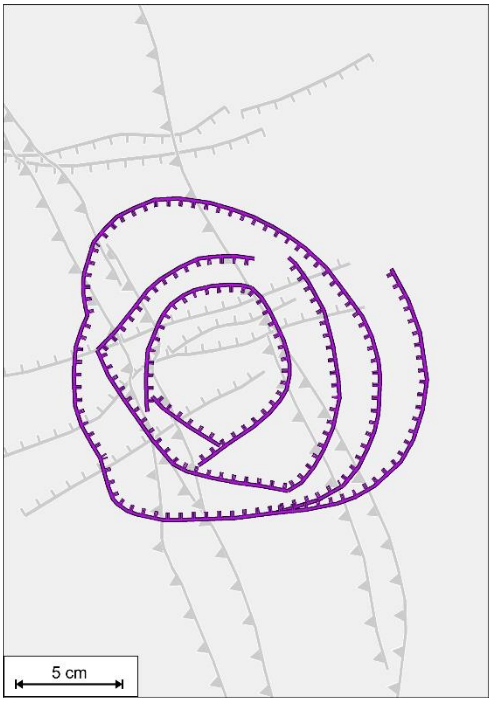

Figure 3.71. Structural sketch map of the analogue model after caldera collapse.

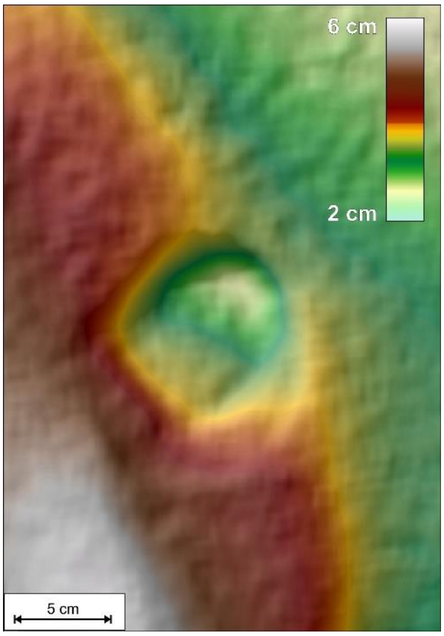

Figure 3.72. DEM of the analogue model after caldera collapse.

5) In step 5 resurgence of the caldera floor is simulated. The results showed that a symmetric, centred, deep- seated intrusion leads to strongly asymmetric uplift of the model surface, deformed by reverse and normal faults (Fig. 3.73, 3.74, 3.75). Most of these faults are roughly parallel to the inherited compressive and tectonic structures in the basement and connect one with the other at high angle (Fig. 3.74). Resurgence sectors at different elevation are delimited by the normal faults in the centre of the resurgence area (e.g. Fig.

3.76). Vertical and horizontal displacements induced by molten vegetable oil intrusion driving caldera resurgence show alignment of eruption point, area with the highest uplift and vector of horizontal displacement in the direction of the inherited normal faults in the basement (Figs. 3.68 and 3.77). Also, the location of the eruption point coincides with the location at surface of the most internal thrust faults (Figs. 3.68 and 3.77).

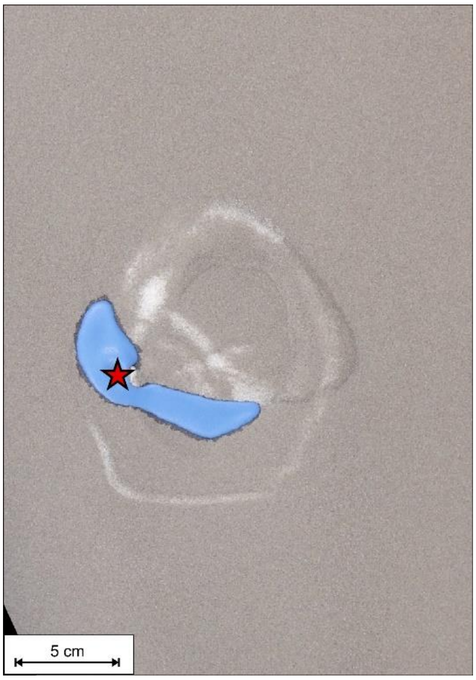

Figure 3.73. Plan view of the analogue model after caldera resurgence. Erupted molten vegetable oil is depicted in blue.

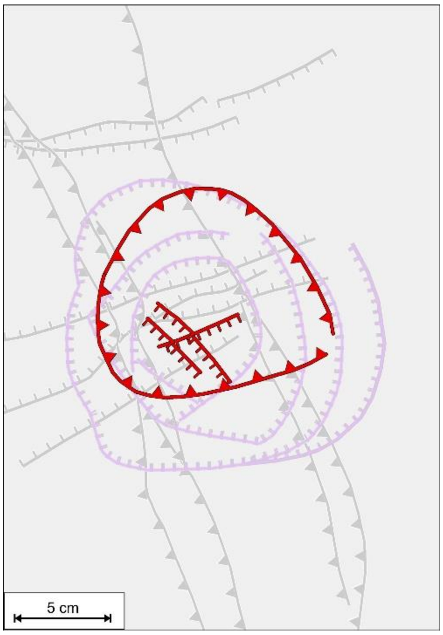

Figure 3.74. Structural sketch map of the analogue model after caldera resurgence.

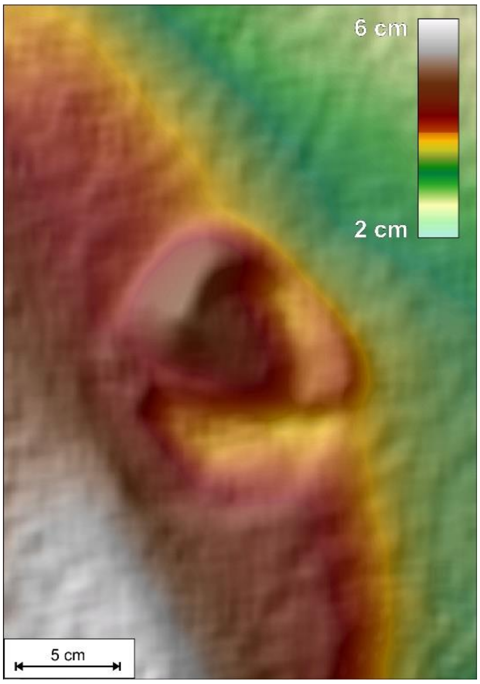

Figure 3.75. DEM of the analogue model after caldera resurgence.

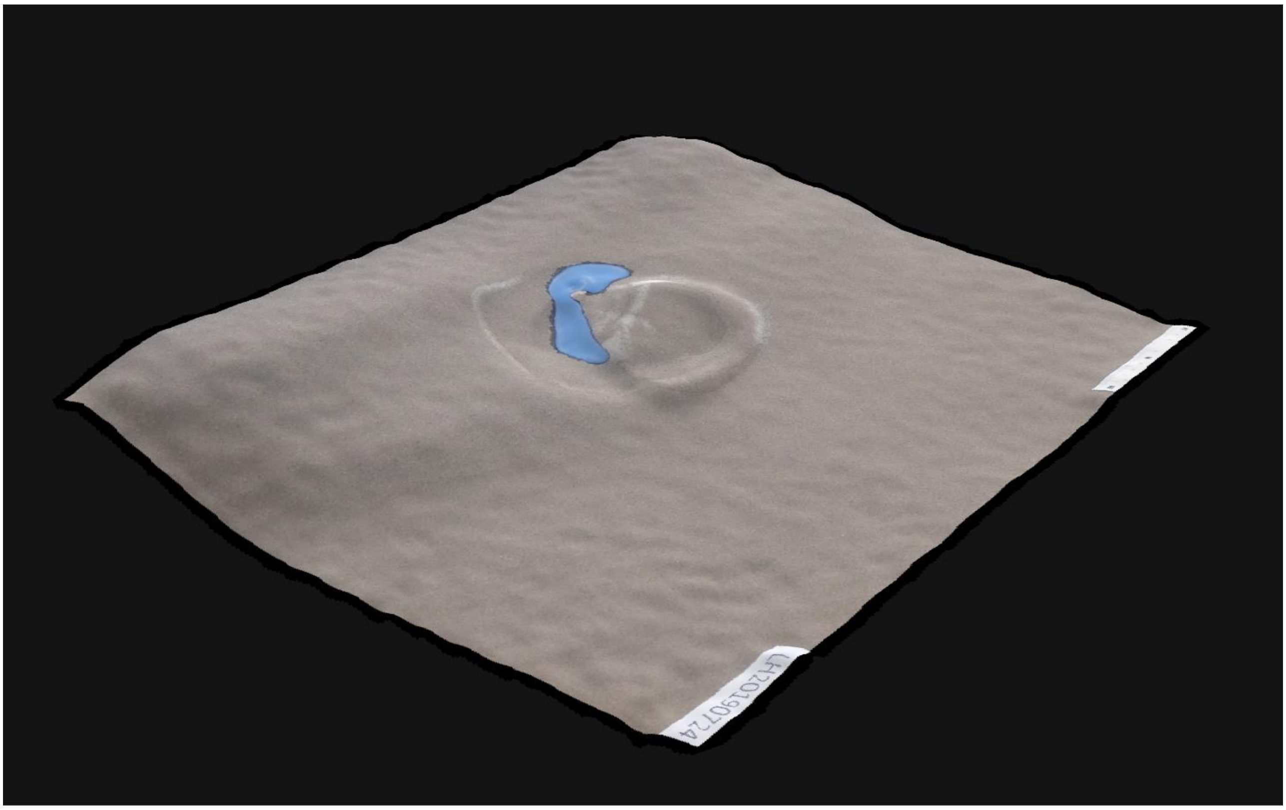

Figure 3.76. Perspective view of the analogue model surface after caldera resurgence. Erupted molten vegetable oil is depicted in blue.

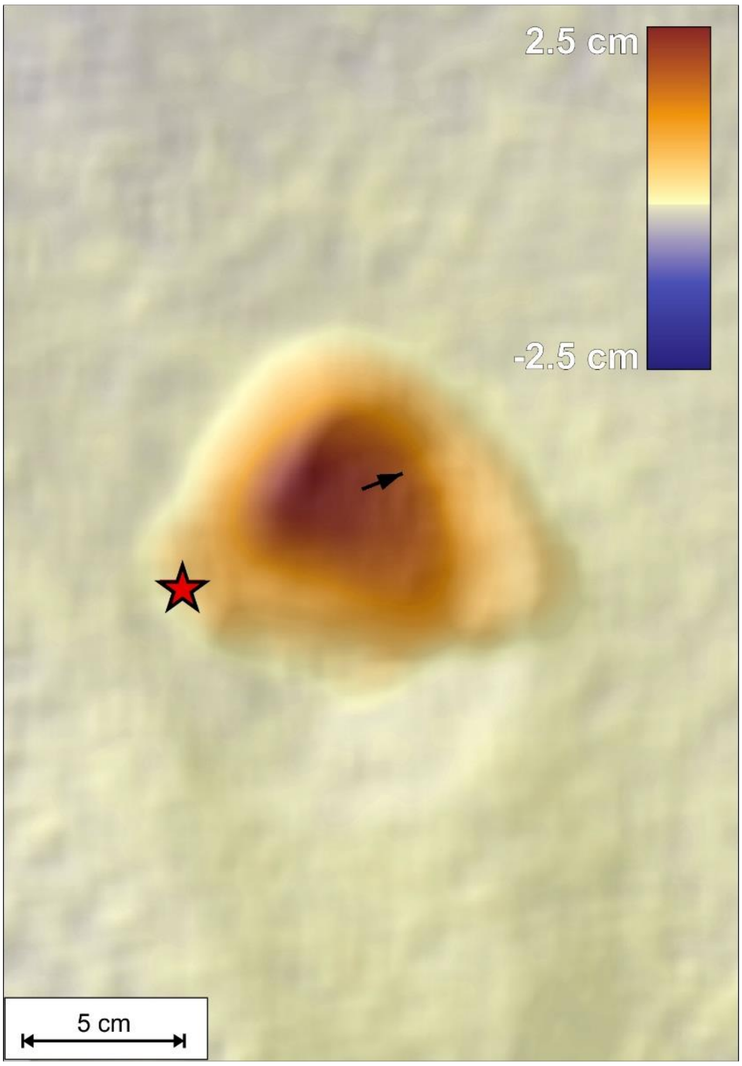

Figure 3.77. Vertical uplift (colour scale) and horizontal displacement (black arrow) of the model surface induced by molten vegetable oil intrusion and caldera resurgence.

In cross-section, the deformed model shows that (Fig. 3.78):

i) the collapse caldera is delimited by outward dipping sub-vertical ring faults at depth, connected with shallow, more external inward-dipping faults corresponding at the surface to the main caldera rims (Figs. 3.71, 3.79);

ii) molten vegetable oil intrusion induces formation of inward dipping reverse faults and doming and tilting of the uplifted surface traversed by normal faults (Figs. 3.74, 3.75, 3.79)

iii) molten vegetable oil intrusion driving resurgence of the caldera floor is strongly asymmetric, rising gradually toward the surface following the inherited extensional tectonic structure of the basement towards the main thrust fault ramps (Figs. 3.77, 3.79).

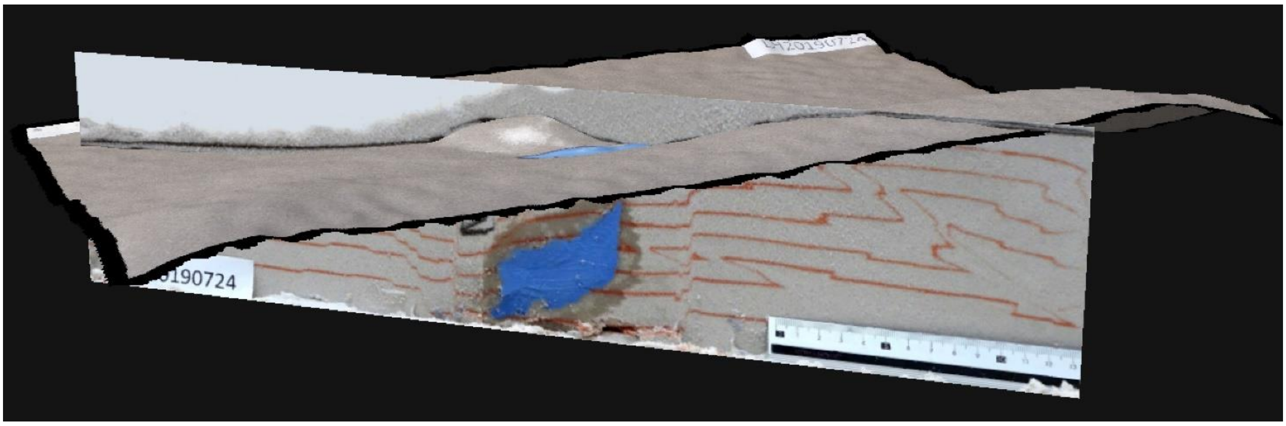

Figure 3.78. **Perspective view of the model after caldera resurgence showing in 3D the location of the cross-section of Fig. 3.79 (vegetable oil intrusion is depicted in blue).**

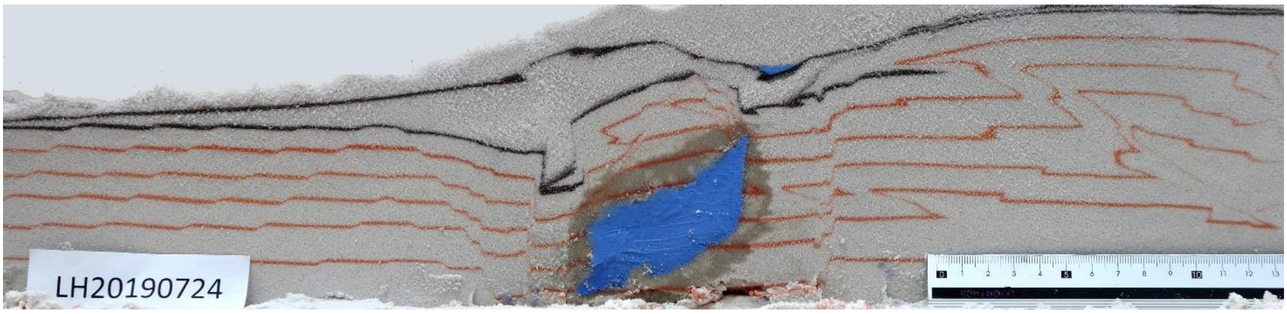

Figure 3.79. Vertical cross-section of the model after caldera resurgence (vegetable oil intrusion is depicted in blue).

3.5 Series D3.6-5: Shallow-intra-caldera intrusions

The experiments show a deformation pattern consisting of a first stage characterized by the uplift of a sub-circular dome, bordered by inward dipping reverse faults, and a second stage characterized by the collapse of the apical part of the dome where normal faulting occurs (graben formation, Fig. 3.80a-z). The top view shape of both the reverse and normal faults is sub-circular and is associated with the formation of radial fractures. A different graben shape is observed with increasing overburden thickness: in the experiments with thinner overburden (10 mm) an annular peripheral graben formed as the silicone reached the surface at the edge of the cylinder (Fig. 3.80a-d, and Fig. 3.80o-r). Conversely, in the experiments with thicker overburden showed (30 and 50 mm) a sub-circular apical graben formed as the silicone reached the surface at the centre of the dome (Fig. 3.80e-n and Fig. 3.80s-z). No significant differences in the surface deformation pattern were observed between the layered and non-layered experiments with T of 10 and 30 mm. Conversely, in the experiments with thicker overburden (50 mm) the apical graben width decreased in the layered experiment (Experiments HUM 6 and HUM 11 with Lg equal to 58 and 80 mm respectively).

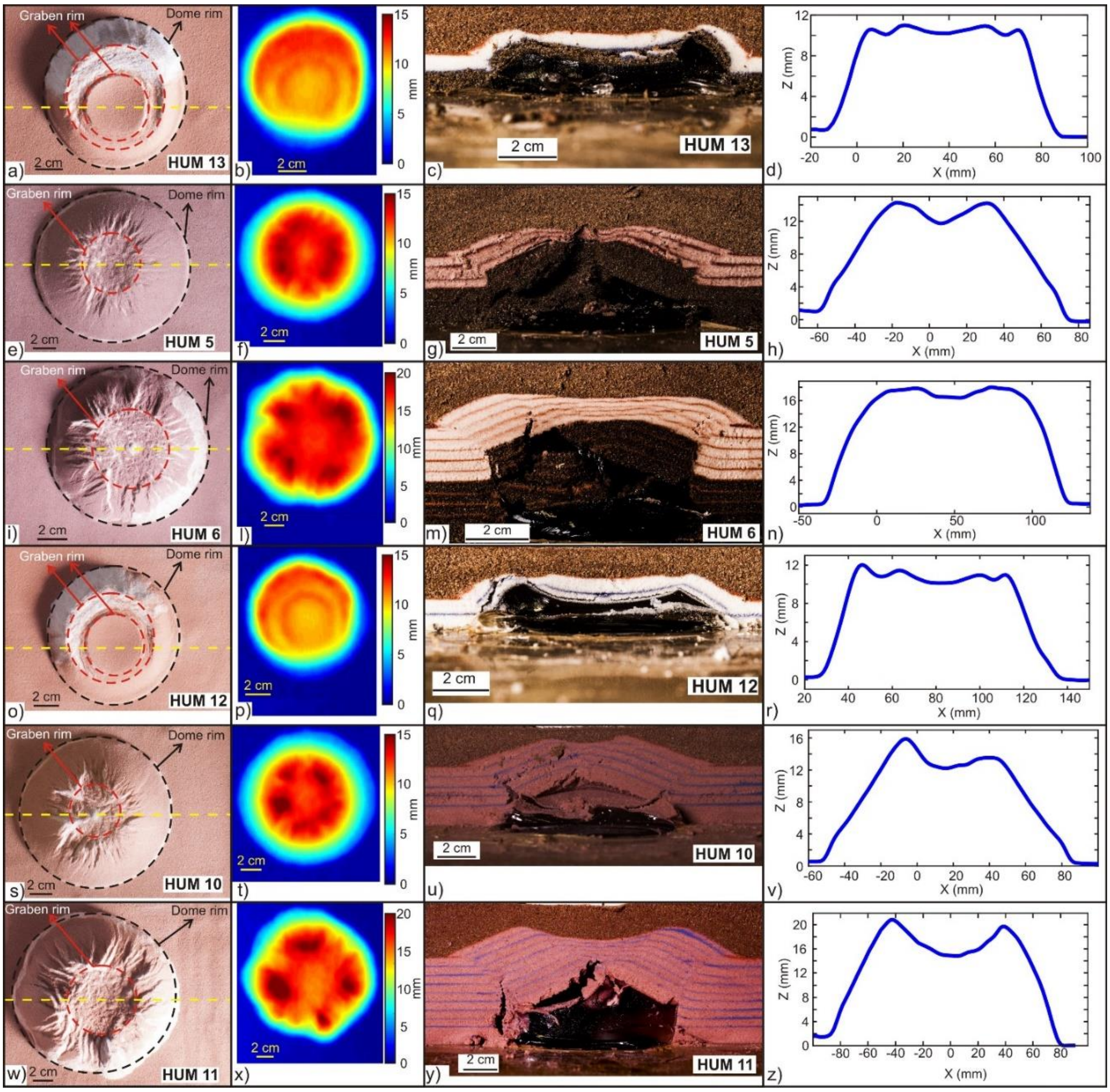

Figure 3.80. (a, e, i, o, s, w) Top view image of the layered (HUM 13, HUM 5 and HUM 6) and non-layered (HUM 12, HUM 10 and HUM 11) experiments. (b, f, l, p, t, x) cumulative vertical displacement; colour scale is proportional to the amount of uplift. (c, g, m, q, u, y) Section view images obtained after cutting the section close to the dome centre. (d, h, n, r, v, z) elevation profile obtained from laser scanner data Z:X=1:4. The yellow dashed line in the top view images indicates the trace of the section views and of the elevation profiles.

All the experiments show that both the dome diamater and graben width increase linearly with the overburden thickness (Fig. 3.81). The dome diameter increases abruptly with time becoming almost constant at an early stage of the experiment (Fig. 3.82a-b); the graben width shows a similar pattern even if it enlarges slightly with time (after the first abrupt increase) as the silicone rises towards the surface suggesting that the intrusion depth has an higher influence on the graben width.

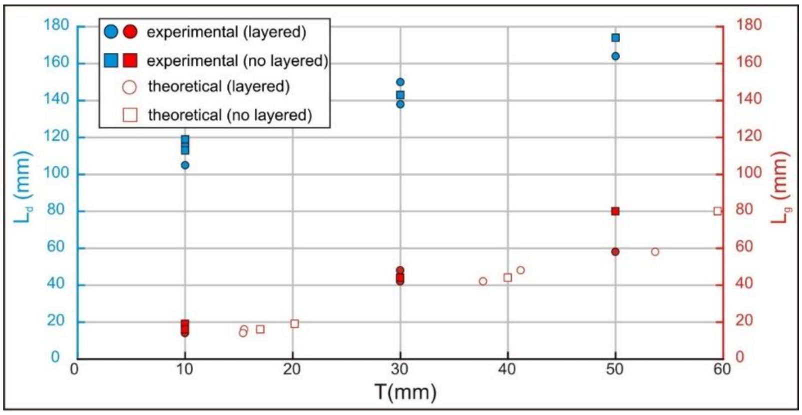

Figure 3.81. Lg (apical graben width) and Ld (dome diameter) versus T. Theoretical values calculated after equation of (Brothelande and Merle, 2015).

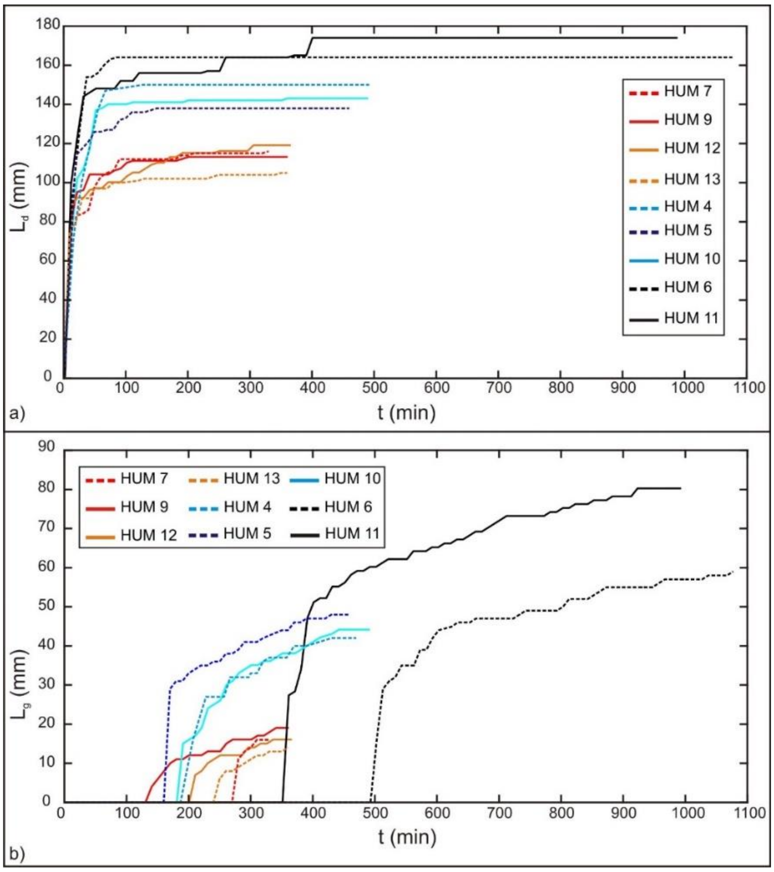

Figure 3.82. (a) Time evolution of the dome diameter (Ld). (b) Time evolution of the apical graben width (Lg). Both Ld and Lg show a similar evolution trend with a first stage of abrupt increase at the beginning of each experiment. In the second stage, Ld becomes constant while Lg increases slightly till the end of the experiment.

4 Caldera collapse and resurgence: Insights from experimental analogue modelling

In the following sections, we discuss the results obtained from analogue modelling carried out in experimental series D3.6-1, D3.6-2, D3.6-3, D3.6-4 and D3.6-5 (Section 4.1). We then compare the experimental results with the natural cases of interest in Section 4.2, discussing in-depth the insights from analogue models into the evolution of the Los Humeros and Acoculco volcanic systems.

4.1 From caldera collapse to resurgence: The control of volcano topography and inherited fabrics

Modelling results are discussed below according to the series of models presented in Chapter 3. This allows systematic description of the main outcomes resulting from the modelling.

4.1.1 Series D3.6-1: Symmetric/asymmetric caldera collapse

The model performed in Series D3.6-1 aimed at investigating the caldera collapse process as well as description of the characteristics of symmetric and asymmetric caldera collapse. Interestingly, models of this series (Section 3.1) developed first-order characteristics similar to models of Series D3.5-2 described in Deliverable D3.5. This warrants model reproducibility, and therefore the soundness of results and interpretation. As mentioned above, the models carried out in this study (series D3.6-1 models, as well as the other series described in the present deliverable) show a first-order evolutionary model that presents similarities with the conceptual model by Acocella (2007) for symmetric caldera collapse developed. In particular, Acocella's (2007) model proposes that caldera collapse is subdivided into successive deformation steps, which involve initial, central down-sagging followed by the formation of outward-dipping reverse faults delimiting a subsiding piston block at the developing caldera centre. Afterward, deformation shifts more externally, where inward-dipping normal faults nucleate and then link with the reverse faults, creating the caldera ring fault system. Notably, Acocella (2007) highlights that not all natural calderas reach the final stage, but can stop their evolution at any stage, depending on the condition of the system (for an in-depth discussion of these aspects, we address the reader to Deliverble D3.5). We then discuss specific aspects of caldera collapse process that can be of interest for further comparison with the study cases of Los Humeros and Acoculco volcanic systems.

Interestingly, as highlighted by analysis of Model-17, symmetric caldera collapse my bear a certain degree of asymmetry, which is important for the understanding of the mechanism leading to caldera collapse. Despite symmetric caldera collapse in some of our models (as well as models performed by other authors with a similar approach, e.g., Komuro, 1987; Martì et al., 1994; Roche et al., 2000; Acocella et al., 2000; 2001b; Walter and Troll; 2001; Troll et al., 2002; Kennedy et al., 2004; Lavellèe et al., 2004; Geyer et al., 2006), show a final circular to slightly elliptical shape with a horizontal central piston roof, the process driving calderas to acquire a symmetric shape often involves steps of asymmetry. For example, Model-17 shows a circular (in top view), counter-clockwise direction of fault propagation (see Fig. 3.2 in Section 3.1.1). After the down-sagging phase, in most cases the inner system of outward-dipping reverse faults does develop synchronously at the caldera centre, but the reverse fault system nucleates from a specific point and then propagate laterally following a circular trajectory (Fig. 4.1a). The direction of fault propagation may occur along one direction (such as the initial stage described form Model-17) or along both directions (i.e., both clockwise and counter-clockwise directions; Fig. 4.1b). This implies that when a side of the developing outward-dipping reverse fault shows an incipient fault scarp at the model surface, the opposite site may show no morphological evidence of reverse faulting because fault propagation has not yet arrived at this point (Fig. 4.1b). This is further complicated by 3D evolution of the system, as in stage where the propagating fault is not yet visible at surface, the fault may be still nucleating at depth and propagating upward producing a 'propagation delay' with respect to the more mature area of initial caldera subsidence.

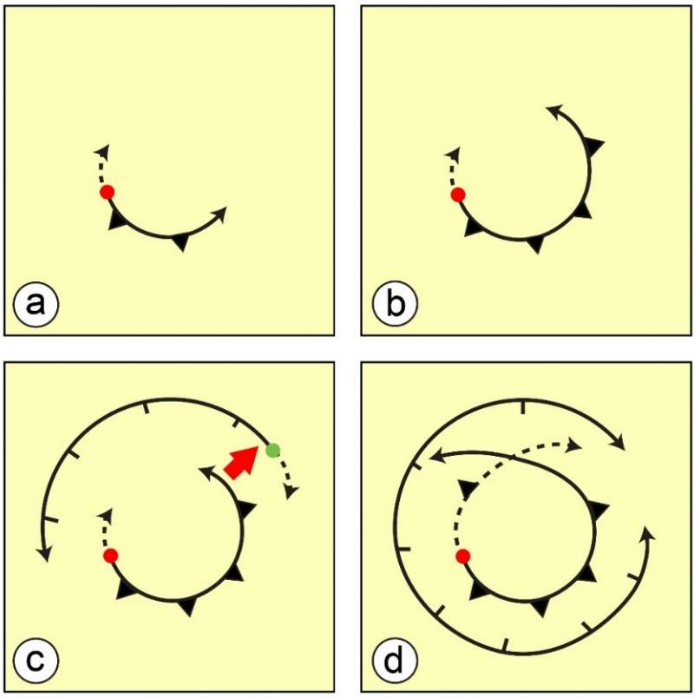

Figure 4.1. Schematic cartoon of top-view fault propagation in a symmetric caldera collapse models. (a) Outward dipping reverse fault starts to propagate from a nucleation point (red dot) in a counter clockwise direction (and/or in clockwise, see dashed arrow). (b) The reverse fault continues to propagate following a circular trajectory, until (c) deformation shifts to peripheral areas (red arrow) to nucleate an inward-dipping normal fault system (green dot indicates the point of nucleation). Afterward, (d) deformation is accommodated by normal fault propagation; in this stage, the inner reverse felt system may increase vertical throw and continue to propagate, up to "closing" the central collapsing piston area, eventually generating a 'fish tail'-like structural pattern.

Similarly, this process can be observed in subsequent caldera stages, during the development of the inward-dipping normal fault system forming the external caldera ring faults (Fig. 4.1c). Interestingly, it is this process to lead to the shift of deformation from the central caldera piston to the more external ring normal faults. In this regard, it is worth noting that:

a) The shift to peripheral areas can happen at different stages of reverse fault development, implying that the inner caldera piston may be only bordered by the reverse fault only partially.
b) After the shift of deformation to peripheral areas, the inner reverse fault system my still keep on propagating laterally to accommodate deformation and to link to the outer normal fault system (Fig. 4.1d). This process is likely responsible for the formation of peculiar features described in Deliverable D3.5 as 'fish tails'-like features that may partly bear a strike-slip kinematics (as highlighted by DPIV analysis).

Nonetheless, even in the case described above, in a symmetric or near-symmetric caldera collapse (i.e., the so called piston-like caldera collapse) the structural pattern developed during model deformation is quite simple. Specifically, apart from some peculiar features (e.g., fish tails features), the main structures can be simply ascribed to the inner outward-dipping fault system and the more external inward-dipping normal fault system (i.e., the caldera ring faults).

On the contrary, an asymmetric caldera collapse induces the formation of a more complicated structural pattern. Such a dissimilar evolution is outlined by comparing a symmetric (piston-like) caldera collapse model (Model-17) with a strongly asymmetric (trap-door) one (Model-7) (Figure 4.2). These two caldera end-members have been considered in our models because most likely representative for the natural case studies. Notably, some kinds of structures are common to both model types (i.e., faults indicated with red lines in Fig. 4.2a,b), and are related to the main fault systems (i.e., outward-dipping reverse faults and inward-dipping normal faults) described above. Nonetheless, despite these similarities and the presence of some secondary structures (faults indicated with blue lines in Fig. 4.2a,b) that may or may not occur, specific faults develop only in models showing trap-door systems (i.e., faults indicated with green lines in Fig. 4.2b).

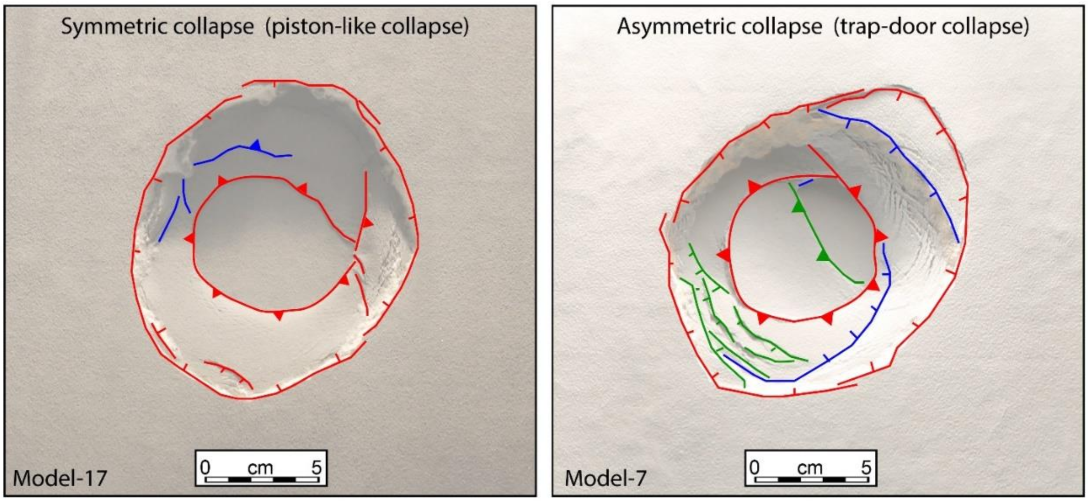

Figure 4.2. End-member models of symmetric (i.e., piston like collapse) and asymmetric calderas (i.e., trap-door collapse). Model-17 (left panel) shows a symmetric caldera collapse, and Model-7 (right panel) shows a highly asymmetric caldera collapse. Line-drawing interpretation marks the main structures. Different colours identify (i) structures that are normally present in both symmetric and asymmetric models (red lines), (ii) secondary structures that may or may not occur in both kinds of caldera collapse (blue lines), and (iii) structures that develop only in asymmetric models (green lines).

Structures deriving from asymmetric collapse (green lines in Fig. 4.2b) are indicative of highly asymmetric trap-door systems and can have both normal and reverse kinematics. It is worth noting that Model-7 represents a highly asymmetric caldera, and such a kind of faults is less developed in models with trap-door calderas showing a less degree of asymmetry. Typically, in these systems, reverse faulting develops inside the subsided and tilted piston block to accommodate its deformation. Furthermore, at the opposite position of the mostly subsided area, a system of (mainly) outward-dipping normal faults develop to accommodate the extension induced by the tilting. The latter faults can be of high interest for the comparison with the natural case study of Los Humeros and Acoculco systems (see Section 4.1.3).

These findings are summarized in Figure 4.3, showing a conceptual evolutionary model both for symmetric piston-like and trap-door caldera systems. In general, after an incipient phase of down-sagging (Fig. 4.3a) calderas can develop symmetric or asymmetric systems.

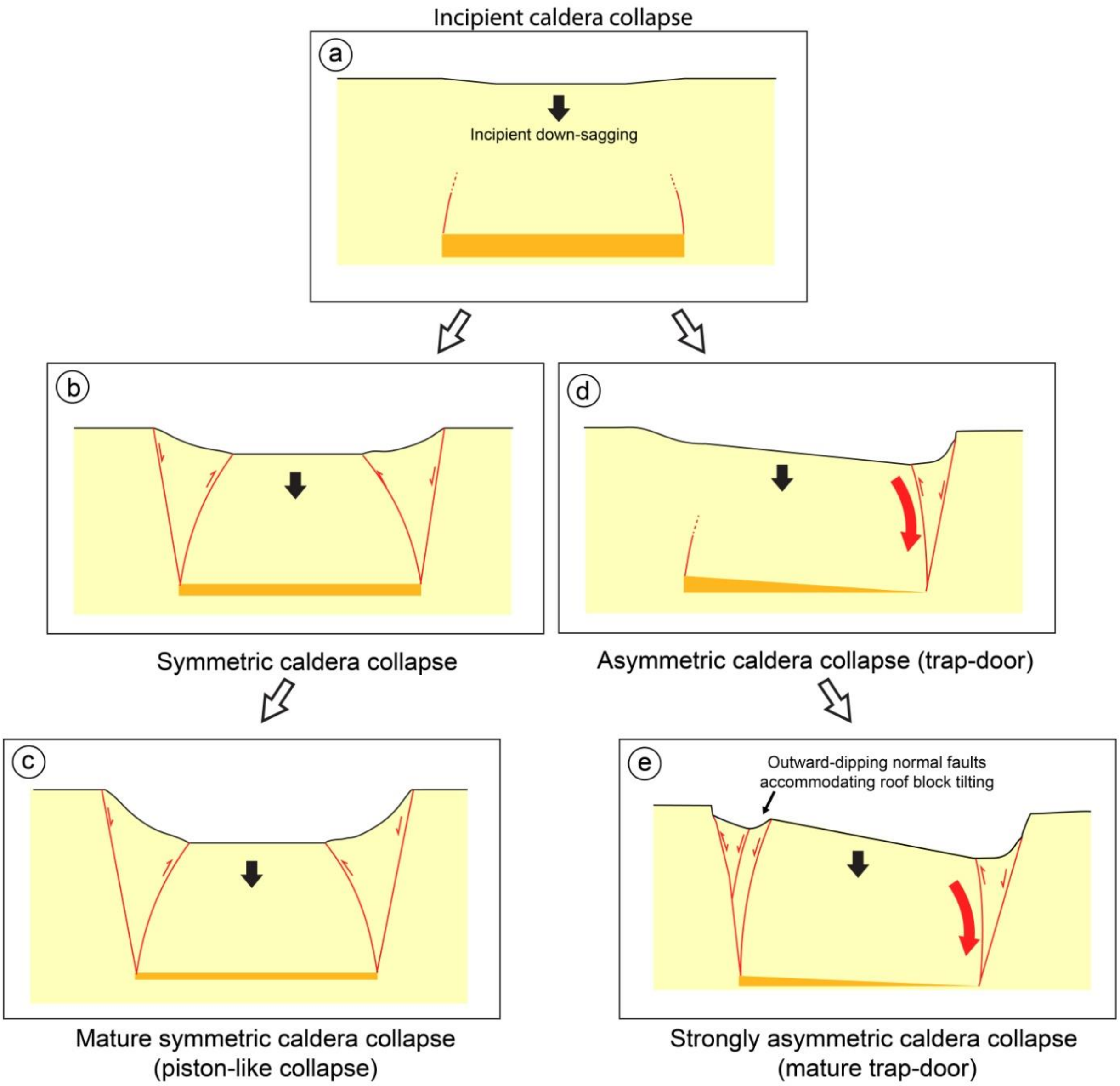

Figure 4.3. Conceptual evolutionary model for symmetric piston-like caldera collapse and trap-door caldera systems. From an initial down-sagging phase (a), models can develop symmetric collapse (b, c) or asymmetric collapse (d, e). See the text for details. Red arrows indicate subsidence of the roof block in asymmetric caldera models. Black arrows indicate caldera subsidence.

Symmetric collapse ends with the development of the system of inward-dipping normal faults forming the peripheral ring faults (Fig. 4.3b) until total subsidence is reached (Fig. 4.3c). In case of asymmetric collapse, after the down-sagging phase, the caldera collapse is accommodated by the tilting of a central roof block. In the initial phases, roof block tilting is accommodated by large displacement along faults located on one side of the caldera, while the opposite caldera side is acting as hinge accommodating the block tilting (Fig. 4.3d). With increasing subsidence, roof block tilting increases and its uplift is typically accommodated by the development of normal faults dipping outwards, namely toward the adjacent caldera rim (Fig. 4.3e).

4.1.2 Series D3.6-2: Role of pre-caldera volcano-related topography

Series D3.6-2 aimed to test the effect of a pre-caldera volcano-related topography on caldera collapse processes. Furthermore, this aspect was test with the coupled effect of inherited structures, and specific models were designed with both artificial discontinuities and an overlying volcanic edifice. Among specific aspects described for each model, results of Series D3.6-2 show several similarities with models of Series D3.6-1. The structural pattern described for comparison of symmetric and asymmetric collapse in Figure 4.2 of the previous section can be easily identified also in models designed with a volcano edifice, implying that the presence of a volcanic edifice does not alter significantly the first-order process of caldera collapse. Beside, the volcanic edifice, depending on its characteristics and position, may play a key role in inducing a symmetric or asymmetric collapse.

Al the performed models were designed and built with a standard analogue volcanic edifice, implying variations of its shape cannot play any influence on caldera collapse. Nonetheless, some models resulted in a symmetric piston-like collapse (e.g., Model- 33, Model-43, Model-46), whereas others showed clear trap-door geometry (e.g., Model-42, Mode-44, Model-45). The development of asymmetric (trap-door) caldera collapse is likely induced by the presence of the analogue volcanic edifice placed in an eccentric position with respect to the underlying analogue magma chamber. This localization induces a differential vertical stress on the analogue magma chamber, resulting in an increased vertical loading beneath the volcano that favours an asymmetric caldera collapse. In contrast, models that evolved in symmetric calderas were designed with a volcano edifice centred over the analogue magma chamber.

Interestingly, the asymmetrically collapsed models of Series D3.6-2 (e.g., Model-42, Fig. 4.4) develop the same features described for Series D3.6-1 models. A strongly subsided area (blue colours in the DEM shown in Fig. 4.4a) is located at the opposite position of a normal fault system accommodating the central piston block tilting, confirming that these structures represent key features in mature trap-door systems. These structures develop in area subjected to extension induced by the piston rotation (green area in Fig. 4.4b), which in this case is induced by an extra loading overload related to the eccentric analogue volcanic edifice (the area of vertical overload is indicated in red in Fig. 4.4b). Clearly, such an extra loading is null when the volcano edifice is located completely external position with respect to the analogue magma chamber, as in Model-41, which deforms according to a piston-like collapse. This setting has been described for natural cases of oblique magma plumbing systems feeding an eccentric volcano with respect to its magma chamber (e.g., Tibaldi, 2015). Under certain conditions, an eccentric volcano may transfer differential stress to the underlying magma chamber, for instance when ductile layers are present in the substrate. However, the setup adopted in our models (with a rigid analogue magma chamber) is unable to transfer stress from highly eccentric analogue volcanoes to the magma chamber, representing one of the limitations of model setup.

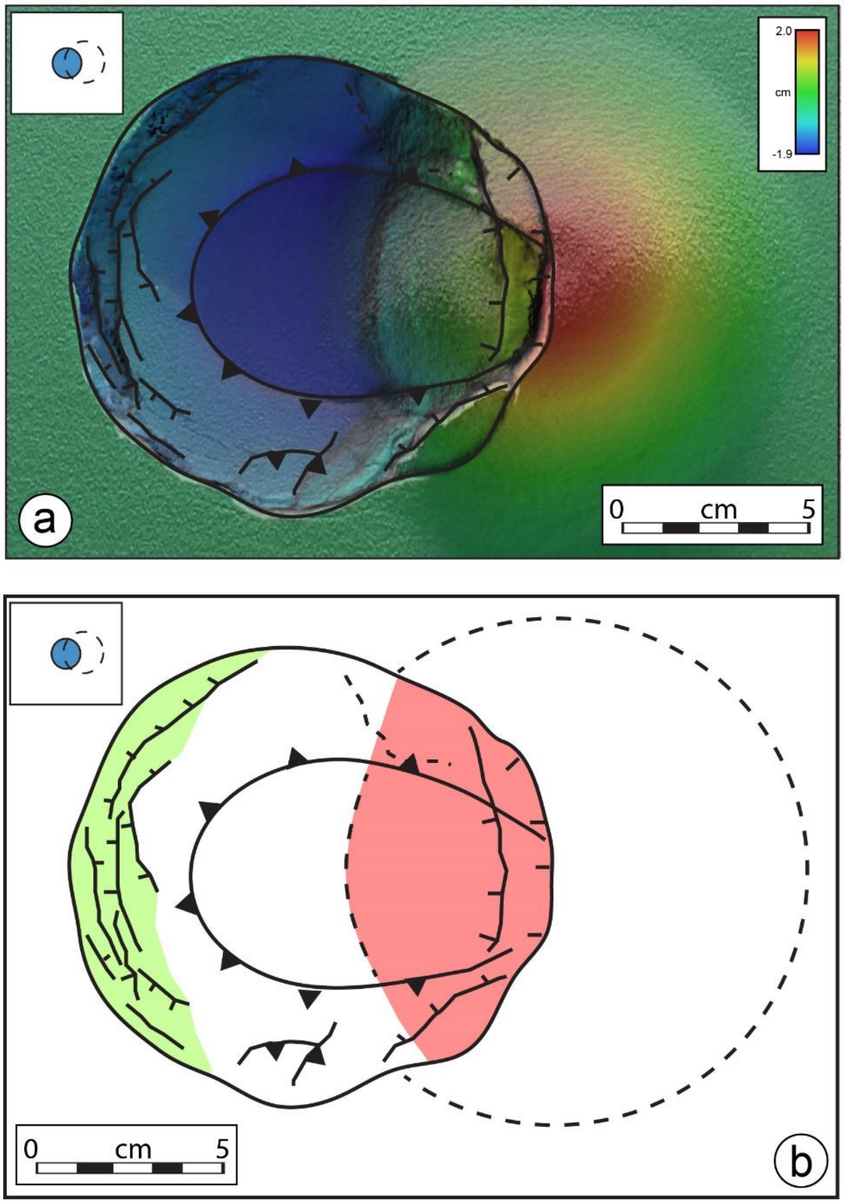

F

Figure 4.4. (a) Digital elevation model (DEM) superimposed onto top view photo of caldera collapse obtained in Model-42, together with line-drawing interpretation of structures. (b) Model-42 interpretation highlighting the areas experiencing extensional stress (green area) and vertical extra loading (red area) due to the presence of the collapsing flank of the analogue volcanic edifice.

The introduction of artificial inherited structures, in models built with variously positioned volcanic edifices, has produced caldera collapse deformation outcomes similar to those described earlier in Series D3.5-2b,c,d of Deliverable D3.5.

4.1.3 Series D3.6-3: Caldera resurgence and interaction with pre-existing structures (both regional inherited fabrics and caldera collapse faults)

Models performed for Series D3.6-3 aims to test various aspects related to caldera resurgence and inherited discontinuities. In sub-series D3.6-3a we have tested the effect of piston-like resurgence both on symmetric (piston-like collapse) and asymmetric (trap-door system) collapsed calderas. Besides, sub-series D3.6-3b has evaluated the effect of localized resurgence, and sub-series D3.6-3c the coupled effect of inherited discontinuities and piston-like vs. localised caldera resurgence.

Model of sub-series D3.6-3a have shown that piston-like (i.e., broad) resurgence applied to a symmetric collapsed caldera have the simple effect to reactivate earlier caldera collapse-related structures. In particular, the latter are forced to recover part of their vertical throw acquired during the collapse in order to accommodate the central piston resurgence. These models have demonstrated that during piston-like symmetric resurgence, formation of new resurgence-related structures is generally absent. This process is summarized in Figure 4.5, and shows caldera collapse and resurgence of a symmetric collapsed system.

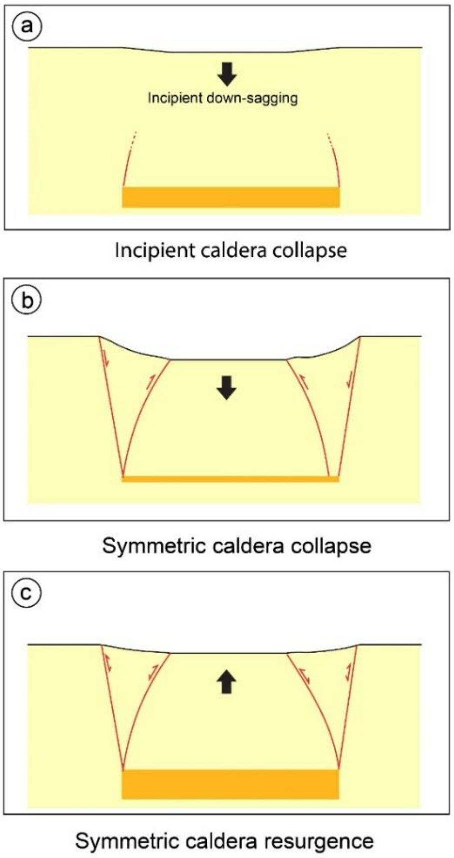

Figure 4.5. Conceptual schematic cartoon showing the process of symmetric caldera collapse and subsequent piston-like (symmetric) resurgence. See the text for details.

However, broad resurgence developing on a mature trap door system can be more complex owing to its asymmetry. As also highlighted in Sections 4.12 and 4.1.3, in our models mature trap door systems often develop peculiar structural features at the opposite position of the maximum area of subsidence. These structures are outward-dipping normal faults forming between the ring fault system and the piston block to accommodate its tilting (e.g. green area in Fig. 4.4b). In case of broad caldera resurgence, these features show a peculiar behaviour, as they increase their vertical normal throw instead of inverting their kinematics as one might expect. DPIV analysis effectively highlights the characteristics of broad (piston-like) resurgence. In particular, DPIV analysis for Model-7 shows that broad resurgence is mainly accommodated by the ring fault system, and, in this specific case of asymmetric collapse, also by the outward-dipping normal faults acting as hinge accommodating uplift of the tilted roof block (Fig. 4.6).

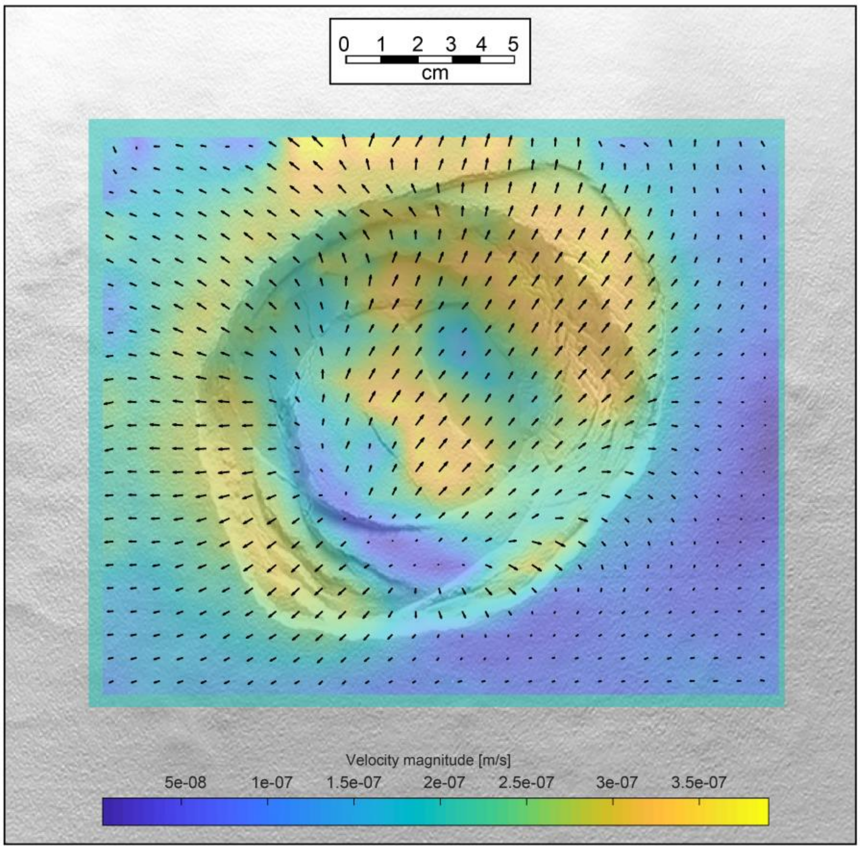

Figure 4.6. DPIV analysis of Model-7 showing asymmetric broad resurgence. Warmer colours indicate higher particle velocities. DPIV is performed on two frames captured with a time interval of 6 minutes.

This evolution is sketched in Fig. 4.7. After asymmetric caldera collapse (Fig. 4.7a,b) and development of a mature trap-door system (Fig. 4.7c), broad resurgence generates a piston uplift re-activating previously formed ring-faults and inner structures. Due to the tilt of the central piston block, the outward-dipping normal faults, located on the margin that has experienced less caldera subsidence, increase their vertical normal throw to accommodate the following caldera resurgence (Fig. 4.7d).

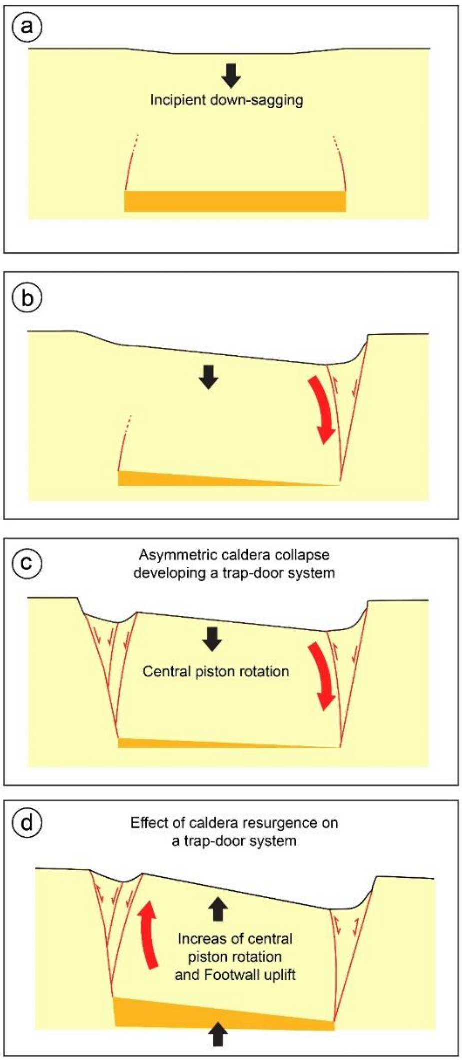

Figure 4.7. Conceptual schematic cartoon showing the process of caldera collapse and resurgence in an asymmetric trap-door system. See the text for explanation.

Sub-series D3.6-3b has tested the effect of localized resurgence that has been obtained by re-intruding analogue magma at different depths below the model surface. These models showed that the geometry of re-intrusion and consequent superficial deformation is influenced by the depth of reinjection. Since we have used for these models the same analogue magma PG3 (i.e., not varying physical parameters of reinjection, e.g., density, viscosity, etc…) and the same velocity of reinjection, we may assume that the geometry and type of re-intrusion is influenced only by the interplay between overpressure of the injected analogue magma and the lithostatic loading above the point of intrusion in the model. A shallow point of re-injection implies low vertical load due to the reduce overburden thickness, which allows the analogue magma to fracture the brittle sand overburden forming a dyke and ultimately extrude at surface (Fig. 4.8a). A deeper point of injection slightly modifies the style of intrusion producing a small sill-like intrusions from which depart shallower dykes. This deformation style thus defines a forced fold cored by magma (e.g., Montanari et al., 2017b; Fig.4.8b). Increasing the injection depth, dimensions of forced fold and sill-like intrusion become larger, while the associated dikes are less developed than in the previous models (Fig. 4.8c). A deep point of reinjection implies a loading generated by the whole overburden thickness, and consequently favours the development of deep sill-like localized resurgence (Fig. 4.8d).

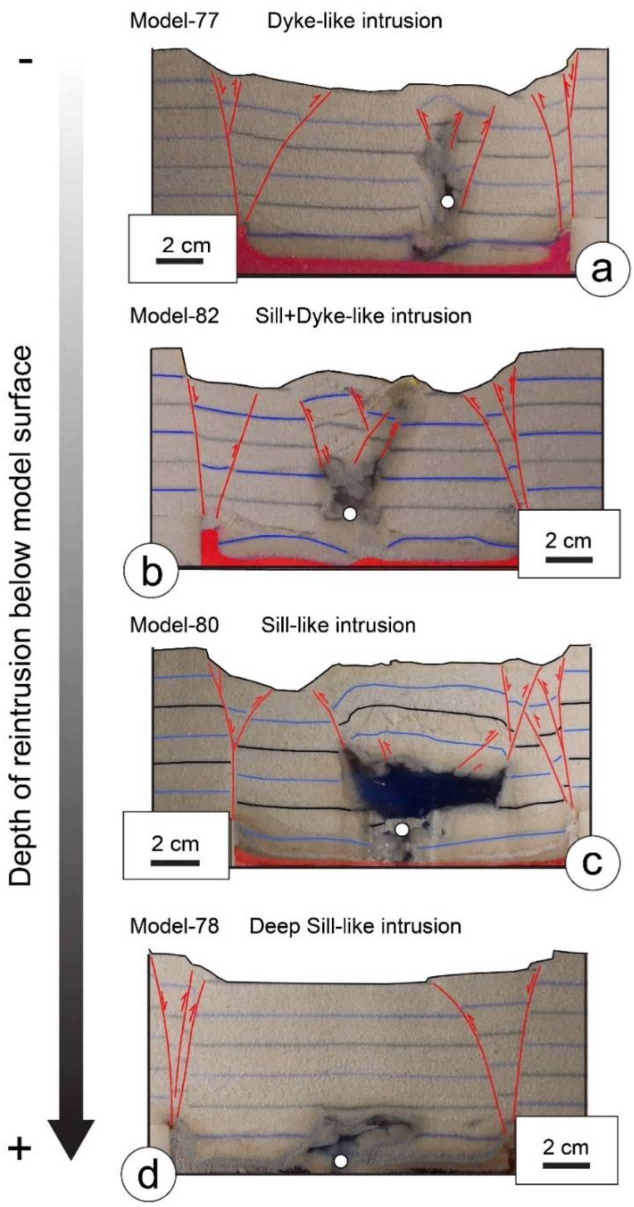

Figure 4.8. Model cross section showing the effect of localized analogue magma reinjection at various depth (a) shallow re-intrusion at 3 cm below the model surface), (b) re-intrusion at 4 cm below the model surface, (c) re-intrusion at 4.5 cm below the model surface and (d) deep re-intrusion at 5 cm below the model surface. White dot indicate the point of reinjection. See the text for discussion.

At surface, localized analogue magma re-intrusion induces doming that eventually may be severely affected by surface extrusion of the analogue magma. Whichever the dome dimension, which is function of intrusion depth (and therefore geometry), its superficial deformation is generally accommodated by radial fracture and small graben systems bordered by rectilinear normal faults. Furthermore, caldera-related ring faults are not exploited by resurgence, which instead localizes deformation at the caldera centre, as highlighted by DPIV analysis (Fig. 4.9)

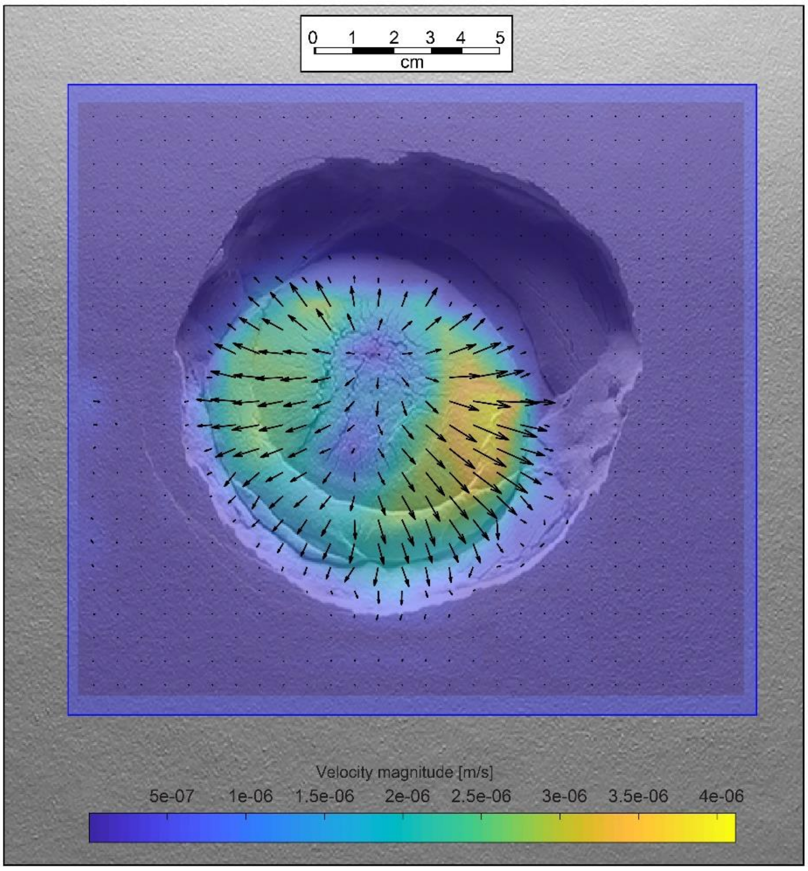

Figure 4.9. DPIV analysis of Model-80 showing localized resurgence. Warmer colours indicate higher particle velocities. DPIV is performed on two frames captured with a time interval of 6 minutes.

Regarding the coupled role of caldera resurgence and inherited structures, sub-series D3.6-3c models showed that discontinuities in the overburden located at the centre of the analogue magma chamber are not reactivated by piston-like resurgence nor by localized resurgence. Notably, this happened also for model that investigated caldera collapse (and not resurgence) described in Series D3.5-2d in Deliverable D3.5. However, these models tested the role of such central discontinuities only for symmetric caldera collapse/resurgence. It is likely that such discontinuities would be reactivated by an asymmetry resurgence, possibly with a reverse kinematics. The inherited discontinuities bounding the analogue magma chamber and crosscutting the brittle overburden are instead easily reactivated during broad caldera resurgence, as discussed for Model-83. Finally, in symmetric collapse/resurgence models, localized resurgence affects only the central area of the collapsed caldera, and does not generally interact with the inherited boundary faults (e.g., Model-85).

4.1.4 Series D3.6-4: Combined effects of compressional and extensional tectonics structures and magmatic processes on the Los Humeros Volcanic Complex (LHVC)

Models realized for Series D3.6-4 have been focused on the LHVC case study, to reproduce in a single experimental set the whole sequence of geological processes that have been identified by the structural study presented in Norini et al. (2019).

The analogue modelling shows that:

a) the two different orders of simulated inherited compressive and extensional regional tectonic structures play a role in the evolution of the magma feeding system, caldera collapses and post-caldera deformations of the experimental caldera complex;

b) geometry of caldera ring faults and rims is characterized by straight segments roughly parallel to and controlled by both inactive thrust faults and normal faults in the basement;

c) Main resurgence faults and post-caldera magma-driven hydrofractures reactivated the inherited tectonic weak planes in the basement underlying the experimental caldera complex. Geometry in plan view of the resurgence faults is controlled by the inherited regional structures and volcanotectonic radial stress field generated by the vegetable oil intrusion;

d) Expect secondary permeability in the geothermal reservoir overlying the post-caldera intrusion should mainly be related to the damage zone of resurgence faults delimiting uplifted and tilted sectors of the caldera floor. Complex geometry of these resurgence faults and local volcanotectonic stress field should be the main factors affecting the variability of secondary permeability within the hydrothermal system.

4.1.5 Series D3.6-5: Shallow intra-caldera intrusions

Our results confirm that the apical graben width shows a linear correlation with the source depth (Fig. 3.80) as estimated in (Brothelande and Merle, 2015). Since (Brothelande and Merle, 2015) performed experiments using elliptical sources with different aspect ratios, our experimental results (using circular sources) suggest that the shape of the source has no influence on the linear correlation with the source depth despite having an influence on the shape of the surface deformation (i.e. elliptical versus circular shape of the dome and the graben). Concerning the effect of layering, our results show that layering has an impact on the results only with the thicker overburden by decreasing the graben width. As this relation contrast with the outcomes of numerical models stating that a soft layer located below a mechanically stiffer layer generates greater tensional stress at surface (i.e. an increasing graben width should be expected, Kinvig et al., 2009) further experiments should test the relation between the apical graben width and layering with thick overburdens to clarify such discrepancy.

Since there is no difference between elliptical vs. circular sources, we constrain the depth of the intrusion (T) from the geometrical parameters measured in the experiments graben diameter (Lg), dome flank dip (θ) and dip of graben master faults (α) using the equation by Brothelande and Merle (2015):

$$T_t = \frac{1}{2} L_g \times \frac{\sin(\theta + \alpha)}{\cos\theta}$$

Comparing the percentage difference between the imposed experimental (T) and theoretical (Tt) overburden thickness values, we calculate the associated error in the evaluation of the intrusion depth in the models (σ, Table 4-1, Fig. 3.81). We then use the above equation for the evaluation of the heat source depth at the Loma Blanca bulge considering σ ~ 40 % (maximum value of the layered experiments with T= 30 and 50 mm). We exclude the σ values of the experiments with T=10 mm as the observed deformation pattern is not consistent with the pattern observed in the field.

Exp	T (mm)	L_g (mm)	L_d (mm)	θ	α	T_t (mm)	σ (%)
HUM 7	10	16	116	59°	26°	15.5	55
HUM 9	10	19	113	62°	27°	20.2	102
HUM 12	10	16	119	62°	27°	17	70
HUM 13	10	14	105	63°	27°	15.4	54
HUM 4	30	42	150	58°	14°	37.7	27
HUM 5	30	48	138	56°	18°	41.2	37
HUM 10	30	44	143	58°	16°	40	33
HUM 6	50	58	164	58°	21°	53.7	7
HUM 11	50	80	174	50°	23°	59.5	19

Table 4-1. Measured parameters in the experiments (layered highlighted in red). T=overburden thickness; Ld= dome diameter; Lg= apical graben width; θ= apical graben fault dip; α= dome flank mean dip; Tt= theoretical overburden thickness calculated with equation of (Brothelande and Merle, 2015); σ= percentage difference between T and Tt.

4.2 Clues from analogue modelling of caldera collapse and resurgence on the evolution of Los Humeros and Acoculco geothermal systems

Model performed in the frame of Series D3.6-1 reported in this deliverable (but also in Deliverable D3.5) have highlighted the structural, evolutionary deformation pattern typical of both symmetric and asymmetric caldera collapse systems. This analysis may help to characterize the structural setting of the Los Humeros volcanic system and Acoculco caldera system. In particular, the comparison with the surface structural style may help to understand the geometry of caldera faults at depth for both case studies. This issues is particularly important, since faults do often represent permeable structures that may localize migrating geothermal fluids. As stated earlier, internal caldera geometry resulting from caldera subsidence is characterized by the presence of outward-dipping reverse faults and more external inward-dipping normal faults. These structures, and/or their interaction with other faults observed in our models (e.g., the outward-dipping normal faults accomplishing uplift of the resurgent block) may be particularly useful when interpreting available geophysical data of the caldera system (e.g., seismic lines, magnetotellurics, etc.) for reconstructing the structural setting internal to the caldera system and the possible geometry of permeable paths.

Series D3.6-2 has investigated the specific case of a magmatic chamber overlaying by a volcanic edifice, a setting that may simulate the original conditions before caldera collapse at both Los Humeros and Acoculco volcanic systems. Obviously, at present the volcanic edifice at the two sites of interest has been mostly dismantled by volcanic processes and meteoric erosion, and thus we are not aware about the specific relationships between the volcano edifice and the related magma chamber. Nonetheless, by applying a systematic variation to modelling conditions (i.e., position of the volcano edifice), we have tested various possibilities, and the results of this modelling might provide useful insights when the original relationship between the magma plumbing system and the resulting volcanic edifice will better defined. Beyond this limit, our models support that a volcanic edifice placed in an eccentric position has the ability to induce asymmetry in the collapsing caldera systems, whereas central volcanoes would favour a mostly symmetric collapse. Therefore, understanding the original volcano setting at Los Humeros and Acoculco volcanic systems may help to distinguish which of the proposed models may fit better the case studies.

Series D3.6-3 investigated the structural pattern resulting from caldera resurgence (both broad, i.e., piston-like, and localized) on symmetric and asymmetric collapsed calderas. These models may be particularly useful when interpreting the internal fault pattern at Los Humeros, particularly at the smaller Los Potreros caldera. The structural pattern of the Los Potreros fault system (a term that is used here to indicate the system of structures including the Maxtaloya, Los Humeros, Las Papas faults and associated structures) is indeed similar to some of the structural patterns obtained in our models, particularly the models addressing localized resurgence. For example, Model-80 and Model-85 developed a structural pattern derived from extension of the resurgent block that is strikingly comparable to the fault pattern of the Los Potreros fault system (Fig. 4.10). Understanding of the fault geometry at depth is an important topic, as the Los Potreros fault system is currently exploited and targeted for geothermal fluids. Both analogue models (Model-80 and Model-85) developed a main normal fault, from which emanate smaller normal fault branches. The surface fault pattern above the analogue magma intrusion is thus characterized by the occurrence of sub-orthogonal fault segments delimiting blocks with differential uplift, a pattern that is very similar to that of the Los Potreros intra-caldera fault system (Fig. 4.10,c,d). This correspondence may thus suggest a similarity in dynamic processes. The main model normal fault shows, in fact, similar features (i.e., geometry, dip and kinematics) to the Maxtaloya fault (Fig. 4.10b), particularly the central position of this fault on the resurgent block system (see Fig. 4.10).

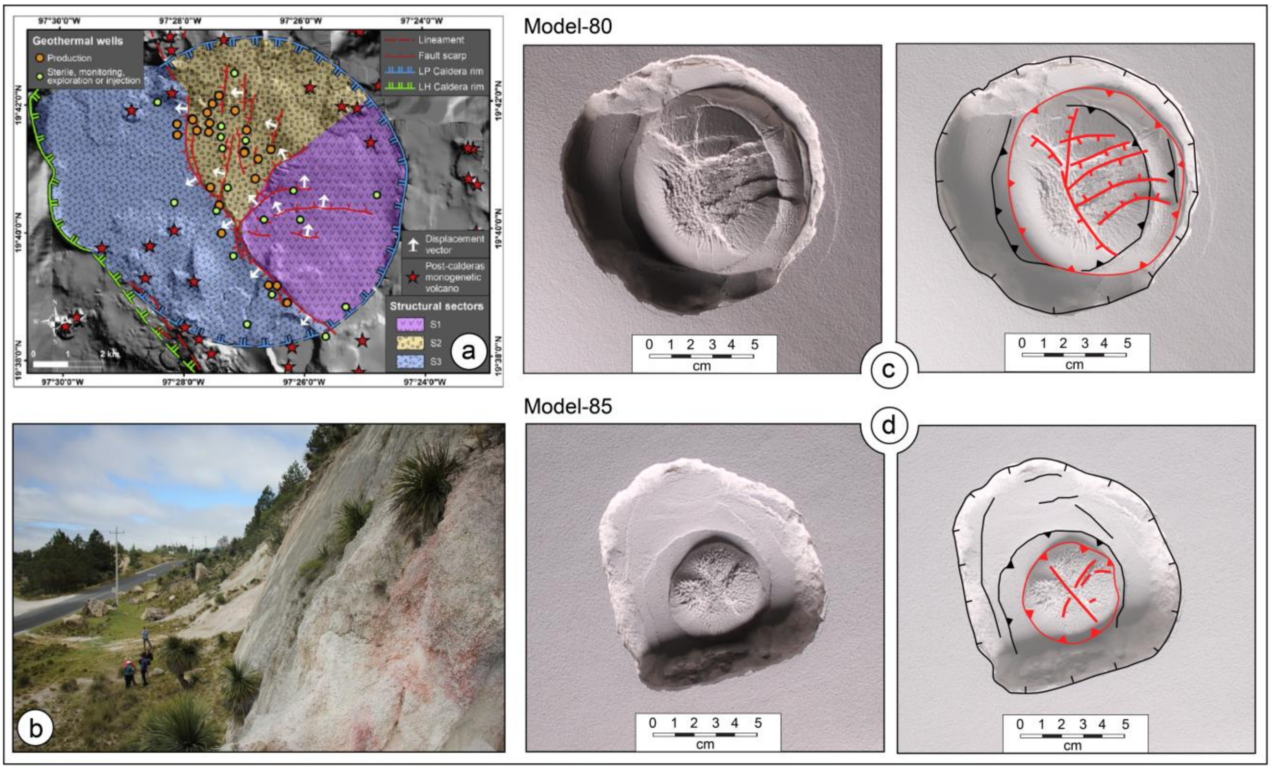

Figure 4.10. Comparison between the Los Potreros structural setting (a) and Maxtaloya fault (b) with models of Series D3.6, showing the effect of localized intra-caldera resurgence (c,d).

These findings are in agreement with those of series D3.6-4 in that secondary permeability in the geothermal reservoir overlying the post-caldera intrusion may be related to the damage zone of resurgence faults delimiting uplifted and tilted sectors of the caldera floor. Complex geometry of these resurgence faults and local volcanotectonic stress field should be the main factors affecting the variability of secondary permeability within the hydrothermal system.

Furthermore, our models provide also alternative ways to explain the Los Potreros structural pattern. These hypotheses aim to compare the natural cases with the geometry observed in the models, and not to provide a unique interpretation. The various hypotheses based on modelling results for the evolution of the Los Humeros and Los Potreros calderas are summarized in Figure 4.11. A first possibility to explain the structural pattern observed at Los Potreros, may consider the Los Humeros caldera collapse exploiting inherited discontinuities (Fig. 4.11a$_1$) and generating a trap-door system with development of outward-dipping normal faults described in asymmetric models (cf. with Fig. 4.2b). The subsequent Los Potreros collapse may have incorporated the older caldera structures at its centre (Fig. 4.11b_1). A variation to this model (Fig. 4.11a_2 and 4.11b_2) may involve the reactivation of these structures by caldera resurgence (Fig. 4.11c_2). This hypothesis is supported by the observation that intra-caldera Los Potreros faults experienced large Holocene slip-rates up to 10 mm yr^{-1} (Norini et al., 2015). At third possibility may consider that after collapse of the Los Humeros and Los Potreros systems (Fig. 4.11a_3, and 4.11b_3) localized resurgence may have generated the formation of the intra-caldera Los Potreros fault system, similar to the structural pattern described in Model-80 and Model-85 (Fig. 4.11c_3). Finally, a further possibility may involve the interplay of caldera collapse and resurgence with inherited faults crosscutting the overburden of the Los Potreros and Los Humeros calderas (Fig. 4.11a_4, 4.11b_4, and 4.11c_4). In this case, reactivation would have been favoured by a certain degree of asymmetry of the collapsed caldera. The integration of these hypotheses with geophysical and geological data may contribute to constrain the structural setting of these volcanic systems.

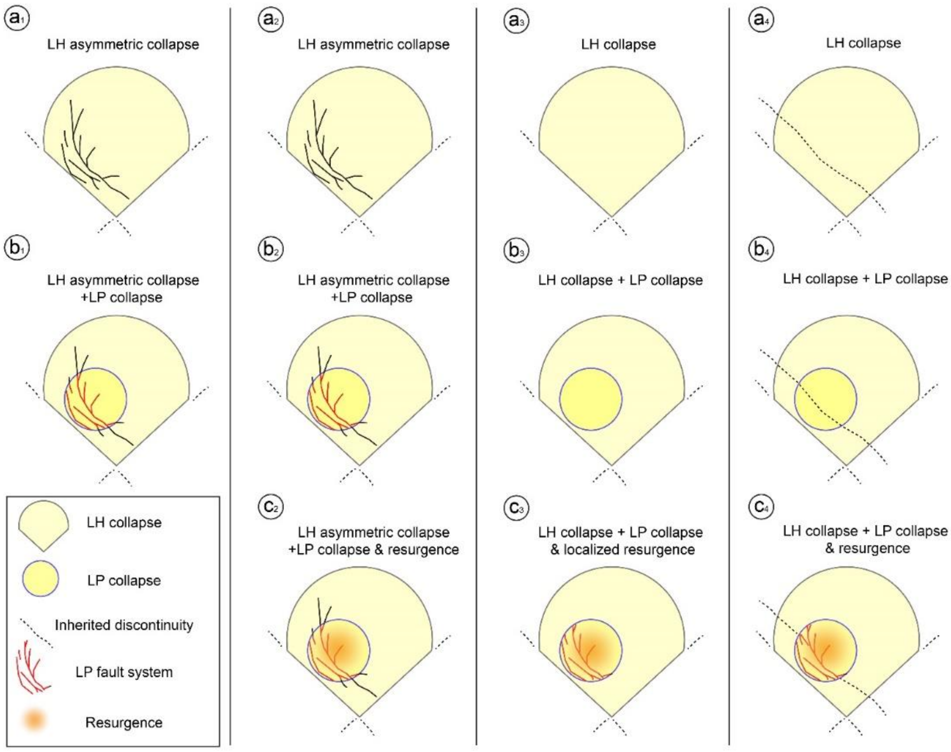

Figure 4.11. Schematic cartoon showing different hypotheses, derived from modelling, for the evolution of the structural pattern of the Los Humeros and Los Potreros caldera systems. See text for details. LH: Los Humeros; LP: Los Potreros.

Finally, the analysis of Series D3.6-5 models provide useful hints for the Los Potreros geothermal system. In particular, for the Loma Blanca bulge Lg= 286 m, θ= 71°, α= 4.5°, the estimated intrusion depth is 425 ± 170 m. Such relatively shallow depth is within the range of depths of acidic domes drilled in geothermal wells (spanning from 300 to 1700 m) and is consistent with the hypothesis that the uplift is driven by small and delocalized magmatic intrusions, as suggested by the field data (Urbani et al. 2019 in review).

It is therefore unlikely that the replenishment of new magma in the caldera forming deep magma chamber accounts for the magnitude (few tens of meters) and discontinuous spatial distribution of the deformation in Los Potreros.

Such a model of the recent uplifting in Los Potreros is supported by field-based petrographic-mineralogical analysis showing that the present-day magmatic plumbing system is characterized by multiple magma levels spanning from a deep (30-33 km) basaltic reservoir to very shallow (~ 1.5 km), smaller, trachyandesitic-trachytic magma batches (Lucci et al. 2019, in review).

A similar model of the plumbing system has been proposed to explain the eruptive activity of Usu volcano (Japan) since 1663, a post caldera cone of the Toya caldera consisting of a basaltic main edifice surmounted by 3 felsic lava domes and more than 10 cryptodomes. Petrochemical data at Usu suggest the presence of multiple magma batches (i.e. sills) at 0.25-2 km deep that originated from partial melting of a metagabbro (Matsumoto and Nakagawa, 2010; Tomya et al., 2010).

This conceptual model has implications for planning future geothermal exploration: siting of future geothermal wells should consider that the presence of shallow heat sources within the caldera may complicate the pattern of isotherms associated with the deeper heat flow.

5 Conclusion

Deliverable 3.6 reports the results obtained in the frame of Task 3.3, investigating collapse of caldera and volcanic edifices and the associated surface deformation through analogue modelling. The present deliverable has reported four experimental series (D3.6-1, D3.6-2, D3.6-3, D3.6-4 and D3.6-5) aiming respectively at the investigation of (1) the processes of symmetric/asymmetric caldera collapse, (2) the effect of pre-caldera volcano-related topography, and (3) caldera resurgence and interaction with pre-existing structures (both regional inherited fabrics and caldera collapse faults), including (4) the compressive structures of the Mexican Fold and Thrust Belt (MFTB), and finally (5) the role of shallow intra-caldera intrusions.

Series D3.6-1 has shown that symmetric caldera collapse is achieved through transient asymmetry steps, which ultimately lead to the formation of a first-order symmetric collapsed system. Nonetheless, specific structures may develop as a response to this transient mechanism, such as the structures here called “fish tail” that may have a strike-slip component. Furthermore, the development of asymmetric caldera collapse leading to the formation of trap-door systems may develop peculiar extensional structures that accommodate the tilting of the caldera block.

The letter structures are also observed in asymmetric models obtained in Series D3.6-2, where the presence of an eccentric volcano edifice induces extra loading on the subsiding block, forcing the caldera to develop a trap-door system. The volcano edifice was introduced in Series D3.6-2 in order to investigate the possible role of a pre-caldera topography. Model demonstrate how a volcano centred above the analogue magma chamber does not induce asymmetric collapse, whereas an eccentric one can easily destabilize the collapsing system to generate a trap-door geometry. This indication may provide insights into the pre-collapsing phase of the Los Humeros and Acocuclo systems and help to interpret the present structural setting.

The models performed in Series D3.6-3 tested the effect of broad (piston-like) and localized resurgence, providing insights into possible interpretations of the structural pattern of the case studies, particularly for the Los Potreros caldera. We have performed three subseries aiming at the investigation of (1) piston-like effect of caldera resurgence, (2) localized resurgence, (3) localized resurgence coupled with the effect of inherited structures. Our models show that a broad resurgence applied to a symmetric collapse simply reactivate the collapse-related structure accommodating the upward movement of the piston block. Broad resurgence of a trap-door system may be instead more complex, with re-intrusion of analogue magma increasing the original normal throw of some collapse-related faults. Localized resurgence is also able to generate various types of intrusion (and consequent surface deformation) as a function of the intrusion depth.

Series D3.6-4 has addressed the role that pre-existing thrust and normal faults may exert on magma resurgence, focusing on the setting specific for the Los Humeros-Los Potreros system.

Finally, Series D3.6-5 addresses the role of shallow intra-caldera intrusion, highlighting that shallow heat sources within the caldera may complicate the pattern of isotherms associated with the deeper heat flow.

Some of the models described above show a high similarity with the considered natural deformation patterns, and may thus help to explain their structural setting and the related evolutionary model.

6 References

Acocella, V. (2007). Understanding caldera structure and development: An overview of analogue models compared to natural calderas. Earth-Science Reviews, 85(3-4), 125-160.

Acocella, V., & Mulugeta, G. (2002). Experiments simulating surface deformation induced by pluton emplacement. Tectonophysics, 352(3-4), 275-293.

Acocella, V., Cifelli, F., & Funiciello, R. (2000). Analogue models of collapse calderas and resurgent domes. Journal of Volcanology and Geothermal Research, 104(1-4), 81-96.

Acocella, V., Cifelli, F., & Funiciello, R. (2001a). Formation of nonintersecting nested calderas: insights from analogue models. Terra Nova, 13(1), 58-63.

Acocella, V., Cifelli, F., & Funiciello, R. (2001b). The control of overburden thickness on resurgent domes: insights from analogue models. Journal of Volcanology and Geothermal Research, 111(1-4), 137-153.

Acocella, V., Funiciello, R., Marotta, E., Orsi, G., & De Vita, S. (2004). The role of extensional structures on experimental calderas and resurgence. Journal of Volcanology and Geothermal Research, 129(1-3), 199-217.

Avellán, D.L., Macías, J.L., Layer,P.W., Cisneros, G., Sánchez-Núñez, J.M., Gómez-Vasconcelos, M.G., Pola, A., Sosa-Ceballos, G., García-Tenorio, F., Reyes Agustín, G., Osorio-Ocampo, S., García-Sánchez, L., Mendiola, I.F., Marti, J., López-Loera H., Benowitz, J. (2018). Geology of the late Pliocene – Pleistocene Acoculco caldera complex, eastern Trans-Mexican Volcanic Belt (México). Journal of Maps, DOI: 10.1080/17445647.2018.1531075Bellahsen, N., Daniel, J.M. (2005). Fault reactivation control on normal fault growth: an experimental study. J. Struct. Geol. 27, 769-780.

Alaniz-Álvarez, S.A., Nieto-Samaniego, Á.F. (2007). The Taxco–San Miguel de Allende fault system and the Trans-Mexican Volcanic Belt: two tectonic boundaries in central México active during the Cenozoic. In: Alaniz-Álvarez, S.A., Nieto-Samaniego, Á.F. (Eds.), Geology of México: Celebrating the Centenary of the Geological Society of México: Geological Society of America Special Paper, 422, pp. 301–316.

Battaglia, J., and P. Bachelery (2003), Dynamic dyke propagation deduced from tilt variations preceding the March 9, 1998, eruption of the Piton de la Fournaise volcano, J. Volcanol. Geotherm. Res., 120, 289–310, doi:10.1016/S0377-0273(02)00410-9.

Byerlee, J. (1978), Friction of rocks, Pure Appl. Geophys., 116, 615–626, doi:10.1007/BF00876528.

Brothelande, E., and Merle, O. (2015). Estimation of magma depth for resurgent domes: An experimental approach, Earth Planet. Sc. Lett., 412, 143–151, https://doi.org/10.1016/j.epsl.2014.12.011.

Burkett, E.R., Billen, M.I. (2010). Three dimensionality of slab detachment due to ridge–trench collision: laterally simultaneous boudinage versus tear propagation. Geochemistry, Geophysics, Geosystems 11, Q11012. doi:10.1029/2010GC003286

Burov, E. B., & Guillou-Frottier, L. (1999). Thermomechanical behavior of large ash flow calderas. Journal of Geophysical Research: Solid Earth, 104(B10), 23081-23109.

Cailleau, B., Walter, T. R., Janle, P., & Hauber, E. (2003). Modeling volcanic deformation in a regional stress field: Implications for the formation of graben structures on Alba Patera, Mars. Journal of Geophysical Research: Planets, 108(E12).

Campos-Enriquez, J., & Garduño-Monroy, V. H. (1987). The shallow structure of Los Humeros and Las Derrumbadas geothermal fields, Mexico. Geothermics, 16(5-6), 539-554.

Carrasco-Núñez, G., McCurry, M., Branney, M.J., Norry, M., Willcox, C. (2012). Complex magma mixing, mingling, and withdrawal associated with an intraplinian ignimbrite eruption at a large silicic caldera volcano: Los Humeros of central Mexico. Geol. Soc. Am. Bull. 124, 1793–1809.

Carrasco-Núñez, G., Hernandez, J., De Leon, L., Davila, P., Norini, G., Bernal, J.P., Lopez, P. (2017a). Geologic map of Los Humeros volcanic complex and geothermal field, eastern Trans-Mexican Volcanic Belt. Terra Digitalis 1 (2), 1–11.

Carrasco-Núñez, G., López-Martínez, M., Hernández, J., & Vargas, V. (2017b). Subsurface stratigraphy and its correlation with the surficial geology at Los Humeros geothermal field, eastern Trans-Mexican Volcanic Belt. Geothermics, 67, 1-17.

Carrasco-Núñez, G., Bernal, J.P., Dávila, P., Jicha, B., Giordano, G., & Hernández, J. (2018). Reappraisal of Los Humeros volcanic complex by new U/Th zircon and 40Ar/39Ar dating: Implications for greater geothermal potential. Geochemistry, Geophysics, Geosystems, 19, 132–149.

Cedillo-Rodríguez, F. (1999). Modelo hidrogeológico de los yacimientos geotérmicos de Los Humeros, Puebla, México. Geoterm. Rev. Mex. Geoenerg. 15, 159–170.

Druitt, T. H., & Sparks, R. S. J. (1984). On the formation of calderas during ignimbrite eruptions. Nature, 310(5979), 679.

Ferrari, L. (2004). Slab detachment control on mafic volcanic pulse and mantle heterogeneity in central Mexico. Geology, 32(1), 77-80.

Ferrari, L., Orozco-Esquivel, T., Manea, V., Manea, M. (2012). The dynamic history of the Trans-Mexican Volcanic Belt and the Mexico subduction zone. Tectonophysics, 522–523, 122–149.

Ferriz, H., Mahood, G. (1984). Eruptive rates and compositional trends at Los Humeros volcanic center, Puebla, Mexico. J. Geophys. Res. 89, 8511–8524.

Galland, O., P. Cobbold, E. Hallot, and J. de Bremond d'Ars (2006), Use of vegetable oil and silica powder for scale modelling of magmatic intrusion in a deforming brittle crust, Earth Planet. Sci. Lett., 243, 786–804, doi:10.1016/j.epsl.2006.01.014.

García-Palomo, A., Macías, J. L., Jiménez, A., Tolson, G., Mena, M., Sánchez-Núñez, J. M., & Lermo-Samaniego, J. (2018). NW-SE Pliocene-Quaternary extension in the Apan-Acoculco region, eastern Trans-Mexican Volcanic Belt. Journal of Volcanology and Geothermal Research, 349, 240-255.

Garduño-Monroy, V., Spinnler, J., Ceragioli, E. (1993). Geological and structural study of the Chapala Rift, state of Jalisco, Mexico. Geoísica Internacional 32, 487–499.

Geyer, A., & Martí, J. (2014). A short review of our current understanding of the development of ring faults during collapse caldera formation. Frontiers in Earth Science, 2, 22.

Geyer, A., Folch, A., & Martí, J. (2006). Relationship between caldera collapse and magma chamber withdrawal: an experimental approach. Journal of Volcanology and Geothermal Research, 157(4), 375-386.

Gudmundsson, A. (2015). Collapse-driven large eruptions. Journal of Volcanology and Geothermal Research, 304, 1-10.

Gudmundsson, A. (2016). The mechanics of large volcanic eruptions. Earth-science reviews, 163, 72-93.

Gudmundsson, A. (1988). Formation of collapse calderas. Geology, 16(9), 808-810.

Gudmundsson, A., Marti, J., & Turon, E. (1997). Stress fields generating ring faults in volcanoes. Geophysical Research Letters, 24(13), 1559-1562.

Guillou-Frottier, L., Burov, E. B., & Milesi, J. P. (2000). Genetic links between ash-flow calderas and associated ore deposits as revealed by large-scale thermo-mechanical modeling. Journal of Volcanology and Geothermal Research, 102(3-4), 339-361.

Heidbach, Oliver; Rajabi, Mojtaba; Reiter, Karsten; Ziegler, Moritz; WSM Team (2016). World Stress Map Database Release 2016. V. 1.1. GFZ Data Services. http://doi.org/10.5880/WSM.2016.001.

Holohan, E. P., Troll, V. R., Walter, T. R., Münn, S., McDonnell, S., & Shipton, Z. K. (2005). Elliptical calderas in active tectonic settings: an experimental approach. Journal of Volcanology and Geothermal Research, 144(1-4), 119-136.

Holohan, E. P., de Vries, B. V. W., & Troll, V. R. (2008). Analogue models of caldera collapse in strike-slip tectonic regimes. Bulletin of Volcanology, 70(7), 773-796.

Holohan, E. P., Walter, T. R., Schöpfer, M. P., Walsh, J. J., van Wyk de Vries, B., & Troll, V. R. (2013). Origins of oblique-slip faulting during caldera subsidence. Journal of Geophysical Research: Solid Earth, 118(4), 1778-1794.

Hubbert, M. K. (1937). Theory of scale models as applied to the study of geologic structures. Bulletin of the Geological Society of America, 48(10), 1459-1520.

Kennedy, B., Stix, J., Vallance, J. W., Lavallée, Y., & Longpré, M. A. (2004). Controls on caldera structure: Results from analogue sandbox modeling. Geological Society of America Bulletin, 116(5-6), 515-524.

Kinvig, H.S., Geyer, A., and Gottsmann, J. (2009). On the effect of crustal layering on ring-fault initiation and the formation of collapse calderas, J. Volcanol. Geoth. Res., 186, 293–304, https://doi.org/10.1016/j.jvolgeores.2009.07.007.

Komuro, H., Fujita, Y., & Kodama, K. (1984). Numerical and experimental models on the formation mechanism of collapse basins during the Green Tuff orogenesis of Japan. Bulletin Volcanologique, 47(3), 649-666.

Komuro, H. (1987). Experiments on cauldron formation: a polygonal cauldron and ring fractures. Journal of Volcanology and Geothermal Research, 31(1-2), 139-149.

Lavallée, Y., Stix, J., Kennedy, B., Richer, M., & Longpré, M. A. (2004). Caldera subsidence in areas of variable topographic relief: results from analogue modeling. Journal of Volcanology and Geothermal Research, 129(1-3), 219-236.

Liotta, D., and WP4 Working Group, (2019). Final report on active systems: Los Humeros and Acoculco. Deliverable 4.1, GEMex project, European Union’s Horizon 2020 programme, 334 pp.

Liotta, D., 2019. Los Humeros and Las Minas. Structural geology and geophysical features. GEMex 3rd Interim Meeting, 18-19 June 2019, Bochum, Germany.

Lipman, P. W. (1997). Subsidence of ash-flow calderas: relation to caldera size and magma-chamber geometry. Bulletin of volcanology, 59(3), 198-218.

López-Hernández, A., García-Estrada, G., Aguirre-Díaz, G., González-Partida, E., Palma-Guzmána, H., Quijano-León, J.L. (2009). Hydrothermal activity in the Tulancingo–Acoculco Caldera Complex, central Mexico: Exploratory studies. Geothermics 38, 279–293

Lucci, F., Carrasco-Núñez, G., Rossetti, F., Theye, T., White, J. C., Urbani, S., Azizi, H., Asahara, Y., and Giordano, G. (2019, in review). Anatomy of the magmatic plumbing system of Los Humeros Caldera (Mexico): implications for geothermal systems, Solid Earth Discuss., https://doi.org/10.5194/se-2019-86.

Mart, Y., & Dauteuil, O. (2000). Analogue experiments of propagation of oblique rifts. Tectonophysics, 316(1-2), 121-132.

Marti, J., Ablay, G. J., Redshaw, L. T., & Sparks, R. S. J. (1994). Experimental studies of collapse calderas. Journal of the Geological society, 151(6), 919-929.

Matsumoto, A., and Nakagawa, M. (2010). Formation and evolution of silicic magma plumbing system: Petrology of the volcanic rocks of Usu volcano, Hokkaido, Japan, J. Volcanol. Geoth. Res., 196, 185–207, https://doi.org/10.1016/j.jvolgeores.2010.07.014.

Merle, O., and B. Vendeville (1995), Experimental modelling of thin-skinned shortening around magmatic intrusions, Bull. Volcanol., 57, 33–43, doi:10.1007/BF00298705.

Montanari, D., Agostini, A., Bonini, M., Corti, G., & Ventisette, C. (2017a). The use of empirical methods for testing granular materials in analogue modelling. Materials, 10(6), 635.

Montanari, D., Bonini, M., Corti, G., Agostini, A., & Del Ventisette, C. (2017b). Forced folding above shallow magma intrusions: Insights on supercritical fluid flow from analogue modelling. Journal of Volcanology and Geothermal Research, 345, 67-80.

Norini, G., Groppelli, G., Lagmay, A.M.F., Capra, L. (2006). Recent left-oblique slip faulting in the central eastern Trans-Mexican Volcanic Belt: seismic hazard and geodynamic implications. Tectonics 25, TC4012. doi:10.1029/2005TC001877

Norini G., Capra L., Groppelli G., Lagmay A.M.F. (2008). Quaternary sector collapses of Nevado de Toluca volcano (Mexico) as consequence of regional tectonics and volcanic evolution, Geosphere, 4, 5, 854-871. ISSN 1553-040X.

Norini G., Acocella V. (2011). Analogue modelling of flank instability at Mount Etna: understanding the driving factors, Journal of Geophysical Research – Solid Earth, 116, 1-21, B07206. ISSN 0148-0227.

Norini, G., Groppelli, G., Sulpizio, R., Carrasco-Núñez, G., Dávila-Harris, P., Pellicioli, C., Zucca, F., De Franco, R. (2015). Structural analysis and thermal remote sensing of the Los Humeros Volcanic Complex: implications for volcano structure and geothermal exploration. J. Volcanol. Geotherm. Res. 301, 221–237.

Norini, G., Carrasco–Núñez, G., Corbo-Camargo, F., Lermo, J., Hernández Rojas, J., Castro, C., Bonini, M., Montanari, D., Corti, G., Moratti, G., Piccardi, L., Chavez, G., Zuluaga, M.C., Ramirez, M., Cedillo, F., (2019). The structural architecture of the Los Humeros volcanic complex and geothermal field. Volcanol. Geotherm. Res., 381, 312–329; doi: 10.1016/j.jvolgeores.2019.06.010.

Ramberg, H. (1981). Gravity, deformation and the earth's crust: in theory, experiments and geological application. Academic press.

Roche, O., Druitt, T. H., & Merle, O. (2000). Experimental study of caldera formation. Journal of Geophysical Research: Solid Earth, 105(B1), 395-416.

Roman, D. C., J. A. Power, S. C. Moran, K. V. Cashman, M. P. Doukas, C. A. Neal, and T. M. Gerlach (2004), Evidence for dike emplacement beneath Iliamna Volcano, Alaska in 1996, J. Volcanol. Geotherm. Res., 130, 265–284, doi:10.1016/S0377-0273(03)00302-0.

Rosas-Elguera, J., Urrutia-Fucugauchi, J. (1998). Tectonic control on the volcano-sedimentary sequence of the Chapala graben, western Mexico. International Geology Review 40, 350–362.

Sosa-Ceballos, G., Macías, J.L., Avellán, D.R., Salazar-Hermenegildo, N., Boijseauneau-López, M.E., Pérez-Orozco, J.D. (2018). The Acoculco Caldera Complex magmas: Genesis, evolution and relation with the Acoculco geothermal system. Journal of Volcanology and Geothermal Research, 358, 288–306

Spence, D. A., and D. L. Turcotte (1985), Magma- driven propagation of cracks, J. Geophys. Res., 90, 575–580, doi:10.1029/JB090iB01p00575

Suter, M., Quintero, O., López, M., Aguirre, G., Ferrar, E. (1995). The Acambay graben: active intraarc extension in the Trans-Mexican Volcanic Belt. Tectonics 14, 1245–1262.

Suter, M., López-Martínez, M., Quintero-Legorreta, O., Carrillo-Martínez, M. (2001). Quaternary intra-arc extension in the central Trans-Mexican volcanic belt. Geological Society of America Bulletin, 113, 693–703. doi:10.1130/0016-7606.

Thielicke, W. & Stamhuis, E. (2014). PIVlab–towards user-friendly, affordable and accurate digital particle image velocimetry in MATLAB. Journal of Open Research Software, 2(1).

Tibaldi, A. (2015). Structure of volcano plumbing systems: A review of multi-parametric effects. Journal of Volcanology and Geothermal Research 298, 85–135.

Tomiya, A., Takahashi, E., Furukawa, N., Suzuki, T. (2010). Depth and evolution of a silicic magma chamber: Melting experiments on a low-K rhyolite from Usu volcano, Japan, J. Petrol., 51, 1333–1354, https://doi.org/10.1093/petrology/egq021.

Troll, V. R., Walter, T. R., & Schmincke, H. U. (2002). Cyclic caldera collapse: Piston or piecemeal subsidence? Field and experimental evidence. Geology, 30(2), 135-138.

Tron, V. & Brun, J.P. (1991). Experiments on oblique rifting in brittle-ductile systems. Tectonophysics, 188, 71-84.

Urbani, S., Giordano, G., Lucci, F., Rossetti, F., Acocella, V., and Carrasco-Núñez, G. (2019, in review): Estimating the depth and evolution of intrusions at resurgent calderas: Los Humeros (Mexico), Solid Earth Discuss., https://doi.org/10.5194/se-2019-100.

Verma, S.P. (1983). Magma genesis and chamber processes at Los Humeros caldera,Mexico – Nd and Sr isotope data. Nature 302, 52–55.

Verma, S.P. (2000). Geochemical evidence for a lithospheric source for magmas from Los Humeros Caldera, Puebla, Mexico. Chem. Geol. 164, 35–60.

Walter, T. R. & Troll, V. R. (2001). Formation of caldera periphery faults: an experimental study. Bulletin of Volcanology, 63(2-3), 191.

Weijermars, R. (1997). Principles of Rock Mechanics. Alboran Science Publishing, Amsterdam, 359 pp.

Weijermars, R., Schmeling, H. (1986). Scaling of Newtonian and non-Newtonian fluid dynamics without inertia for quantitative modelling of rock flow due to gravity (including the concept of rheological similarity). Physics of the Earth and Planetary Interiors 43, 316– 330.

Williams, H. (1941). Calderas and Their Origin, by Howel Williams. University of California Press.

Coordination Office, GEMex project
Helmholtz-Zentrum Potsdam
Deutsches GeoForschungsZentrum
Telegrafenberg, 14473 Potsdam
Germany